

**EXCLUDED-VOLUME EFFECTS IN MOLECULAR  
BIOLOGY AND EXTRACELLULAR MATRIX  
BIOCHEMISTRY: BIOPHYSICAL CONSIDERATIONS  
AND MOLECULAR MODELING**

**HARVE SUBRAMHANYA KARTHIK  
MBBS, MMST**

**A THESIS SUBMITTED FOR THE DEGREE OF DOCTOR  
OF PHILOSOPHY IN BIOENGINEERING**

**DIVISION OF BIOENGINEERING  
NATIONAL UNIVERSITY OF SINGAPORE**

**2008**

## **Acknowledgements**

Sincere thanks and gratitude to Prof. Raghunath, Prof. Rajagopalan, Dr. Ricky Lareu, Dr. Andrew Thomson, Prof. Jiang, Dr. Dimitrios Zeugolis, and all members of the TML team, Irma Arsianti, Shriju Joshi, Peng Yanxian, Benny Paula, Wang Zhibo, Felicia Loe, Clarice Chen, Ariel Tan, Yuan Sy Wong, Pradeep Paul, Lewis Tan, Siah Wanping, Dr. Yin Jian, Vignesh, Dhawal and last but not the least, my family, who guided, supported and helped me making every moment of my PhD life memorable.

# Table of Contents

Acknowledgements	ii
Table of Contents	iii
1. List of Figures	vi
2. List of Tables	viii
3. List of Abbreviations and Symbols	ix
4. Summary	xi
5. Introduction	1
6. Review of Literature	4
6.1 Macromolecular Crowding and its Effects on DNA and the Nucleus	5
6.2 Macromolecular Crowding and Cellular Homeostasis	6
6.3 Macromolecular Crowding influences Intra-cellular Trafficking	7
6.4 Macromolecular Crowding on Protein-folding and Stability	7
6.5 Macromolecular Crowding Effects on Protein-Aggregation	9
6.6 Macromolecular Crowding Effects on in vitro Biological Processes	10
6.7 Macromolecular Crowding and Enzymatic Processes in vitro	11
6.8 Macromolecular Crowding can trigger Reverse Proteolysis	11
6.9 Mixed Macromolecular Crowding: An Emerging Concept	12
6.9.1 Crowding is a feature seen in all Biological Systems	13
6.9.2 An Evolving Facet of Crowding in Multi-Cellular Organisms: the ECM	15
6.9.3 Macromolecular Crowding in Extremophiles	15
6.9.4 Challenges for Quantitative Estimation of the degree of ‘Crowdedness’	16
6.9.5 Macromolecular Crowding and Confinement: the Biological Equivalence	18
6.9.6 Summary of Literature	19
7. Objectives and Study Design	20
7.1 Aims and Rationale	20
7.2 Study Design	21
8. Biophysical Approaches to Quantitate Crowding	22
8.1 Aims and Rationale	22
8.2 Study Hypothesis	23
8.3 Biophysical Tools for Crowding Quantification	23

8.3.1 Theory of Dynamic Light Scattering	24
8.3.2 Readouts from a typical DLS Experiment and Interpretation	26
8.3.3 Theory of Zeta Potential	27
8.3.4 Readout from a typical ZP run and Interpretation	28
8.3.5 Materials and Methods	30
8.3.5.1 Sample preparation	30
8.3.5.2 DLS Methods	30
8.3.5.3 Viscosity Measurements	30
8.3.5.4 Zeta Potential Measurements	31
8.4 Results	32
8.4.1 Charged Macromolecules have Significantly Larger Hydrodynamic Radii	32
8.4.2 A Concentration-dependent Decrease in Hydrodynamic Radii	33
8.4.3 A Retrograde Approach from the “Self-Crowding point”	34
8.4.4 Mixed Macromolecular Crowding: PVP360 enhances Fc70 Multimerization	35
8.4.5 Surface Charge Characterization of Macromolecules	36
8.5 Discussion	37
9. Macromolecular Crowding of Molecular Biology Reactions	42
9.1.1. Biomolecular Reactions and the Need for Crowding	42
9.1.2. RT-PCR as a Model for Testing Crowding Effects	43
9.1.3. Rationale of Crowding the RT-PCR	45
9.1.4 Aims	46
9.1.5 Study Hypotheses	46
9.2 Materials and Methods	47
9.2.1. General Materials.	47
9.2.2. Thermostability Screening of Macromolecules.	47
9.2.3. RNA Extraction	47
9.2.4. Reverse Transcription Reaction	48
9.2.5. Polymerase Chain Reaction	48
9.2.6. Processivity Experiments	49
9.2.7. Agarose Gel Electrophoresis	49
9.3. Results	51
9.3.1 Sensitivity	51
9.3.2 Specificity	54
9.3.3. Processivity of Taq Polymerase and Reverse Transcriptase	55

9.3.4	PCR Product Yield is enhanced under Crowded Conditions	57
9.3.5	Crowding stabilizes Pre-stressed Enzymes against Heat	59
9.4	Discussion	60
10.	Semi-Empirical Modeling of Crowding Nucleic Acid Interactions	64
10.1	Introduction	64
10.2	Aims and Rationale	66
10.3	Hypothesis	66
10.4	Materials and Methods	67
10.4.1	Real-time Measurement of DNA Hybridization	67
10.4.2	Molecular Dynamics Simulations	68
10.5	Results	70
10.5.1	Rationale of Modeling MMC as Macromolecular Confinement	70
10.5.2	Double-stranded DNA is stabilized at Temperature Cycles of a typical PCR	71
10.5.3	<i>In vitro</i> Crowding enhances Thermal Stability of Nucleic Acids	77
10.5.4	Macromolecular Confinement enhances Hydrogen	78
10.5.5	<i>In silico</i> Confinement Models predict Structural Stabilization	80
10.5.6	MMC enhances Duplex Formation of Single-stranded Hair-pin	81
10.6	Discussion	83
10.6.1	MMC drives Duplex Formation from Nucleic Acid Single Strands	83
10.6.2	Mixed MMC greatly enhances DNA-thermal Stabilizing Effects	84
10.6.3	A Combined <i>in vitro-in silico</i> Approach	86
10.6.4	Crowding Effects by Confinement	87
11.	Macromolecular Crowding of <i>in vitro</i> Cell Culture	89
11.1	Rationale and Aims	89
11.1.1	Collagen Biosynthesis	89
11.1.2	Hypotheses	91
11.2	Experimental Design, Readouts and Interpretation	92
11.3	Materials and Methods	92
11.4	Results	95
11.5	Discussion	100
12.	Final Conclusions and Outlook for the Future	104
13.	References	106
	Appendix (publications and patent information)	

# 1. List of Figures

1. A schematic illustration of the various extremophiles found on earth
2. Crowded state of cytoplasm in eukaryotic and *E. coli* cells
3. Crowding principle
4. Crowded environments drive protein folding
5. *In vitro* biology: Illustrating the shortcomings of current *in vitro* cell culture
6. Reverse proteolysis
7. Crowding in the ECM
8. Dependence of the folding rates as a function of concentration and the radius
9. A schematic outlay of the study design
10. A schematic outlay of the biophysical approach to quantify crowding
11. The set up of a dynamic light scattering experiment.
12. A DLS Instrument for collecting scattered light
13. A typical DLS readout
14. Electric potential profile
15. A schematic representation of the electrode set-up
16. Charged Macromolecules have larger hydrodynamic size than neutral
17. The 'self-crowding' phenomenon
18. Hydrodynamic radii: Maxima and Minima
19. Mixed Macromolecular Crowding
20. Mean negative zeta potentials of anionic macromolecules
21. The contribution of electrostatic exclusion of anionic macromolecules
22. A schematic illustration of reverse transcription *in vivo*
23. A schematic to show the target molecular biology reactions
24. Macromolecular crowding enhances sensitivity of RT-PCR (Amplification)
25. Macromolecular crowding enhances sensitivity of RT-PCR (Dissociation)
26. Amplification plots and dissociation curves of the GAPDH PCR
27. Macromolecular crowding increased primer binding specificity
28. Macromolecular crowding enhances enzyme processivity
29. Macromolecular crowding enhances activity of Taq DNA polymerase

30. Taq DNA polymerase-thermal stability testing
31. A simplified confinement model
32. Real time readings of SG I fluorescence due to 20-mer DNA hybridization
33. Dissociation Curves of 20-oligomer DNA-DNA hybrids
34. Dissociation curves of DNA duplexes between mismatched oligo(20)-mers
35. Snapshots of simulated single DNA-DNA hybrid
36. Dissociation Curves of 20-mer hair-pin DNA-DNA hybrids
37. Schematic representation of Mixed Crowding effects on DNA stability.
38. Collagen biosynthesis in vivo
39. Schematic illustration of the proposed hypothesis
40. Dextran sulfate (DxS) promotes collagen deposition
41. Dose-dependent stimulation of collagen deposition by DxS
42. Immunocytochemical detection of deposited collagen
43. SDS-PAGE of cell fractions from cultures
44. PSS is a greater volume excluder than DxS500

## **2. List of Tables**

1. A schematic illustration of crowding in cellular organelles
2. List of macromolecules tested for their biophysical profiles
3. Charged macromolecules are larger than neutral macromolecules
4. Mean Zeta potentials of macromolecules
5. Comparing the relative diffusion coefficients of DNA and crowders
6. Real-Time monitoring of thermal stability of nucleic acid hybrids
7. Summary of MD Simulations on nucleic acid hybrids
8. Marginal effects of Neutral Dextran 670 on collagen deposition



### 3. List of Abbreviations and Symbols

aP2, Fatty Acid Binding Protein

Asc, Ascorbic acid

C<sub>T</sub>, Threshold Cycle

° C, degrees Celsius

cDNA, Complementary DNA

DLS, Dynamic Light Scattering

dNTPs, Deoxy-ribose Nucleotide Triphosphates

DxS, Dextran Sulfate

ECM, Extracellular Matrix

EVE, Excluded-Volume Effect

Fc70, Ficoll 70kDa

Fc400, Ficoll 400kDa

FtsZ-GDP, Filament Temperature-Sensitive Mutant Protein Z- GDP

Ψ, Fractional Volume Occupancy

GAG, Glycosaminoglycan

GAPDH, Glyceraldehyde Phosphate Dehydrogenase

GroEL, Molecular Chaperone Protein

HBSS, Hanks Balanced Salt Solution

K, Kelvin

MMC, Macromolecular Crowding

MM-CK, Muscle Creatinine Kinase

MD, Molecular Dynamics

μm, micrometer

nm, nanometer

ND 410, Neutral Dextran 410 kDa

ND 670, Neutral Dextran 670 kDa

$R_H$ , Hydrodynamic Radius

RT, Reverse Transcriptase

RMSD, Root-Means-Squared-Displacement

PCR, Polymerase Chain Reaction

PDI, Protein Disulfide Isomerase

PEG, Polyethylene Glycol

PSS, Polystyrene Sulfonate

PVP360, Polyvinyl Pyrrolidone 360 kDa

SEM, Standard Error of Mean

SG I, SYBR Green I

$T_m$ , Melting temperature

TIM, Triose Phosphate Isomerase

ZP, Zeta-( $\zeta$ )- Potential

## 4. Summary

Macromolecular crowding is a vital biophysical principle governing the structure and function of all biological systems both at the intra- and extra-cellular levels. Crowding of biological spaces leads to the excluded volume effect (EVE). This favors macromolecular association, influences enzymatic reactions and evolutionary structural organization of living systems. In the current study, EVE was created by dissolving macromolecular crowders of defined molecular weights and surface charge in physiological solutions. Quantitative characterisation of crowding molecules was done by Dynamic Light Scattering, Viscometry and Zeta potential measurements. We found that anionic macromolecules like dextran sulfate (DxS; 500 kDa) have larger hydrodynamic radii (~46.3nm) than neutral macromolecules of comparable molecular weight like dextran (670 kDa; ~21.2nm). However, among the negatively charged crowders, those with a higher negative surface charge density (and zeta potential) like polystyrene sulfonate (PSS; 200kDa) showed a massive gain in hydrodynamic radius (21.2nm). Hydrodynamic radius and negative surface charge therefore are critical determinants of EVE by a crowder to a 'test' molecule. Crowding was applied on *in vitro* models, namely the reverse-transcriptase-polymerase chain reaction (RT-PCR) by adding neutral macromolecules (Ficoll) to the reaction. Sensitivity of the RT-PCR was improved by ~10-fold at an enhanced specificity of amplification. Thermal stability and processivity of DNA polymerase enzymes were enhanced by crowding demonstrated by synthesis of longer DNA products. Crowding enhances PCR efficiency and product yield by ~2-fold. Effects of crowding on the thermal stability of nucleic acid hybrids (critical for many molecular biology reactions such as RT-PCR), was investigated. Melting temperatures

were increased by 5-8 °C under crowded conditions for DNA-DNA hybrids of different length, sequence and conformations and DNA:RNA hybrids. Crowding thus enhances stability of nucleic acid structure in thermally stressed environments. An *in silico* modeling based on a Molecular Dynamics platform was done to understand the mechanics of crowding induced thermal stability of nucleic acid hybrids. Crowding was found to minimize structural distortion as shown by a 3-fold decrease in Root-Means-Squared-Deviation and to reduce breaking of hydrogen bonds between complementary nucleotides in the double helix upon heating to denaturation. The study was then taken to a higher level of complexity by introducing crowding into fibroblast cultures, a more complex system than PCR in terms of composition, target biological reactions and read-outs. We chose extracellular collagen deposition as a read-out, as it is an enzymatically controlled step. Collagen deposition is very slow in standard non-crowded culture conditions which represent a bottleneck in tissue engineering applications. Crowding by negatively charged macromolecules such as DxS and PSS enhanced collagen deposition by ~10-fold. As expected from biophysical measurements, EVE created by charged macromolecules and, in turn, collagen deposition, was greater than in the presence of neutral macromolecules of comparable size. As predicted, PSS led to greater collagen deposition than DxS due to greater surface charge density. In conclusion, the presented studies demonstrate the manifold effects of crowding and EVE in molecular biology and extracellular matrix biochemistry with a wide-range of potential applications in academic research, industrial R & D and clinical translation.

## 5. Introduction

All living systems are highly crowded (Fulton, 1982). This is true of the interiors and exteriors – of all cells, whether bacterial, animal, or plant. The Crowding element is derived from macromolecules such as proteins, carbohydrates, lipids and nucleic acids, that form macromolecular complexes and supra-molecular assemblies such as cellular organelles and membranes (Minton, 2000a) so much so that up to 40% of the cytoplasmic volume is occupied by macromolecules (Ellis & Minton, 2003; Ebel & Zaccai, 2004). Viruses, archaea and prokaryotes considered the earliest life forms, have been found to have crowded structural and functional units. Further, the archaea and prokaryota have been found to be extremophilic, i.e. they have the ability to survive under extremely harsh conditions of temperature (thermophiles, hyperthermophiles and psychrophiles), salt (halophiles), pH (acidophiles and alkaliphiles), aridity (xerophiles), hydrostatic pressure (piezophiles) and so on (Fig. 1).

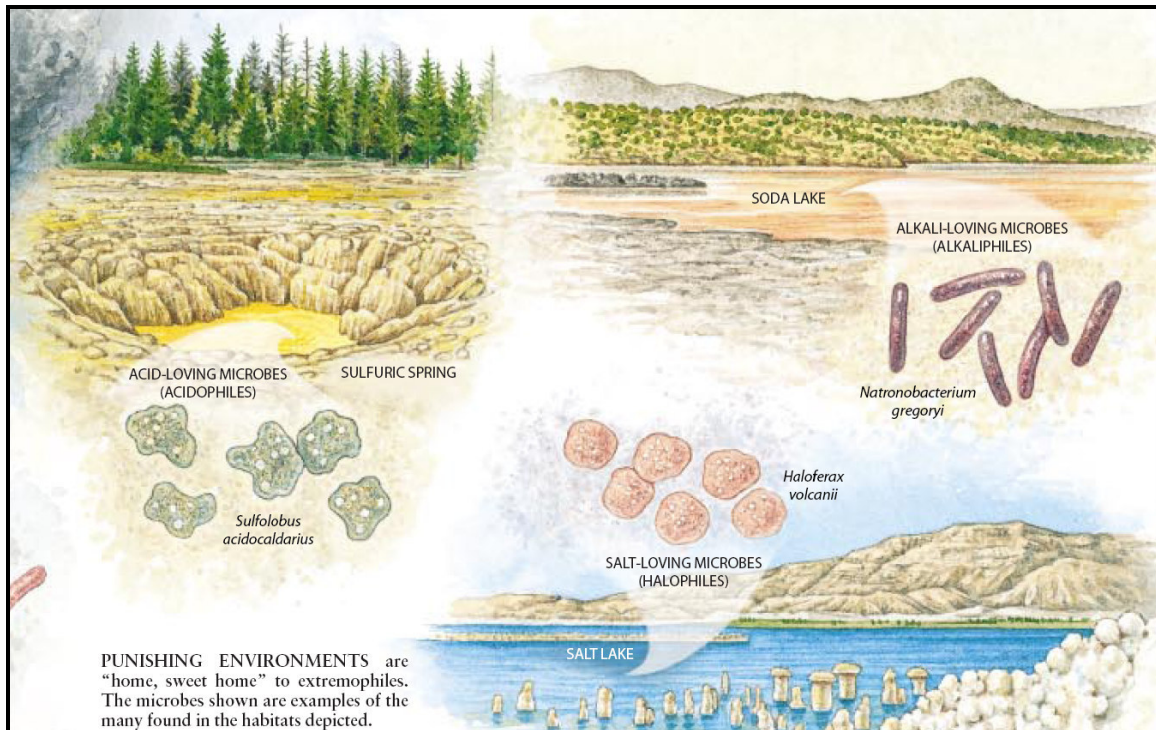


**Figure 1.** A schematic illustration of the various extremophiles found on earth (Adapted with permission from Roberto Osti Illustrations, illustrated in an article by Madigan *et al.*, 1997).

The extremely hardy nature of these organisms has been explained as being due to many factors. One of them is Macromolecular Crowding. Still in the hypothetical domain, this attribution needs to be thoroughly investigated experimentally and the mechanisms explained. Crowding functions by way of the excluded-volume effect (EVE). *Excluded volume* refers to the volume of a solution that is excluded to the center of mass of a ‘test’ molecule by the presence of one or more background (crowder) molecules in the medium. The volume exclusion effect is greatest between like-sized crowder and ‘test’ molecules. *Fractional volume-occupancy* ( $\Psi$ ) denotes the fraction of the total volume occupied by macromolecules. Structurally and chemically, the macromolecule could be derived from carbohydrate/ protein/nucleic acid/lipid family or their analogues like the glycosaminoglycans. However, the Crowding behavior is entirely dependent on the

physical property of the macromolecule. Biological macromolecules such as enzymes and proteins function in highly crowded environments. The total concentration of protein and RNA inside bacteria like *E. coli* is in the range of 300-400 g/l. Crowding has multiple effects in biological systems *in vivo*. They include effects on reaction rates and equilibria, macromolecular self-assembly, genome structure and function as well as folding of biopolymers (eg. nucleic acids and proteins). These resulting effects are so large, that many estimates of reaction rates and equilibria made with uncrowded solutions in the test tube differ by orders of magnitude from those of the same reactions operating under crowded conditions within cells or the extracellular compartment (Minton, 2005). However, EVE and its roles have not been appreciated in the biological domain and applications have yet to be fully discovered (Ellis, 2001b). The cell culture is a typical example wherein the cells anchored to the culture plate find themselves bathed in an ocean of medium that is hardly representative of the *in vivo* conditions. Biological reactions in such *in vitro* conditions proceed at significantly slower rates than their *in vivo* counterparts. Thermodynamically, volume exclusion lowers the configurational and conformational freedom (entropy) and this leads to raised basal free energy of the reactant macromolecules and a number of downstream effects (Hall & Minton, 2003). These may be identified as (1) folding of proteins into native states optimal for function (Cheung *et al.* 2005) (2) stronger macromolecular transition complexes with longer half-lives (eg. enzyme-substrate) leading to more products and (3) buffering effect of crowded environments on biological function under conditions of adverse pH, temperature or ionic strength (Goobes *et al.* 2003).

## 6. Review of Literature

The role of Macromolecular Crowding (MMC) in shaping the cell and extra-cellular environments and its influence on most biological processes both at the intra- and extra-cellular levels *in vivo* are the focus of many current studies.

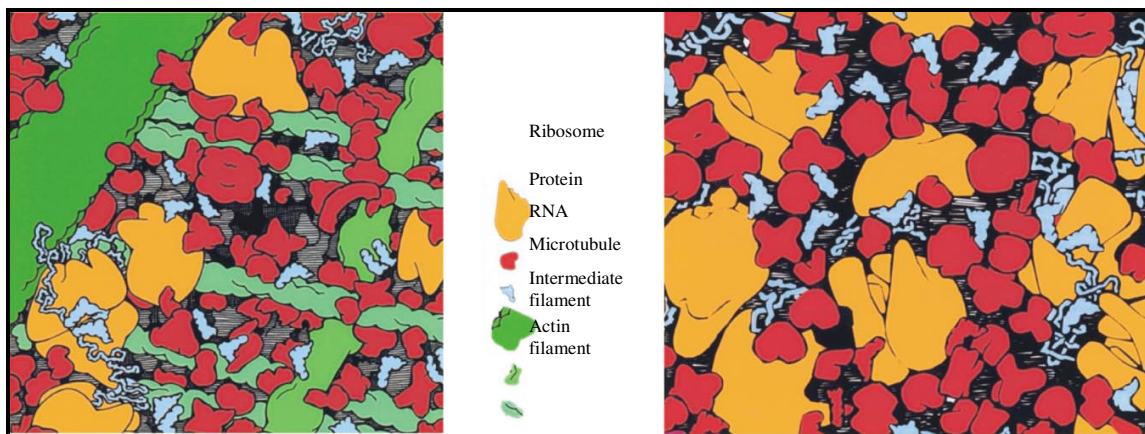


**Figure 2.** Crowded state of cytoplasm in eukaryotic and *E. coli* cells (adapted from *The machinery of life* by Goodsell D.S., Springer-Verlag, 1993 with kind permission of Springer Science and Business Media; see reference for full citation).

In a medium containing multiple species of soluble macromolecules, even if no species is found at high concentrations, but when considered collectively all the different species account for a significant fraction (20-30%) of the volume of the medium; then this medium is called “crowded” instead of being “concentrated” (Minton & Wilf, 1981; Zimmerman, 1993; Rivas *et al.* 2004). The term ‘Macromolecular Crowding’ was thus introduced to underscore that the effect of Crowding by large molecules is not significant on the activity of metabolites and small ions but on other large molecules; that is, the effect is exerted by large molecules on like-sized large molecules (Fig. 3).



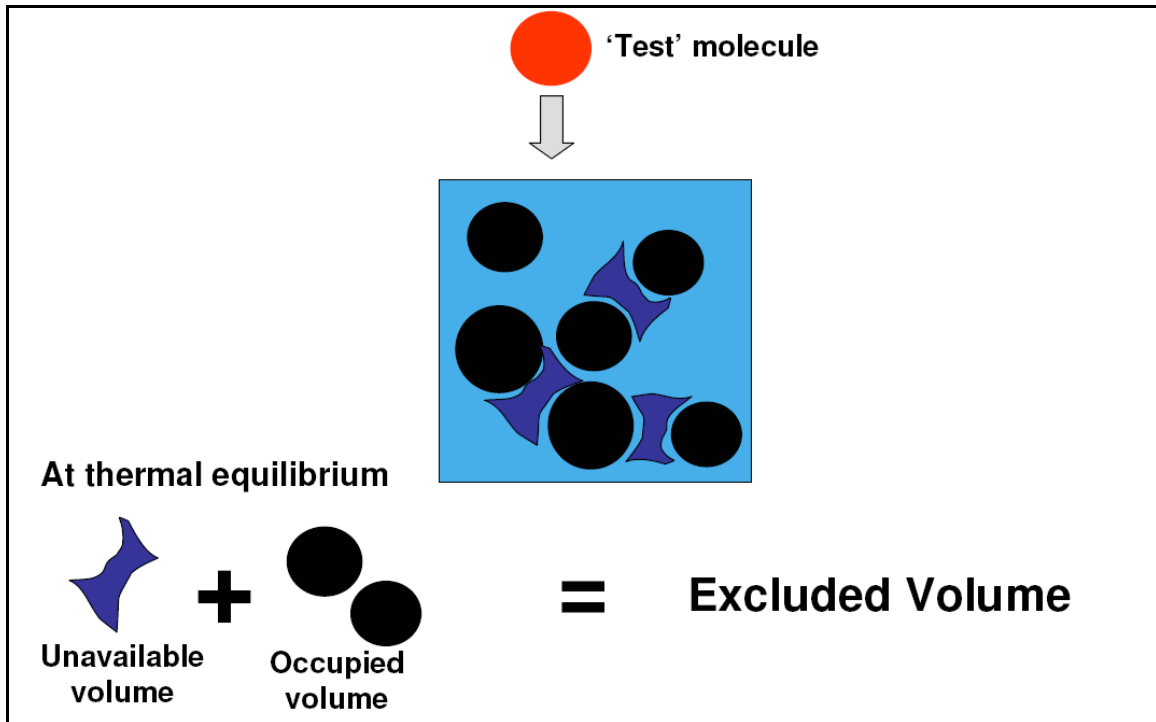


**Figure 3.** Crowding principle: At thermal equilibrium of the solution, the total excluded volume to a 'test'\* (red) molecule of size comparable with the crowders (black) is a summation of the unavailable volume (dark-blue) and the occupied volume (black). This is due to the geometric shape constraints of the crowders modeled here as rigid hard spheres.

### 6.1 Macromolecular Crowding and its Effects on DNA and the Nucleus

Crowding determines genome structure and function by its effects on both the organization of DNA into nucleosomes by folding-packaging and the interactions between DNA and histones (Zimmerman, 1993; Zimmerman & Murphy, 1996). Crowding has been shown to contribute to enhance the free energy of binding between two individual DNA strands or between a protein and a DNA interaction (Goobes *et al.* 2003; Record *et al.* 1998). Crowding thus influences the structural and functional integrity of nuclear compartments *in vivo* (Hancock, 2004). Moreover, it has been reported that the initiation of DNA replication depends on nucleus formation (Walter *et*

---

\* The 'test' molecule refers to the molecule that will be crowded by the crowding macromolecules

*al.* 1998; Depamphilis, 2000), which emphasizes the role of Crowding for the operation of the replication machinery, as shown by *in vitro* experiments (Walter *et al.* 1998; Jarvis *et al.* 1990).

## **6.2 Macromolecular Crowding and Cellular Homeostasis**

The living cell depends entirely on the enzyme-driven metabolic reactions as suggested by Arthur Kornberg as one of the ten ‘commandments’ in enzymology (Kornberg, 2003). The seventh ‘commandment’, according to Kornberg describes the crowded nature of the cell and a reminder that all enzymatic reactions *in vitro* with cell-free systems need to include this crowding element. All the enzymes function at optimal conditions of salt concentration, pH and temperature. However, if any of these conditions are altered, the enzyme function is perturbed. However, under crowded conditions the enzymatic activity is still maintained. As an example, experiments were done on the nick-translation and polymerizing functions of *E. Coli* DNA polymerases (Zimmermann and Harrison, 1987). The optimal salt (KCl) concentration for nick-translation under non-crowded conditions was 0.1M. However when the salt concentration was increased by 3-fold, the enzyme activity was inhibited. But under crowded conditions (due to Ficoll 70), the enzyme activity was still well detectable at 0.3M salt concentrations. This was explained to be due to the sustained binding of the polymerases to their template-primer complexes under Macromolecular Crowding conditions even in highly unfavorable conditions (in this case, the ionic strength) that are introduced, the enzymes remaining active and hence widening the range of conditions/environments in which the cell can remain viable. It has also been found that Crowding effects resulting from changes in the amount of water seem to compensate for the effects of changes in cytoplasmic  $K^+$  ions

and contribute to maintaining protein–nucleic-acid equilibria and kinetics in the range required for function *in vivo* (Record *et al.* 1998).

### **6.3 Macromolecular Crowding influences Intra-cellular Trafficking**

The viscoelastic properties of a cell determine how it reacts to the environment (Guigas, 2007a). Macromolecular Crowding contributes to the viscoelasticity of the cytoplasm and nucleoplasm which results in anomalous sub-diffusion<sup>†</sup> of macrosolutes (Weiss *et al.* 2004; Guigas *et al.* 2007) leading to slow apparent translational diffusion of molecules in the cytosol (Elowitz, 1999). Crowding has also been associated with cell signal transduction pathways (Bray, 1998). Crowding in cells greatly favors macromolecular associations involved in signal transmission, frequently increasing the binding strength by at least an order of magnitude (Wilf & Minton, 1981).

### **6.4 Macromolecular Crowding on Protein-folding and Stability**

Crowding influences protein stability by driving proteins into compact from expanded states and enhancement of self- and hetero-associations of protein macromolecules provided there is a tendency for the interacting molecules to associate (Ellis 2001). For instance, the dependence of oxygen affinity of erythrocytes containing sickle cell hemoglobin can be quantitatively explained by Crowding induced-steric repulsion between hemoglobin molecules (Minton, 1976). The increased thermal stability of proteins under crowded conditions has been shown by many *in vitro* experiments. Crowding tends to force binding of the enzyme to the substrate and increased strength of binding could, in principle, stabilize both components to denaturation (Zimmerman &

---

<sup>†</sup> A phenomenon when the mean-squared-displacement of a diffusing molecule does not increase linearly with time

Harrison, 1987). Theoretical considerations (Cheung *et al.* 2005) have predicted that Crowding can enhance the thermal stability of the folded state relative to that of the unfolded state (Fig. 4). Crowding also influences the rate of protein folding. It has been found that the refolding of hen lysozyme occurs in two distinct separate fast and slow tracks (Radford *et al.* 1992; Dobson *et al.* 1994; Matagne *et al.* 1997; Kulkarni *et al.* 1999). Another study (Van den Berg, 1999b) reported that, in experiments done on the oxidative refolding of hen lysozyme under crowded conditions, while there is acceleration of fast-track refolding rate by 2- to 5-fold relative to refolding in dilute solution, it could decrease slow-track refolding rate by nearly 50%.

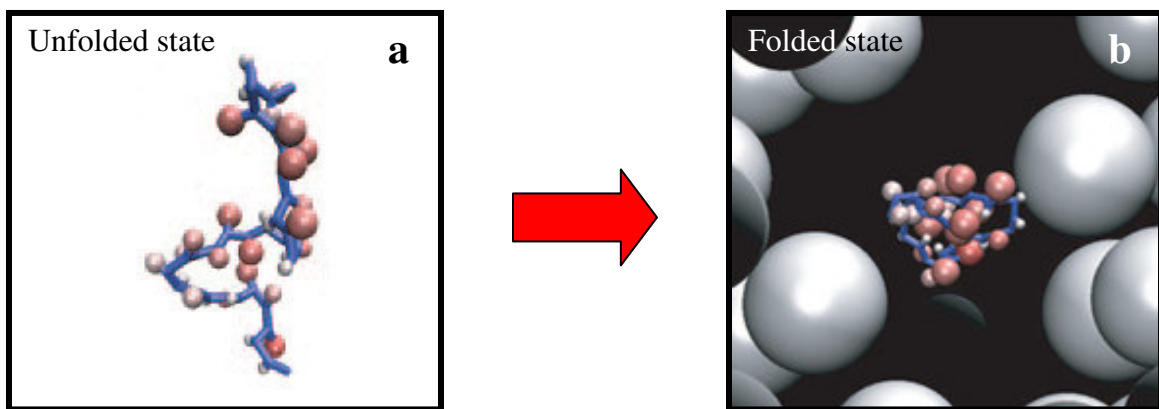


**Figure 4.** Crowded environments (b) contribute to protein folding into compact state by reducing the conformational entropy for the unfolded state (a) (Modified from Cheung *et al.*, PNAS, 2005).

The relative unfolding of one population of proteins could affect the folding of other proteins in the same environment and Crowding acts as a regulator of the thermal stability of proteins (Despa *et al.* 2005). The thermal stability of the proteins found in the interior of an eye lens increases with concentration (Steadman *et al.* 1989), and the exceptional heat stability of an intact lens has been attributed in part to the stabilizing effects of Macromolecular Crowding inside the lens cell (Bloemendal *et al.* 2004). In the

*in vitro* scenario, the thermal stability of  $\alpha$ -lactalbumin is increased as indicated by a raise in melting temperature by 25–30 °C by encapsulation in a silica matrix (Eggers & Valentine, 2001), an example also of the ‘caging effect’ that Crowding exerts on proteins (Thirumalai, 2003). Studies of Crowding effects on the refolding rates of proteins have been done on reduced lysozyme (van den Berg *et al.* 2000; Zhou *et al.* 2004), glucose-6-phosphate dehydrogenase (Li *et al.* 2001), glyceraldehyde-3-phosphate dehydrogenase (Ren *et al.* 2003), protein disulfide isomerase (PDI) (Li *et al.* 2001), and GroEL (Galan *et al.* 2001).

### **6.5 Macromolecular Crowding Effects on Protein-Aggregation**

Although the above mentioned works have shown that Crowding enhances protein folding to the native state, there have also been reports of Crowding-induced aggregation (van den Berg *et al.* 1999b; Ellis, 2001b). Several experiments show that the oligomerization of actin (Lindner & Ralston, 1997), spectrin (Lindner & Ralston, 1995), tubulin (Rivas *et al.* 1999) and FtsZ-GDP (Rivas *et al.* 2001) were augmented under crowded conditions, as well as the self-association of fibrinogen (Rivas *et al.* 1999). In the intra-cellular context, it was shown that the association of ribosomal particles was increased under crowded conditions (Zimmerman & Trach, 1988b). The aggregation has been explained as being due to increases in the thermodynamic activity of partially folded polypeptide chains, and this effect being particularly pronounced for small as well as slow-folding chains (Ellis, 2001b). For slow-folding chains, it was shown that the protein-folding catalyst PDI was especially effective in preventing proteins such as reduced hen lysozyme from aggregating under crowded conditions (van den Berg *et al.* 1999b), due to the enhancement of PDI’s chaperone function by Crowding. The

association of chaperones with partly folded chains might be enhanced under crowded conditions, thus reducing the encounter rate of these chains with each other and hence the probability of them aggregating (Ellis, 2001b).

## 6.6 Macromolecular Crowding Effects on *in vitro* Biological Processes

The realization of the importance of Macromolecular Crowding notwithstanding, many studies continue to be conducted in *in vitro* under uncrowded conditions. For example, in the cell culture the total concentration of macromolecules is typically 1-10 mg/ml and Crowding effects are negligible (Ellis, 2001b). Thus we can appreciate that current *in vitro* culture media are actually “an ocean of dilution” (Fig. 5). However, Crowding effects needed to be taken into account when attempting to relate biochemical and biophysical observations made *in vitro* to physiological processes observed *in vivo* and therefore Crowding is an important parameter to be applied *in vitro*. Further, excluded-volume effects in physiological media demand careful consideration when associating a role *in vivo* for any macromolecular reaction conducted *in vitro* (Minton, 2001). An important observation here is that many estimates of reaction rates and equilibria made with uncrowded conditions *in vitro* differ by orders of magnitude from those made under crowded conditions *in vivo* (Ellis, 2001b).



**Figure 5.** *In vitro* biology: the shortcomings of current *in vitro* cell culture: An “ocean of dilution” illustrating how the newsprint can be easily read through the flask containing dilute culture medium (Picture courtesy: Prof. M. Raghunath, Tissue Modulation Laboratory, NUS).

Crowding effects can be replicated and examined in *in vitro* studies by using single or combinatorial solutions of ideal Crowding agents, i.e. those that are chemically inert, highly pure, water-soluble, of varied shapes (ideally globular) and with a molecular weight range of 50-500 kDa such as dextrans and their derivatives, Ficolls or inert proteins (Munishkina *et al.* 2004).

### **6.7 Macromolecular Crowding and Enzymatic Processes *in vitro***

Crowding effects on the function of enzymes have been studied *in vitro*. As was mentioned before, studies on DNA polymerases (Zimmerman & Harrison, 1987) of *E. coli* showed that Macromolecular Crowding enhanced the binding of the polymerases to the template-primer complex and increased enzyme activity even at highly inhibitory conditions of high ionic strength. Hence Crowding helps extend the range of environments in which the enzyme still remains functional.

### **6.8 Macromolecular Crowding can trigger Reverse Proteolysis**

An interesting effect of Macromolecular Crowding is observed called as reverse proteolysis. Crowding enhances the association of macromolecules into compact complexes, and it was found that some enzymes which catalyze degradative reactions such as limited proteolysis *in vitro* might catalyze the reverse reaction *in vivo*, i.e. cause reverse proteolysis (Somalinga & Roy, 2002; Fig. 6), and thus function as synthetic rather than degradative enzymes *in vivo*. This study showed that Crowding could trigger transformation of a non-covalent protein complex obtained by limited proteolysis to the native (covalent) form, but only if the formation of the native protein resulted in

significant compaction leading to substantial volume reduction, thereby enabling greater translational entropy for the compacted protein under crowded conditions.

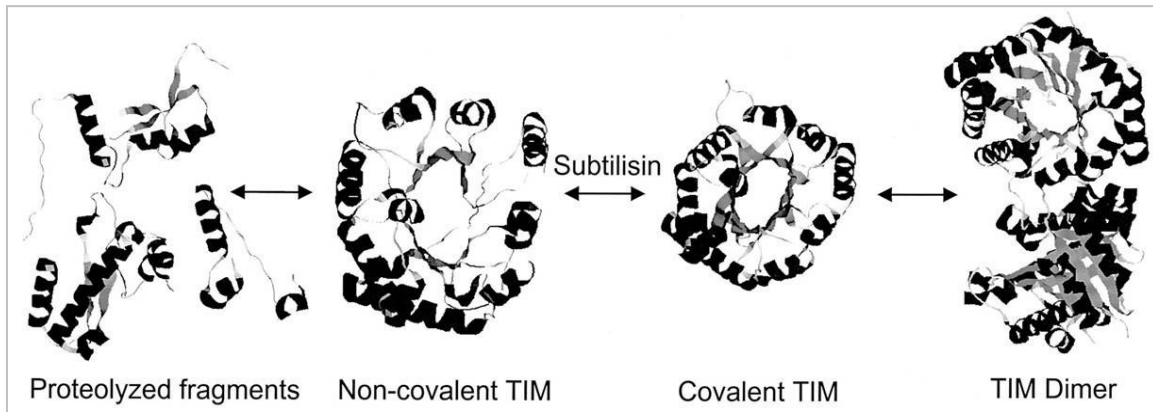


**Figure 6.** Reverse proteolysis: Crowding causes a proteolytic enzyme to function as a synthetic enzyme (Adapted from Somalinga *et al.* *JBC*. 2002).

### 6.9 Mixed Macromolecular Crowding: An Emerging Concept

Conceptually, this is an extension of the principle of Crowding that takes origin from earlier findings that the cellular environment is a collection of a variety of different macromolecules within the same confined space; different types of inert macromolecules (in terms of size, shape and surface charge) in varying amounts could in principle be added to cell cultures to more accurately mimic the *in vivo* conditions. Studies conducted to test this theory have produced interesting results. For example, Du *et al.* (2006) observed that the refolding yield of rabbit muscle creatine kinase (MM-CK) in the presence of a Mixed Crowding agent (in which the weight ratio of calf thymus DNA to Ficoll 70 is 1:9) increased by up to 23% as compared to single Crowding agents. The refolding rate of MM-CK was also greatly accelerated by Mixed as opposed to single Crowding agents. It can thus be concluded that Mixed Macromolecular Crowding







conditions are arguably more favorable for protein folding and also better mimic the physiological environment than single Macromolecular Crowding conditions.

### **6.9.1 Crowding is a feature seen in all Biological Systems**

The native structures of proteins and other intracellular moieties are usually compact and most nuclear compartments are spherical or quasi-spherical in shape (Rivas *et al.* 2001). DNA occurs in highly compact structures such as nucleoids (prokaryotes) or nucleosomes (Watson *et al.* 1987) and condensed rather than extended DNA is possibly the more efficient and a more physiologically relevant state of DNA (Sikorav & Church, 1991). In multi-cellular organisms like vertebrates, we see that the intra-cellular crowded environment develops into a more ordered structure. Thus the cellular interior is nano-compartmentalised by the microtubules, intermediate filaments and actin fibers that form the cytoskeletal framework. The cytoskeletal framework in fact provides the “Macromolecular Confinement”, an effect equivalent to Crowding (Cheung *et al.* 2005). Cellular nano-compartmentalisation is evident by the formation of cellular organelles such as the nucleus, mitochondrion, endoplasmic reticulum, and Golgi bodies. For a typical eukaryotic cell, the nucleus has been found to have a total macromolecular concentration of 400 mg/ml, the cytoplasm 50-400 mg/ml, the ER 100mg/ml and mitochondria a substantial 270-560 mg/ml (see Table 1). However, it has to be noted that the macromolecules making up this number are a diverse collection of molecules differing in size, shape and net surface charge sub-serving different functions but together occupying a significant fraction of the total volume. The volume of exclusion to a given molecule however, depends on its size relative to the Crowding molecules. Thus the concentrations indicated may not be exact measures of the volume excluded. This is

therefore the quantitative challenge in measuring the excluded-volume effect. Crowding in organelles such as the ER can have a bearing on how proteins fold once they are synthesized. Mitochondrial Crowding has been correlated with the high metabolic activity in that organelle and an interesting new concept called as “metabolic channeling” has been described for the mitochondrial metabolism (Partikian *et al.* 1998). A study (Guigas *et al.* 2007a) investigated the cytoplasm and nucleoplasm of mammalian cells and found that nanoscale viscoelasticity – a result of Macromolecular Crowding – showed minimal variation amongst different cell types, suggesting the conservative nature of cytosolic and nuclear Macromolecular Crowding across prokaryotic, eukaryotic and higher mammalian cells.

**Table 1.** A schematic illustration of Crowding in cellular organelles.

	Crowding concentration (mg/ml)		
<b>E Coli</b>	<b>300-400</b>		Ellis, R.J. <i>Trends. Biochem. Sci.</i> <b>26</b> , 597-604 (2001)
<b>Eukaryotic cell</b>			
-nucleus	<b>400</b>		Hancock, R. <i>Biol. Cell</i> <b>96</b> , 595-601 (2004)
-cytoplasm	<b>50-400</b>		Ellis, R.J. <i>Trends. Biochem. Sci.</i> <b>26</b> , 597-604 (2001)
-mitochondria	<b>270-560</b>		Partikian A et al. <i>J. Cell Biol.</i> <b>140</b> , 821-829 (1998)
<b>Serum</b>	<b>80</b>		Ellis, R.J. <i>Trends. Biochem. Sci.</i> <b>26</b> , 597-604 (2001)
<b>in vitro culture</b>	<b>&lt;10</b>		Lareu R.R. et al. <i>Tiss. Eng.</i> <b>13</b> , 385-391 (2007)

### 6.9.2 An Evolving Facet of Crowding in Multi-Cellular Organisms: the ECM

As we trace up the evolution ladder from uni- to multi-cellular organisms like vertebrates, we see that the cells have evolved to survive in an extracellular matrix (ECM). In the extra-cellular compartment, the nature of the Crowding macromolecules differs from one tissue to another in multi-cellular species. For example, the main crowders in the ECM of brain and cartilage are the glycosaminoglycans (GAGs) (Fig. 7).

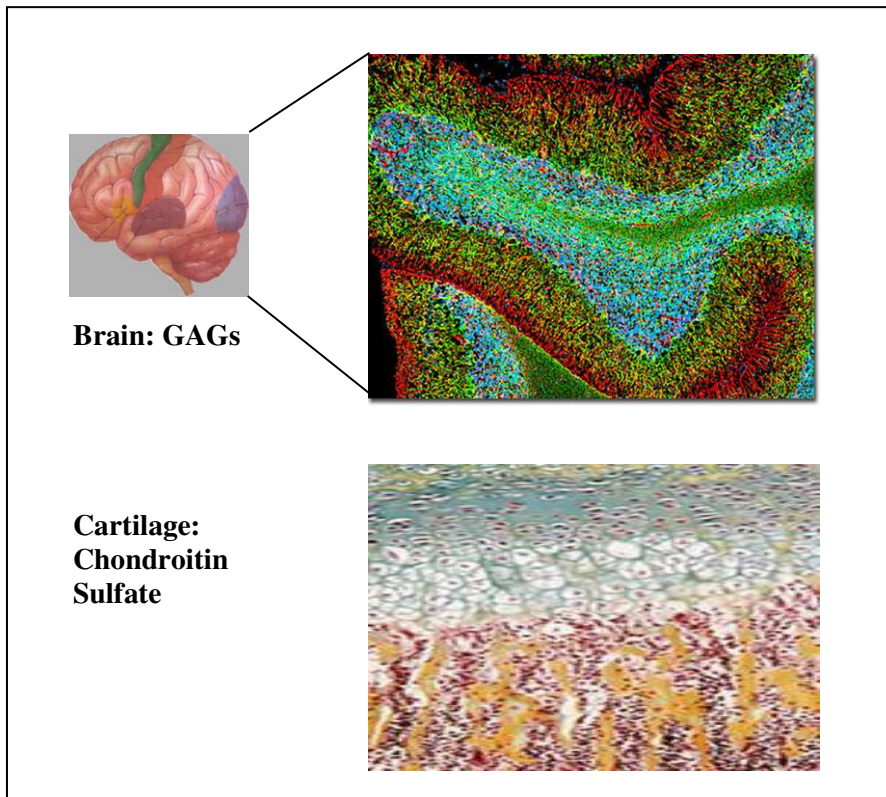


**Figure 7.** Crowding in the ECM: Brain and Cartilage are crowded by Glycosaminoglycans. (Picture adapted with permission from: [www.spineuniverse.com](http://www.spineuniverse.com)).

### 6.9.3 Macromolecular Crowding in Extremophiles

Macromolecular Crowding has been speculated to play a role in the molecular adaptation of microorganisms to survive in extreme environments, i.e. the extremophiles. Interactions of macromolecules with each other as well as with the solvent (water) in

biological systems involve weak forces such as van der Waals forces. These types of interactions can be strengthened by crowded conditions. These interactions are necessary in the correct folding and sub-unit assembly of the macromolecules such as proteins and nucleic acids to function in harsh conditions such as boiling or freezing temperatures, acidic or highly alkaline pH in organisms that live in such environments thus highlighting the importance of Crowding. Moreover, the stabilization of a compact macromolecular structure by Crowding could affect the structure's dynamics at the pico- to nano-second time scale. The increasing stability observed in going from psychrophile to hyperthermophile cells could be due in part to Macromolecular Crowding effects. This possibility has been partially verified by the ability of crowding to enable the optimum functioning of the vital DNA polymerizing enzyme even under a 3-fold increase in salt concentration (Zimmermann and Harrison, 1987). Another support to this statement is the finding that in hyperthermophiles, carbohydrate molecules such as cycloamylose have been detected in abundance. These carbohydrates have been shown to contribute to the enhanced thermostability of these organisms (Fujii, 2005).

#### **6.9.4 Challenges for Quantitative Estimation of the degree of 'Crowdedness'**

Current biophysical methods to quantify Crowding effects have been largely limited to specific models. These include non-ideal tracer sedimentation centrifugation technique (Rivas 2001), Magnetic Relaxation Dispersion (Snoussi *et al.* 2005) and diffusion measurements (Verkman, 2002). A recent study identified that the hydrodynamic radius measurements by Dynamic Light Scattering (DLS) can be a useful parameter in applying Crowding conditions in biological models *in vitro* (Harve *et al.* 2006). Theoretical models based on statistical mechanics have been developed by Minton

to further enhance the understanding of the excluded volume effect. However, a ready-to-apply relationship between the crowder profile and the volume excluded, is what a biologist needs at the bench-side for incorporating the appropriate Crowding macromolecule into the biological reaction in question. Some examples of quantitative estimation methods of Crowding are determining reaction rate of a biomolecular reaction versus crowder concentration or enzymatic activity against concentration. However, if we could derive a relationship between the volume of exclusion and the concentration of crowder, that would be more generic in terms of quantitation for all the biological applications of Crowding.

### 6.9.5 Macromolecular Crowding and Confinement: the Biological Equivalence

Crowding can be mimicked by confinement. Encapsulation of polypeptide chains in nanopores has been used to mimic Macromolecular Crowding. Several reports of confinement hint at biologic equivalence of confinement with Crowding. In an interesting study (Purohit, Kondev & Phillips, 2002), it was shown how much force is needed to package DNA into a viral capsid, an example of a confined space. According to Cheung *et al.* 2005, at a volume fraction  $\psi_c$ , a polypeptide chain could be localized in a spherical region with the most probable radius

$$R_s = \left( \frac{4\pi}{3\varphi_c} \right)^{1/3} R_c$$

These results show that Crowding and confinement affect the stability of the native state of a polypeptide chain to the same extent when compared to each other (Fig. 8) and thus may be biologically equivalent.

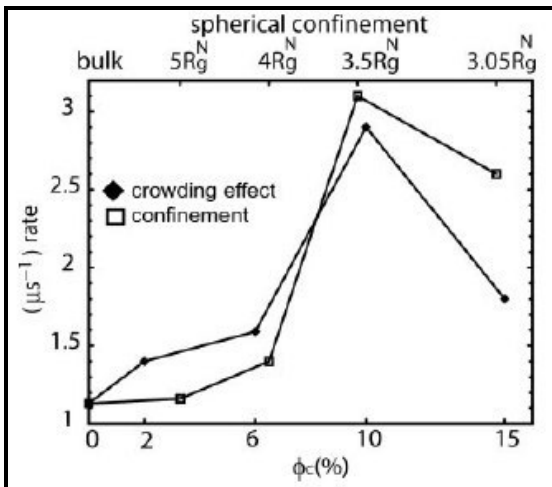


**Figure 8.** Dependence of the folding rates as a function of concentration and the radius of the volume-fraction-dependent confining sphere, This figure shows that Crowding effects can be mimicked by encapsulation in a spherical pore with radius  $R_s$  (From Cheung *et al.*,2005)

### 6.9.6 Summary of Literature

Crowded conditions are prevalent in all organisms– from bacteria to human, fungi to plants, both inside and outside the cell. Inside the cell, the degree of crowding ranges from 5 to 40%. The extracellular milieu in higher organisms shows a heterogeneous composition depending on the tissue in question. For example, the blood plasma is mainly composed of protein up to 80 g/l. We estimated the degree of crowding in plasma that works out to be 10-15%. Macromolecular Crowding influences folding and stabilization of compact states, and it has to be noted that major macromolecular structures typically have compact assemblies in their optimal functioning states. Crowding effects also have a profound influence on many biological processes, and may contribute to the survival of the organism. Current *in vitro* systems are hardly representative of the *in vivo* situation due to their highly dilute nature and Macromolecular Crowding could be the missing link between the two systems. However, there are conceptual facts about Crowding that need to be investigated and understood prior to application in a defined biological reaction. Firstly, the optimum concentration of a Crowding agent always falls within a certain window and has to be carefully tailored for the biological application. Secondly, a quantitative relationship between the concentration of crowders and the magnitude of excluded volume provides the biologist with a tangible parameter for optimizing/maximizing the application in a given biological model.

## **7. Objectives and Study Design**

### **7.1 Aims and Rationale**

#### **7.1.1. To develop simple methods to quantitate Macromolecular Crowding within a biophysical domain**

The principal aim of this study was to develop a readily applicable biophysical parameter of macromolecular crowders to tailor an optimum crowded condition for a given *in vitro* setting. Selection criteria for the biophysical methods were: (1) The method has to be simple and yield fast readouts that are applicable as screening tools, (2) The method should not interfere with the structural and other physical properties of the crowder itself and (3) The measurement method should ideally require only small sample volumes for measurement.

Dynamic light scattering, viscometry and zeta potential measurement were employed as the biophysical methods to identify the point of onset of Crowding, the point of maximum effects and the concentration beyond which the effects were negligible or even adverse.

#### **7.1.2 To apply the biophysical observations of quantitative estimates of Crowding on *in vitro* biological models**

Since enzyme-substrate reactions are ideal targets to determine the effects of Macromolecular Crowding and also serve as useful *in vivo* surrogates, we chose a few biological models to test our biophysical observations based on a few selection criteria:

1. The biological model should yield a readily measurable output.
2. The model should allow application of a range of crowder concentrations.
3. The output measurement of the model reaction should not be affected by the presence of the crowder. Crowding was



applied on the reverse transcriptase-polymerase chain reaction (RT-PCR) and then on a cell culture model of collagen biosynthesis.

## 7.2 Study design

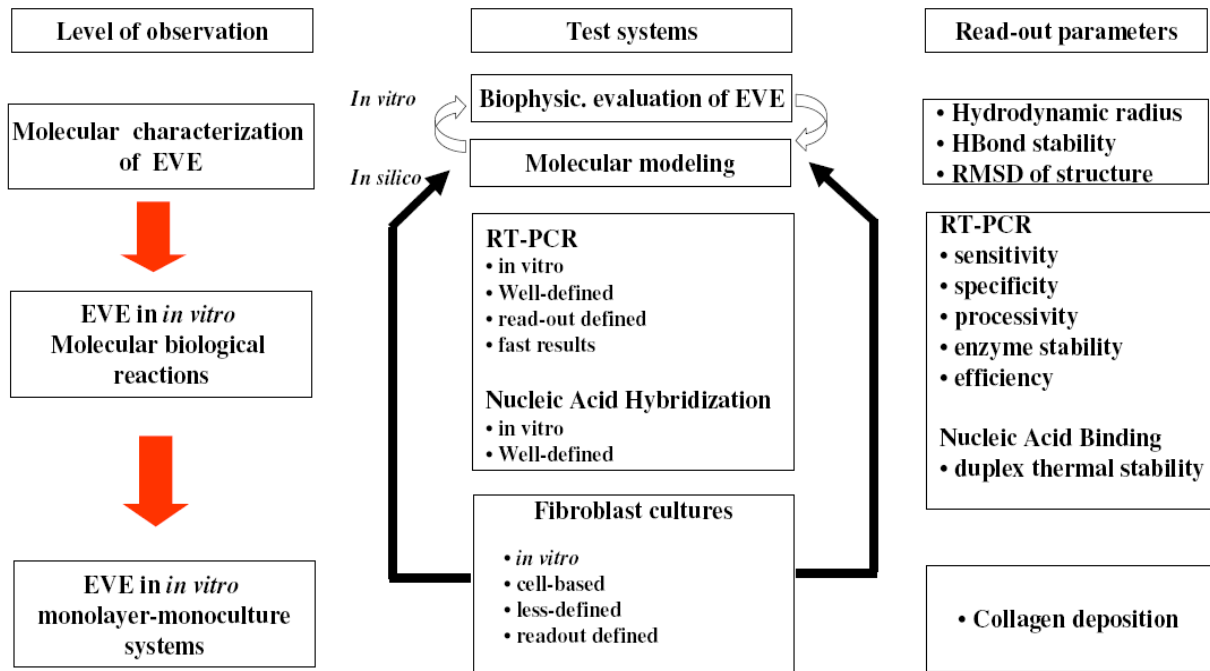


**Figure 9.** A schematic outlay of the approach to study Crowding in biological models describing the target systems, the methods and the corresponding read-outs for each method.

The study was designed to do an estimation of biophysical properties of macromolecular crowders, then applied on *in vitro* models such as the RT-PCR, followed by applying Crowding on a more complex system such as the *in vitro* cell culture. The corresponding read-outs are shown towards the right.

## **8. Biophysical Approaches to Quantitate Crowding**

### **8.1 Aims and Rationale**

#### **8.1.1. To devise simple biophysical tools that can predict optimal Crowding conditions for biological applications**

Since all biological reactions occur in aqueous environments, the concentration of the crowder in an aqueous medium critically determines the fraction volume occupancy of the crowder. Dynamic Light Scattering in combination with Viscometry and Zeta potential measurement were employed as screening tools to identify the onset of Crowding and the point where the effects are maximum.

#### **8.1.2. To determine the attributes of a macromolecular crowder in relation to their physical properties for optimal EVE**

The aim is to identify a physical property of a crowder in solution that directly influences the volume of exclusion. The crowders selected are water-soluble by definition and hydrophilic. The hydrophilicity implies that there exist solvation layers around the macromolecule in solution. The hydrodynamic radius of a macromolecule that accounts for both the macromolecular size and the hydration layers is therefore a measurable parameter by DLS studies. The aim is therefore to determine if measuring the hydrodynamic radius can yield meaningful data on the net volume of exclusion in combination with measurement of viscosity of the macromolecular solution.

## 8.2 Study Hypothesis

Crowder size, Fractional Volume Occupancy, macromolecular surface charge and charge density are collective quantitative determinants of the net volume of exclusion for biological applications.

## 8.3 Biophysical Tools for Crowding Quantification

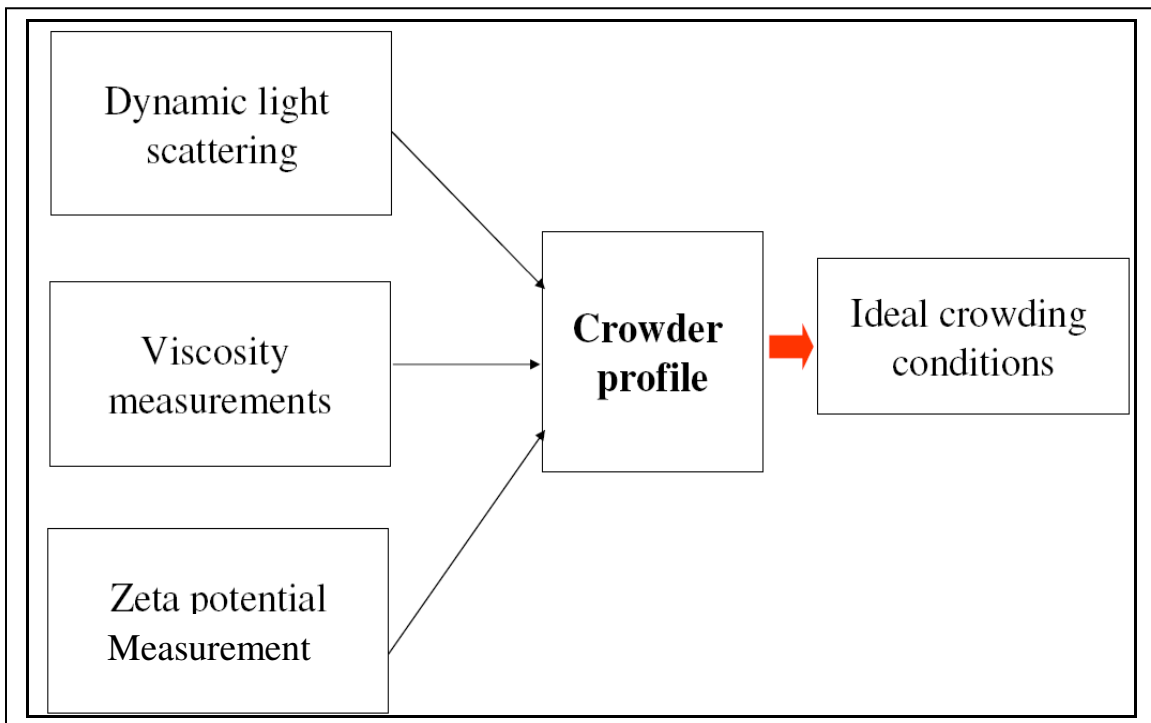


**Figure 10.** A schematic outlay of the biophysical approach to quantify Crowding: The biophysical studies help to determine the physical properties of macromolecular crowders that could be readily applied on *in vitro* biological models.

### 8.3.1 Theory of Dynamic Light Scattering

According to the light scattering theory when light impinges on matter, the electric field of light induces an oscillating polarization of electrons in the molecules. The molecules then serve as secondary sources of light and subsequently radiate (scatter) light. The frequency shifts, the angular distribution, the polarization, and the intensity of the scattered light are determined by the size, shape and molecular interactions in the scattering material (Lomakin *et al.* 2004).

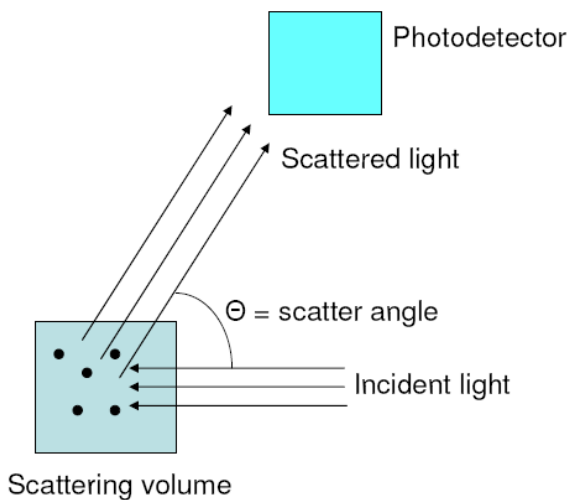


**Figure 11.** The set up of a dynamic light scattering experiment.

A beam of monochromatic light is directed through a sample and the fluctuation of the intensity of scattered light by the molecules is analyzed by a photodetector. The photodetector then sends electrical pulses to the Digital Signal Processor which counts the number of photons detected in each successive time sample. The similarity between the signal wave form and a slightly time delayed copy of itself is determined by

multiplying the two wave forms together and then summing to give the autocorrelation function. The second order auto-correlation function of the intensity  $I(t)$  is defined as:

$$g^2(q; \tau) = \frac{\langle I(t)I(t + \tau) \rangle}{\langle I(t) \rangle^2}$$

In the above formula, the angular brackets denote an average over time  $t$ . This time averaging is necessary to extract information from the random fluctuations in the intensity of the scattered light. From this, the Translation Diffusion Coefficient,  $D_T$  can be calculated by performing a nonlinear least squares fit of the autocorrelation coefficients to an exponential decay. Under the assumption of Brownian motion and that the molecules in solution are spheres, the Hydrodynamic Radius,  $R_H$  can be calculated by using Stokes' Equation as shown below:

$$R_H = k_b T / 6\pi\eta D_T$$

$k_b$  = Boltzmann's Constant  
 $T$  = Temperature in Kelvin  
 $\eta$  = Solvent Viscosity

The DLS instrument that records the signal and feeds it to the software is shown below:



**Figure 12.** The instrument that was used for DLS collects the intensity signals of scattered light due to molecules moving randomly in solution

For spherical molecules such as the globular proteins (BSA) and Ficoll, this equation can be reliable. However, for molecules that are rod-like or irregular in shape, this may not be as accurate and therefore is a limitation of the Stokes'-Einstein calculation while applying the method on macromolecules that are non-spherical.

### 8.3.2 Readouts from a typical DLS Experiment and Interpretation

The principal readouts from a DLS run are shown in figure 13 panels A and B. Panel A is a size distribution of the given macromolecule in solution and is a collection of 20 readings. Panel B is a regularized histogram of the % intensity against hydrodynamic radius.

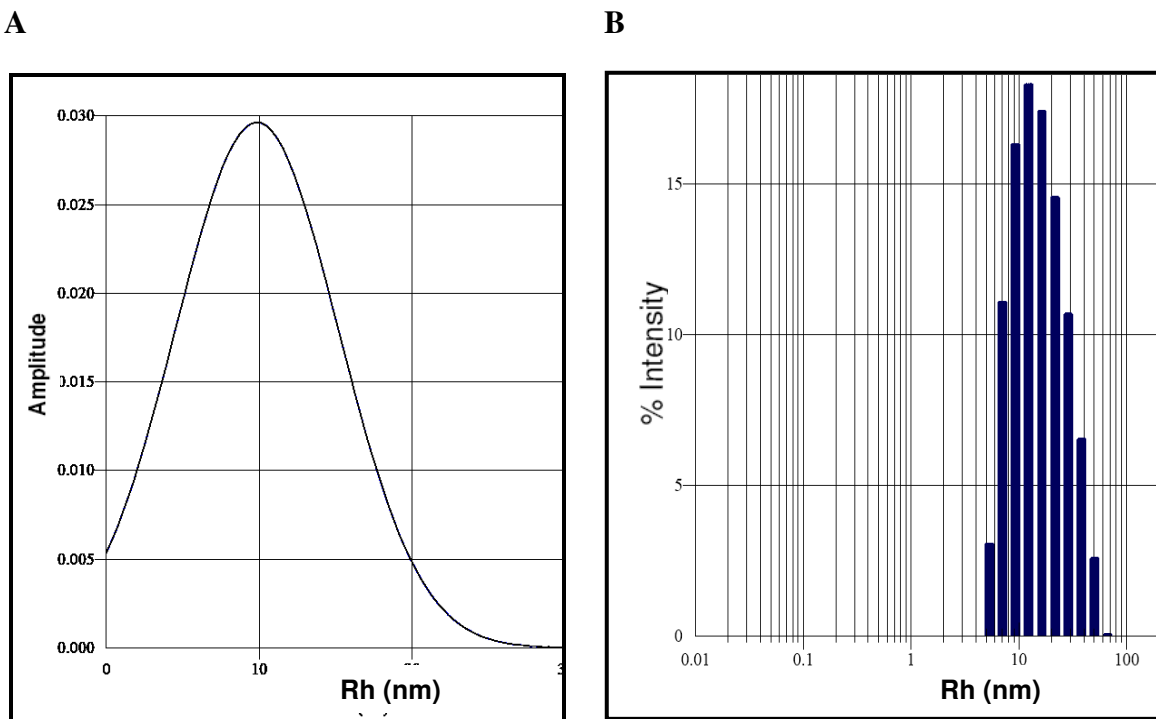


**Figure 13.** A typical DLS readout of a macromolecular solution of Fc400 dissolving in HBSS showing a mean hydrodynamic radius (Rh) of  $\sim 13.6 \text{ nm} \pm 0.3 \text{ nm}$ : (A) A single peak is detected suggesting the presence of a single population of macromolecular scatterers (B) A histogram demonstrates a uniform size-distribution of the Ficoll 400 macromolecule in solution.

### 8.3.3 Theory of Zeta Potential

Zeta potential refers to the electrostatic potential generated by the accumulation of ions at the surface of a particle or a macromolecule in an electrolytic solution which is organized into an electrical double-layer consisting of the Stern layer and the diffuse layer (see Fig. 14).

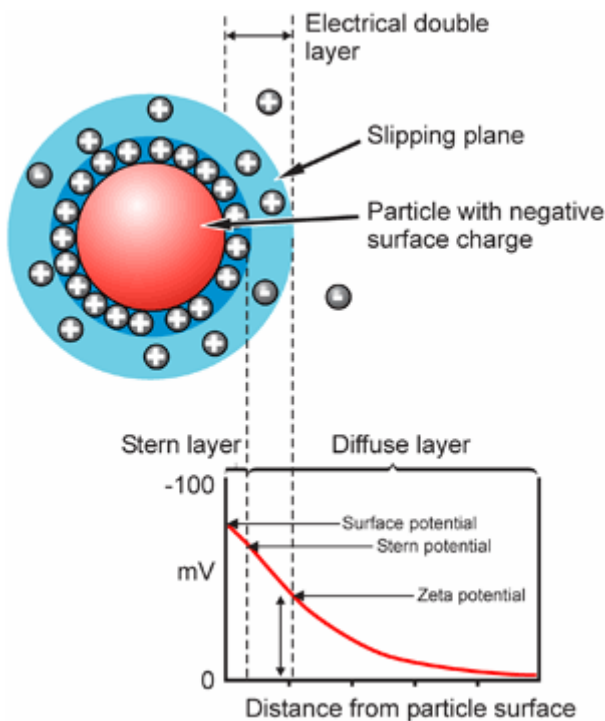


**Figure 14.** Electric potential profile as measured from the surface of a macromolecule in solution (Image courtesy: with permission from Malvern Instruments Ltd. [www.malvern.com](http://www.malvern.com) )

The zeta potential of a particle can be calculated if the electrophoretic mobility of the sample is known by Henry's Equation (under appropriate conditions; see Hiemenz and Rajagopalan, 1997):

$$U_E = \frac{2\varepsilon z f(ka)}{3\eta}$$

where  $U_e$  is the electrophoretic mobility,  $\varepsilon$  is the dielectric constant of the sample,  $Z$  is the zeta potential,  $f(ka)$  is Henry's Function (most often used are the Huckel and Smoluchowski approximations of 1 and 1.5, respectively) and  $\eta$  is the viscosity of the solvent.

### 8.3.4 Readout from a typical ZP run and Interpretation

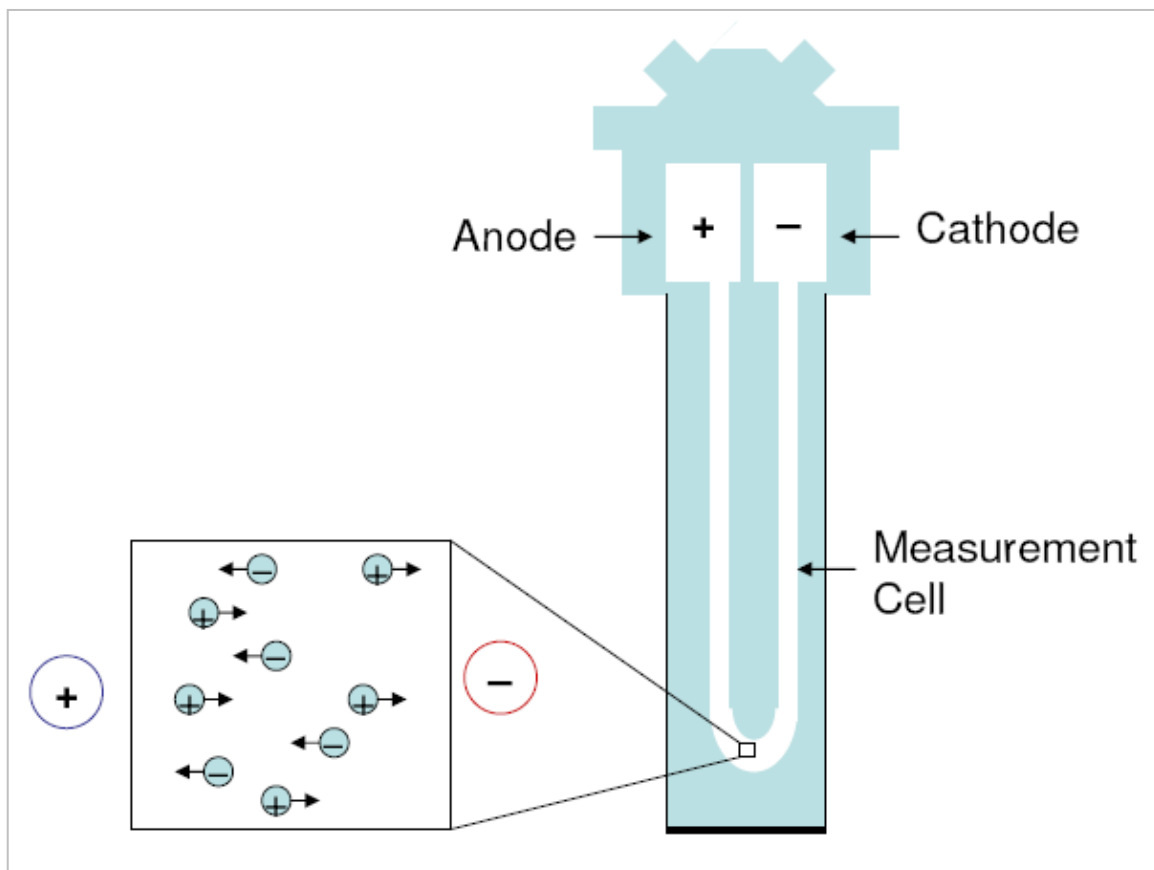


**Figure 15.** A schematic representation of the set-up for measurement of zeta potentials around macromolecular surfaces. The macromolecular solution is introduced into the capillary flow cell and when the electric field is applied, positive charges move towards cathode and negative towards anode slipping across each other where a potential can be detected and measured.



Zeta potential is measured by applying an electric field across the dispersion. Particles within the dispersion with a zeta potential will migrate toward the electrode of opposite charge with a velocity proportional to the magnitude of the zeta potential. Thus a negatively charged particle in a polyelectrolyte solution will have a sheath of oppositely charged particles and vice-versa (see Fig. 15). When an electric field is applied across the solution, the positively charged particles surrounding the negatively charged particle move towards the cathode and a negative potential is recorded which marks the negative zeta potential of the negatively charged particle. Thus the zeta potential is actually recorded some distance away from the surface of the particle. However this zeta potential strongly depends on the potential at the surface of the negatively charged particle, i.e. the surface potential which further depends on the surface charge and the way it is distributed over the surface of the particle. Hence we can conclude that the surface charge density critically determines the zeta potential and therefore zeta potential measurement can be used as an index to compare the surface charge distribution of anionic macromolecules of different types as shown in the next section.

## 8.3.5 Materials and Methods

### 8.3.5.1 Sample preparation

Solutions of macromolecules covering a series of concentrations were prepared in Hanks Balanced Salt Solution (HBSS) to mimic physiologic conditions of electrolyte concentration and pH.

**Table 2.** List of macromolecules tested for their biophysical profiles

<b>Macromolecule</b>	<b>Mol. weight (kDa)</b>	<b>Remarks</b>
Dextran Sulfate	500	Polyanionic
Polystyrene Sulfonate	200	Polyanionic
Ficoll PM70	70	Neutral
Ficoll PM400	400	Neutral
Dextran	410	Neutral
Dextran	670	Neutral

### 8.3.5.2 DLS Methods

Dynamic light scattering experiments were performed at an incident laser wavelength of 825.8 nm. Scattering from a 20  $\mu$ l sample of macromolecular solution (20 °C) was detected by a photomultiplier tube at 90° and processed by a Flex-99-adn digital correlator. From each run 20 readings were obtained and average values for the hydrodynamic radius determined.

### 8.3.5.3 Viscosity Measurements

Viscosities of macromolecular solutions at different concentrations were estimated using the *ARES100 FRT Rheometer*.

#### **8.3.5.4 Zeta Potential Measurements**

For zeta ( $\zeta$ )-potential measurements, anionic macromolecular solutions of Dextran Sulfate (pK chemicals; 500 kDa) and Polystyrene Sulfonate (Fluka; 200 kDa) were taken separately in sample volumes of 2 ml in glass cuvettes. Neutral macromolecules Ficoll (Amersham; Fc400; 400 kDa) and Dextran 670 (Sigma; 670 kDa) were employed as controls. Zeta potentials were measured using a ZetaPlus analyzer (Brookhaven Instruments Corporation, NY, USA) at 25 °C. Zeta-( $\zeta$ )-potential was expressed as the mean of 10 readings and tabulated with the standard error of mean.

## 8.4 Results

### 8.4.1 Charged Macromolecules have Significantly Larger Hydrodynamic Radii compared to Neutral Macromolecules of Similar Molecular Weights under Physiologic Conditions<sup>‡</sup>

Dextran sulfate (DxS, polyanionic; 500 kDa) was dissolved in Hanks Balanced Salt Solution (HBSS) at various concentrations from 100  $\mu\text{g/ml}$  to 10  $\text{mg/ml}$ . Diffusion coefficients and hydrodynamic radii ( $R_H$ ) were determined for each concentration point. The mean hydrodynamic radius for DxS is  $46.4 \text{ nm} \pm 0.39 \text{ nm}$  at a concentration of 100  $\mu\text{g/ml}$  in HBSS (Table 3; Harve *et al. Biophys. Rev. Lett.* 2006; see reference for full citation). When measured in water, the mean  $R_H$  for DxS500 was  $\sim 134 \text{ nm}$  at similar concentrations. The observed reduction of size in HBSS is probably due to the charge-screening effects of salts on DxS when dissolved in HBSS and is discussed later. Dextran 670 (neutral; 670 kDa) was dissolved in HBSS and DLS measured an  $R_H$  of  $21 \text{ nm} \pm 0.2 \text{ nm}$  at 100  $\mu\text{g/ml}$  (Fig.16).

**Table 3.** Charged macromolecules are larger than neutral macromolecules of similar molecular weight in physiological solutions at concentrations of 100  $\mu\text{g/ml}$ .

MACROMOLECULE	MW (kDa)	CHARGE	$R_H$ (nm)
Dextran sulfate	500	polyanionic	$46.4 \pm 0.3$
Polystyrene Sulfonate	200	polyanionic	$21.6 \pm 2$
Ficoll PM400	400	neutral	$13.6 \pm 0.3$
Dextran	670	neutral	$21 \pm 0.2$

<sup>‡</sup> Harve *et al. Biophysical Reviews Letters*. Vol. 1(3) 2006; see reference for full citation

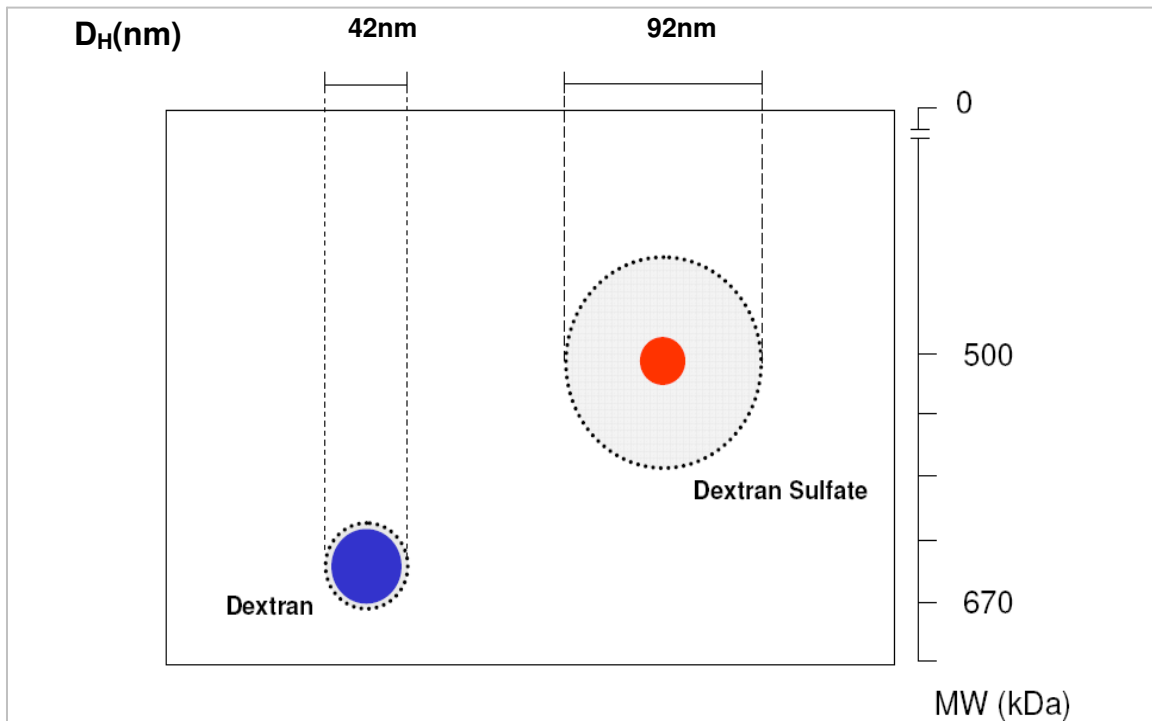


**Figure 16.** Charged Macromolecules have larger hydrodynamic size than neutral macromolecules of similar molecular weights. Dextran Sulfate has a net negative surface charge and is more than double than that of neutral Dextran of comparable molecular weight.

#### 8.4.2 A Concentration-dependent Decrease in Hydrodynamic Radii of Crowding Macromolecules in Physiologic Solutions: the Phenomenon of ‘Self-Crowding’

When increasing concentrations of the macromolecular solutions were subjected to DLS, at a particular concentration (e.g. 1 mg/ml for DxS), the  $R_H$  dramatically decreases and at 10 mg/ml, there is a 3-fold decrease in the  $R_H$  after correcting for viscosity. Similar observations were made for all the macromolecules tested irrespective of surface charge. But the magnitude of decrease in the  $R_H$  was maximum for the negatively charged DxS and minimum for the neutral Fc70 (Fig. 17). This is significant because with increasing concentration of molecules in solution, the diffusion would be expected to slow down with additional contributions from hydrodynamic interactions (HI; the role of HI is to

reduce the mobility of a molecule/particle) that also contribute to crowding-mediated slowing down of diffusion and an apparent *increase in*  $R_H$ . However, because of self-crowding, the crowder molecules themselves undergo compaction resulting in reduction of  $R_H$  and the increase in translational diffusion as observed here.

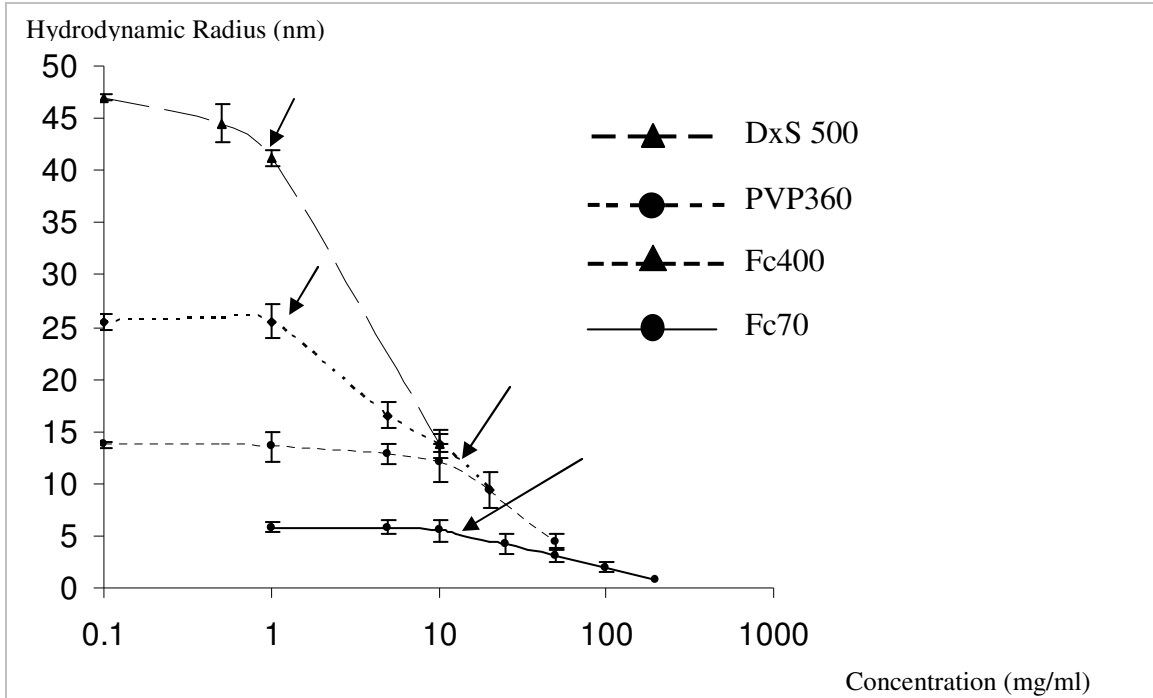


**Figure 17.** The ‘Self-Crowding’ phenomenon: A concentration-dependent decrease in hydrodynamic radii beyond a threshold concentration (see arrows) is observed for all the tested macromolecules. Each value is an average of 3 independent experiments at 20 readings/trial (Modified from Harve *et al.* Biophys. Rev. Lett. 2006; see reference for full citation). Error bars represent Standard Error of Mean (SEM).

#### 8.4.3 A Retrograde Approach from the “Self-Crowding point” could identify Onset-of Crowding Concentrations

From our previous results (Fig. 17), it could be inferred that actual Crowding onset might be occurring at much lower concentrations from the “Self-Crowding” point. To validate this hypothesis, another series of concentrations of Ficoll PM70 were made in HBSS in the range 1 mg/ml to 2.5 mg/ml (Fig. 18). Interestingly the hydrodynamic radius

shows a slight but significant increase while going from 1 to 1.5 mg/ml and stabilizes between 1.5 to 2 mg/ml. It then falls off at concentrations greater than 2 mg/ml.

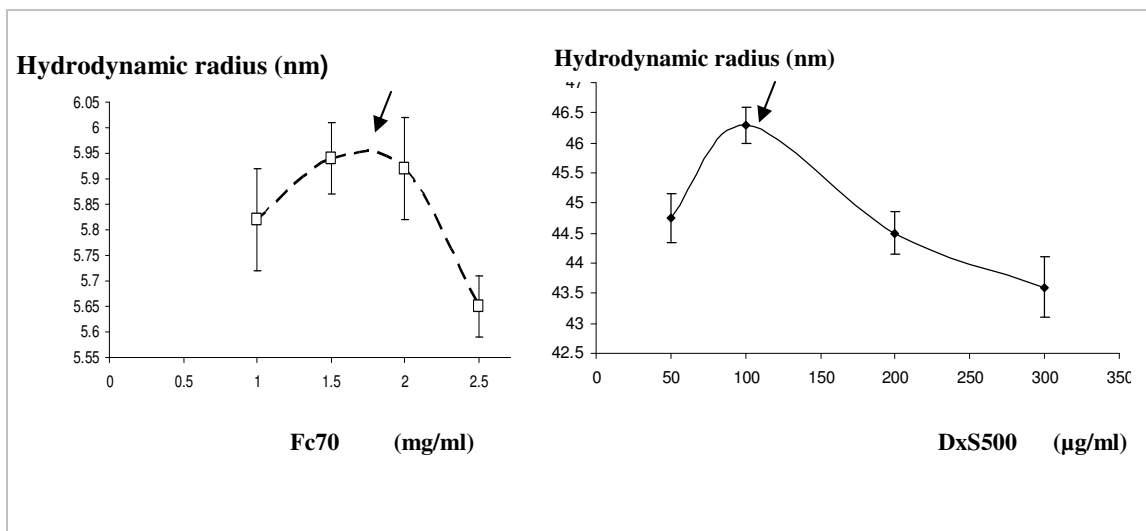


**Figure 18.** Points of maxima (arrow) can be observed due to an apparent increase in hydrodynamic radius resulting from slowing of diffusion in the concentration range 1 mg/ml to 2.5 mg/ml of Fc70 and 100 µg/ml to 200 µg/ml of DxS500 in HBSS (Harve *et al.* 2006). Error bars represent Standard Error of Mean (SEM).

#### 8.4.4 Mixed Macromolecular Crowding: PVP360 enhances Fc70 Multimerization

In order to determine whether Fc70 which is much smaller than PVP360 is affected in the presence of PVP in the same solution, a binary mixture of Fc70 (12.5 mg/ml) and PVP360 (100 µg/ml) was examined by DLS. The PVP concentration was deliberately kept below the detection threshold of the DLS instrument so that a potential multimerization of Fc70 could be detected without interfering noise from the second crowder. A pure solution of Fc70 showed a uniform size distribution with an average hydrodynamic radius of 5.2 nm (Fig. 19a). However, in the presence of PVP the Fc70 size distribution showed an additional distinct population with a mean radius of 9.4 nm suggesting multimerization of Fc70 (Fig. 19b).

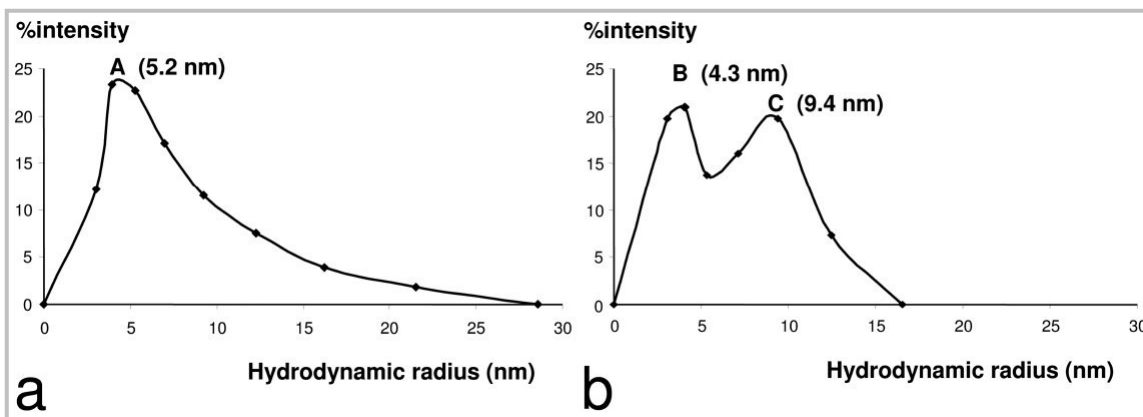


Figure 19. Mixed Macromolecular Crowding: PVP360 enhances multimerization Fc70 when present together in solution (see double-peak in panel ‘b’) compared to a single peak in panel ‘a’ which represents the size distribution of a physiological solution of Fc70 alone.

#### 8.4.5 Surface Charge Characterization of Macromolecules by Zeta Potential Measurement

As can be appreciated from the table below, neutral macromolecules showed a zero zeta potential confirming that they had zero net charge on their surface. In comparison, anionic macromolecules DxS500 and PSS demonstrated a mean negative zeta potential of -11 mV and -79 mV respectively.

**Table 4.** Mean Zeta potentials of macromolecules: neutral macromolecules have net zero zeta potential and anionic macromolecules have a net negative zeta potential

Macromolecule	Zeta-potential (mV) (10 mg/ml)
Fc400	0.0
Dextran 670	0.0
DxS	-11 ± 3
PSS	-79 ± 10

When a series of concentrations of these macromolecules was tested, DxS500 showed consistently lower values than PSS (see Fig. 20). At 1 mg/ml, the detection threshold of



the instrument (which is concentration dependent) was higher than the zeta-potential of DxS500 and hence no signal was detectable. However, a value of  $-73.89$  mV was recorded for PSS. At higher concentrations, PSS showed a significant increase in ZP over and above DxS500.

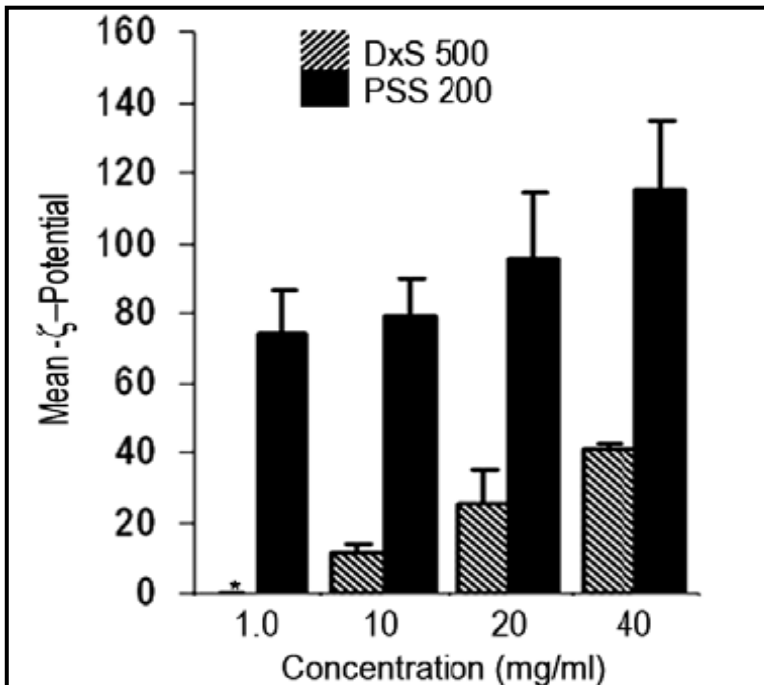


**Figure 20.** Mean negative zeta potentials of anionic macromolecules DxS and PSS at concentrations from 1 to 40 mg/ml. Note the consistent increase in the ZP of PSS compared to DxS. At 1 mg/ml, the ZP of DxS was below the detectable threshold. All values are Mean  $\pm$  SEM (Lareu *et al.* *FEBS Lett.* 2007).

## 8.5 Discussion

The hydrodynamic radius of a macromolecule in solution is an important parameter that determines how much of volume is occupied by the macromolecule, thus contributing to the total volume of exclusion. The term ‘hydrodynamic’ accounts for not only the actual size of the molecule, but also the hydration shell surrounding it. Surface charge on a macromolecule also contributes for the hydrophilicity of the macromolecule in addition to the electrostatic effects on like-charged molecules in solution. The hydrodynamic radius of the polyanionic DxS500 was  $\sim 3$  fold lower than the  $R_H$  of DxS

dissolved in water (~ 134 nm at 100 µg/ml). This can be explained as due to the charge screening effects of ionic solutions favoring internal folding of the coils of anionic DxS molecule. Similar observations have been made earlier when the hydrodynamic size of Hyaluronic Acid was measured when it was dissolved in water and in salt solutions (Gibbon *et al.*1999). However, comparing DxS500 and Dextran 670 with MW close to each other (500 & 670 kDa respectively), it is appreciated that charge screening effects of HBSS on DxS notwithstanding, there is still more than a 2-fold difference in  $R_H$  of DxS compared to Dextran 670. This implies that for the same volume occupancy, far less DxS molecules than would be needed than Dextran 670 and hence a lower concentration of the charged macromolecule compared to a neutral molecule for similar Crowding effects. This would mean that, a charged macromolecule such as DxS could still be a better crowder compared to a neutral polymer of similar size under physiologic conditions for similar concentrations. This might be advantageous because at high concentrations macromolecular solutions tend to be more viscous, which is undesirable for biological reaction kinetics.

An interesting observation was made when a concentration series of the macromolecules in HBSS was subjected to DLS<sup>§</sup>. With increasing concentrations of the Crowding agent, at a particular concentration (e.g. 1 mg/ml for DxS), the  $R_H$  dramatically starts to decrease. This observation is attributed to the phenomenon of “Self-Crowding”. That is, as the concentration of the macromolecules increases, above a certain concentration, the steric interaction between molecules triggers an intra-chain-folding-transition within the macromolecules leads to a compaction of the macromolecules. Such observations have been made in earlier studies (Tokuriki *et al.* 2004; Wenner &

---

<sup>§</sup> Harve *et al.* *Biophysical. Reviews and Letters*. Vol.1(3) 2006; see reference for full citation

Bloomfield, 1999). This indicates that concentrations equal to or greater than this value would offset Crowding effects and so do not create ideal Crowding conditions for a 'test' molecule that is to be crowded. A retrograde approach from this point to identify an optimum Crowding concentration, as determined by the hydrodynamic size and the number density (to estimate fraction volume occupancy) of the macromolecules, is therefore required. But it has to be noted here that these observations pertain to a single macromolecular species system, a physiologic solution of the crowder in HBSS. It has to be seen whether a system of 2 or more different species of macromolecules mixed in solution also demonstrates a similar behavior.

The hydrodynamic radius shows a slight but significant increase while going from 1 to 1.5 mg/ml and stabilizes between 1.5 to 2 mg/ml. It then falls off at concentrations greater than 2 mg/ml. This seems to suggest the existence of a maximum in the concentration interval 1.5 mg/ml - 2 mg/ml and is perhaps due to decrease in diffusion of the molecules whose mutual interactions with other molecules become significant around this concentration (~ 1.5 mg/ml). This hints at possible onset of Crowding at this point. A corollary to be inferred from this observation is that at this concentration window, we found that viscosity was unchanged and was ~ 1 centiPoise, which is very close to that of water. Therefore at this point, the slowing of diffusion that was observed could be attributed solely to EVE with no contribution from any viscosity changes. An earlier study on molecular Crowding in intracellular compartments showed that diffusion depends on Crowding independently of viscosity (García-Pérez *et al.* 1999). Therefore, by studying diffusion behavior of solutions at concentrations which have viscosities close to water would help us in determining the contribution of

Crowding alone in decreasing the diffusion of the macromolecules. Hence the concentration at the maximum point could well mark the optimum Crowding concentration for Fc70. But this needs to be further validated by applying the putative concentrations on biological reactions. Whether this behavior holds true for other macromolecules also would also need to be investigated.

Macromolecular Crowding contributes to EVE, by way of the mutual impenetrability of all solute molecules. This non-specific steric repulsion is always present, regardless of any other attractive or repulsive interactions that might be occurring between the solute molecules. The steric exclusion is valid for species with large hydrodynamic radii such as proteins, nucleic acids and glycosaminoglycans (GAGs). However, this effect of Crowding may be amplified greatly if the interacting macromolecules have surface-charge, the resulting electrostatic exclusion magnifies the already present steric effects and enhances EVE by several folds of magnitude (Gyenge *et al.* 2003). Together, the macromolecular surface area and shape determine how this surface charge is distributed around it, i.e the surface charge density. Our calculations show that the surface charge density for DxS500 =  $-0.0159 \text{ C/m}^2$  and that for PSS200 =  $-0.04 \text{ C/m}^2$ . Therefore PSS has a ~3-fold higher surface charge density than DxS. These calculations are based on the degree of sulfation of the two macromolecules. From this data, the number of fixed negative charges in each monomer of the macromolecules was determined and then multiplied by the number of monomers for each macromolecule based on the number average molecular weights. This increase in surface charge density for PSS therefore results in much higher surface potentials and hence correlates with the experimentally obtained higher zeta potential values. A point to be discussed here is how

relevant the zeta potential measurement can be. This potential is actually measured at a certain distance away from the surface of the macromolecule. However, the advantages of measuring this potential are that: (1) It sensitively depends on the potential that is present at the surface of the macromolecule. Since it is difficult to measure the surface potential, an indirect measure albeit at a distance from the surface can be a valuable indicator of the surface potential, (2) While comparing two anionic macromolecules, measuring the zeta potential of the macromolecules dissolved in solution is a rapid screening method in combination with Dynamic Light Scattering, of determining the ideal charged macromolecule for crowding (see Fig. 21). Therefore measuring the zeta-potential is a very reliable and useful means to screen anionic macromolecules for their electrostatic exclusion magnitude and correlating with their effects on biological models such as fibroblast cultures as described later in the thesis.

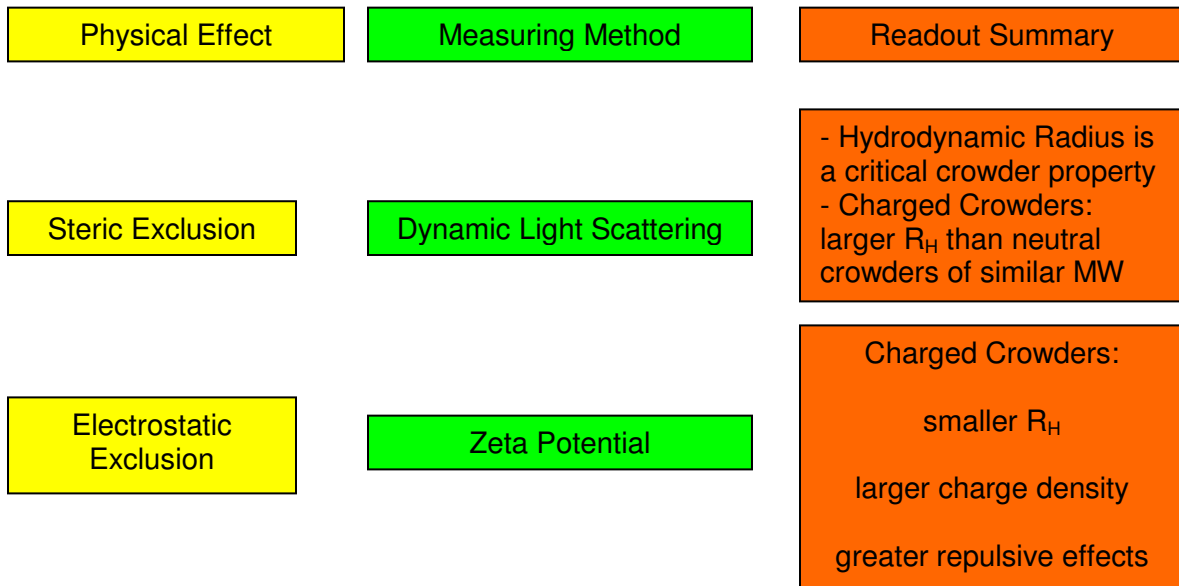


**Figure 21.** The contribution of electrostatic exclusion of anionic macromolecules to their steric effects: By a combined DLS and Zeta Potential measurement enable selecting the ideal crowding agent.

## 9. Macromolecular Crowding of Molecular Biology Reactions

### 9.1.1. Biomolecular Reactions and the Need for Crowding

Biochemical reactions in cells function in a carefully controlled intracellular environment which biologists have, to a limited extent, reproduced *in vitro* by controlling factors such as pH, ionic strength, temperature, and supply of cofactors which constitute the buffer system. In fact, all DNA modifying enzymes that are commonly used today (e.g. polymerases, nucleases, ligases) have evolved to function efficiently within the crowded interior of cells. Biological Crowding occurs in the range of 5-40% w/v solute content which translates to even higher excluded volume (Ellis, 2001). It has been postulated that Macromolecular Crowding is a key factor responsible for the phenomenally high rates of reactions and molecular interactions *in vivo* while seemingly relatively low amounts of reactants are present, at least when compared to their *in vitro* use. Our general aim is to more closely emulate the intracellular biophysical environment of the bacterium in the *in vitro* setting and thus enhance molecular biology reactions exemplified by reverse transcription (RT) and polymerase chain reaction (PCR).

### 9.1.2. RT-PCR as a Model for Testing Crowding Effects

The protein synthesis cycle is broken down into two components, transcription and translation of specific parts of DNA to form proteins. Normal transcription involves RNA synthesis from DNA and the processing of the RNA, before translation occurs, which translates the nucleotide sequence of RNA into encoded proteins using the genetic code. Reverse transcription is a molecular biological process of making a double stranded DNA molecule from a single stranded RNA template. Key component that is required is reverse transcriptase, also known as RNA-dependent DNA polymerase, a DNA polymerase enzyme that transcribes single stranded RNA into single stranded DNA (cDNA; see Fig. 22).

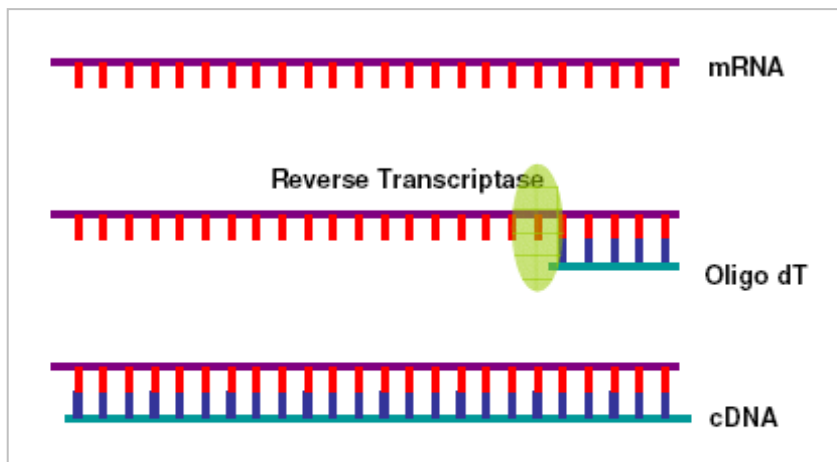


**Figure 22.** A schematic illustration of how an RNA-dependent DNA polymerase (reverse transcriptase) is able to use RNA as a template and add nucleotides to a short oligo-dT primer and thus synthesize a complementary DNA (cDNA) as the product in the presence of  $MgCl_2$  as cofactor.

All *in vivo* systems function in highly crowded environments. This is particularly true for DNA replication occurring in the crowded *in vivo* conditions. However, *in vitro* DNA synthesis with or without amplification cycles such as the PCR, catalyzed by the respective enzymes, are routinely done in aqueous media that lack Crowding with a fraction volume occupancy of the PCR of  $<0.01\%$ . As there is a huge amount of uncrowded space in the reaction volume, the RT-PCR reaction can be targeted to test the

effects of Crowding. PCR lends itself as a model to test Crowding because it consists of four constituents within the reaction, namely, the DNA (template), DNA (primer), the enzyme and the dNTPs dispersed in water. Thus the RT-PCR represents a simple and well-defined system with an effective and reliable readout, namely the creation of amplicons over time, helps to determine the effects of Crowding by applying the biophysically derived data to quantitate the volume exclusion effects of Macromolecular Crowding.



### 9.1.3. Rationale of Crowding the RT-PCR

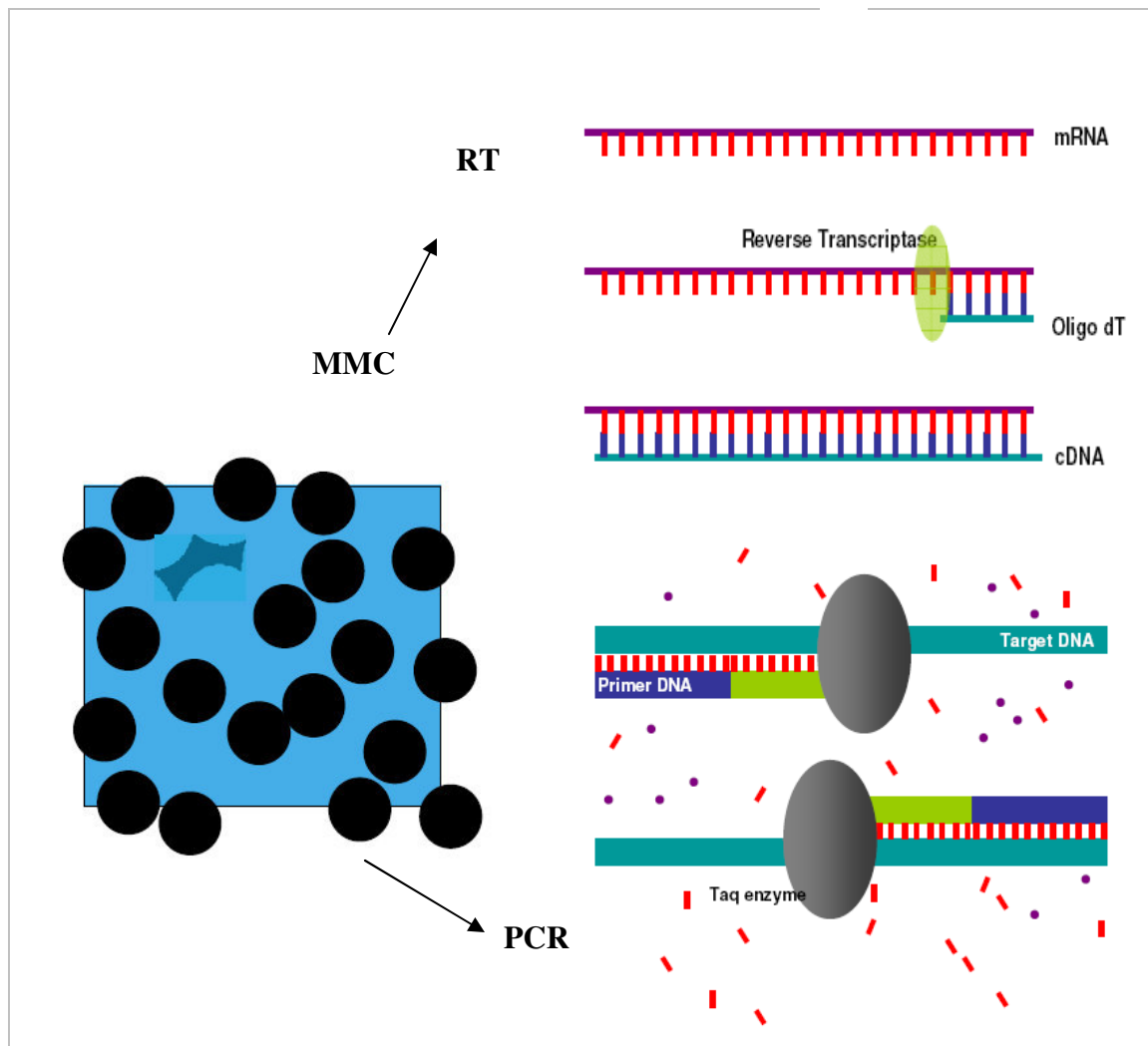


**Figure 23.** Crowding (MMC) the target molecular biology reactions, the reverse transcription (RT) and the Polymerase Chain Reaction (PCR) by macromolecules.

As can be appreciated from the above schematic, our target reactions are the reverse transcriptase catalyzed cDNA synthesis and the *Taq* polymerase catalyzed DNA amplification. In order to further clarify the readout methods for faster output, a real-time monitoring of the DNA amplification was employed in the current study. For this purpose SYBR Green I that binds selectively to double stranded DNA was employed as explained later. In order to crowd the reaction, macromolecules were added to the mix. Certain

criteria had to be considered for the crowders. Preliminary studies showed that negatively charged macromolecules such as D<sub>x</sub>S are not useful to crowd RT-PCR because of their ability (anionicity) to chelate Mg<sup>2+</sup> which is an important co-factor for DNA polymerase activity. Therefore neutral macromolecules were used as the Crowding macromolecules. Among the neutral crowders, globular macromolecules like Ficoll were preferred since their globular nature does not increase the viscosity of the reaction mix significantly above than that of water in these water-based systems.

#### **9.1.4 Aims**

1. To demonstrate effects of Crowding on the yield of first strand cDNA synthesis.
2. To demonstrate the effects of Crowding on the PCR read-out parameters.
3. To demonstrate the effects of Crowding on the processivity of DNA polymerases.
4. To determine the effects of Crowding on thermal stability of *Taq* DNA polymerase.

#### **9.1.5 Study Hypotheses**

1. Macromolecular Crowding enhances the activity and processivity of reverse transcriptase enzyme leading to yield of longer and greater amounts of cDNA.
2. Macromolecular Crowding enhances the activity, processivity and yield of *Taq* polymerase.
3. By improved structural and functional properties of reverse transcriptase and *Taq* polymerase, the RT-PCR sensitivity, specificity, yield and efficiency can be improved.

## **9.2 Materials and Methods**

### **9.2.1. General Materials.**

All reactions were performed on the real-time Mx3000P (Stratagene, CA, USA). Macromolecules: Ficoll (Fc) 70 kDa (Fc70) and Fc400 kDa (Fc400) (Amersham Pharmacia, Uppsala, Sweden); trehalose (Fluka-Sigma-Aldrich, Singapore); proline (Sigma-Aldrich) and polyethylene glycol (PEG; Sigma) 4 kDa. Additives were dissolved in nuclease-free water as a concentrate and added freshly to the reaction buffers each time.

### **9.2.2. Thermostability Screening of Macromolecules.**

To screen macromolecules for thermostability, solutions of macromolecules were made in Hanks buffered salt solution at different concentrations (Fc70: 5 mg/ml to 25 mg/ml; Fc400: 5 mg/ml to 50 mg/ml; ND410 & ND670: 100 µg/ml to 10 mg/ml; PVP360: 100 µg/ml to 10 mg/ml) and 20 µl of each sample was subjected to 35 thermal cycles sequentially at 56 °C-72 °C-94 °C. DLS runs before and after thermal cycling were done and data analysed in the Dynapro software.

### **9.2.3. RNA Extraction**

RNA was extracted from human WI-38 fibroblasts (American Tissue Culture Collection, VA, USA) from which complementary DNA (cDNA) was prepared for all PCR assays except for aP2 (fatty acid binding protein 2) which used RNA from adipocytes differentiated from human mesenchymal stem cells. Extractions were performed with RNeasy (Qiagen, Crawley, UK) according to the Manufacturer's protocol.

#### **9.2.4. Reverse Transcription Reaction**

Complementary DNA synthesis was carried out according to the Manufacturer's protocol for SuperScript II reverse transcriptase with oligo(dT) primers with the following modifications when macromolecules were used. Fc70 (7.5 mg/ml) was added to the annealing buffer and mixture of Fc70/400 (7.5 and 2.5 mg/ml) was added to the polymerization step.

#### **9.2.5. Polymerase Chain Reaction**

Two microliters of cDNA was used as target for all PCRs in a final volume of 20  $\mu$ l and all samples were run in duplicates. Negative Controls were run ('No Template Control') in which no target DNA was added. This was to rule out non-specific amplification of genomic DNA that could have contaminated the reaction mix. Another set of negative controls were included with only the crowders and SYBR Green to rule out any enhancement or quenching of SYBR Green Fluorescence due to the crowder macromolecules. Reactions were run as follows unless otherwise stated: 1 U Platinum Taq DNA polymerase in 1X reaction buffer, 300 nM primers and 2.5 mM MgCl<sub>2</sub>. The thermal cycling program for all PCRs was the following, unless otherwise stated: 94 °C/5 min, 94 °C/30 s, 56 °C/30 s, 72 °C/30 s, for (collagen I set 1, 30; GAPDH, 35;  $\alpha$ P2 and M13, 40; collagen I set 2, 42) cycles with a final dissociation step of 60-94 ° C at 1.1° C/s. Fluorescence was detected with SYBR Green I (Molecular Probes-Invitrogen). Optimization of the concentration of Mg<sup>2+</sup> was done by running PCR of each target sequence at a concentration series of MgCl<sub>2</sub> from 1mM to 10mM. The MgCl<sub>2</sub> concentration that gave the lowest C<sub>T</sub> and the sharpest melt peak was chosen as the ideal MgCl<sub>2</sub> concentration for the subsequent 'test' PCR. Similar optimization runs were done to identify the optimum annealing temperature for a given target sequence.

The dissociation run was done to determine the melting temperature of the double-stranded PCR product. At the melting point of duplex-DNA (50% breaking into single strands, the  $T_m$ ) there is a sudden drop in the SYBR Green I fluorescence. The real-time software then computes a negative derivative of the fluorescence at this point which is seen as a melt peak. The annealing temperature for collagen I set 1 and set 2 was 55 °C. The Primer sequences were as follows:

GAPDH: GTCCACTGGCGTCTTCACCA, GTGGCAGTGATGGCATGGAC;

Collagen I set 1: AGCCAGCAGATCGAGAACAT, TCTTGTCCTTGGGGTTCTTG;

aP2: TACTGGGCCAGGAATTTGAC,GTGGAAGTGACGAATTTTCAT;

M13: TTGCTTCCGGTCTGGTTC, CACCCTCAGAGCCACCAC;

Collagen I set 2: GTGCTAAAGGTGCCAATGGT, CTCCTCGCTTTCCTTCTCT.

### **9.2.6. Processivity Experiments**

The single-stranded M13 (ssM13) processivity assay for Taq DNA polymerase was modified from Bambara *et al.* Briefly, 100 nM of primer (GTAAAACGACGGCCAGT) was added to 100 nM ssM13mp18 DNA (New England Biolabs Inc., MA, USA) in buffer with 1 U Taq DNA polymerase in the absence or presence of Fc400 (2.5 mg/ml). The samples were heated to 94 °C/5 min, cooled to 55 °C/1 min followed by 72 °C for 1 and 3 min, respectively. For the reverse transcriptase processivity assay, a standard RT was performed without and with the macromolecules Fc70/Fc400 mixture, as above. Reaction products were separated on a denaturing 0.6 % agarose gel.

### **9.2.7. Agarose Gel Electrophoresis**

Reaction products were either resolved in 1X TAE agarose (Seakem, ME, USA) gels or in

formamide-denaturing agarose gels at the stipulated concentrations of 0.6% or 2.0%. The molecular weight markers were 1 kb (Promega Corporation, WI, USA), 50 and 100 bp (Invitrogen) DNA ladders. Post-staining was done with SYBR Gold (Molecular Probes-Invitrogen), images were captured with a Versadoc<sup>TM</sup> (Bio-Rad), and analysed using Quantity One v4.5.2 (Bio-Rad). Calculation of the area-under-the-curve and late phase PCR efficiency: The method of Rasmussen *et al.* using the NCSS software helps calculate the area-under-the-curve from the PCR dissociation curves raw data values derived from the Stratagene software MxPro v3.20. The late-phase efficiency of PCR amplification was calculated according to the method of Liu and Saint. Agarose Gel Electrophoresis enables separation of DNA/RNA of different lengths. DNA or RNA dissolved in a loading dye (containing a tracker-bromophenol dye) is loaded onto an Agarose gel submerged in a running buffer (1X Tris-Acetate-EDTA; TAE) and a horizontal electric field is set up. The negatively charged DNA then starts migrating towards the anode of the electric field, the distance traveled could be tracked by the colored tracker dye. After the dye has reached three-fourths of the distance of the gel, the electric field is switched off and the gel taken out for staining in 1X TAE buffer containing SYBR Gold that by percolating into the gel, stains the DNA. The fluorescence emitted is then detected by a dark reader and the images of the bands are captured in a versadoc scanner. The DNA migration distance is proportionate to their molecular weights. Therefore, by running a molecular weight standard alongside the DNA samples, the actual size of the separated DNA can be determined. Staining the separated DNA bands by SYBR Gold is both specific and quantitative. The fluorescent dye binds efficiently to the nucleic acids and the fluorescence emitted is directly proportional to the amount of DNA that is present.

### 9.3. Results

#### 9.3.1 Sensitivity

Total RNA (1000 and 50 ng) was reverse transcribed in the presence and absence of a macromolecule mixture (Fc70 and Fc400) followed by amplification with collagen I PCR assay in the presence and absence of a single macromolecule (Fc400), respectively. Crowding resulted in a reduction of greater-than 3 Ct (threshold cycle) (green) compared to standard (i.e. uncrowded) RT-PCR samples (orange) (Fig. 24). This translates to enhanced sensitivity of >10-fold. The dissociation curves (Fig. 25A) in conjunction with the agarose gel electrophoresis (Fig. 25B) confirm amplification of the specific target.

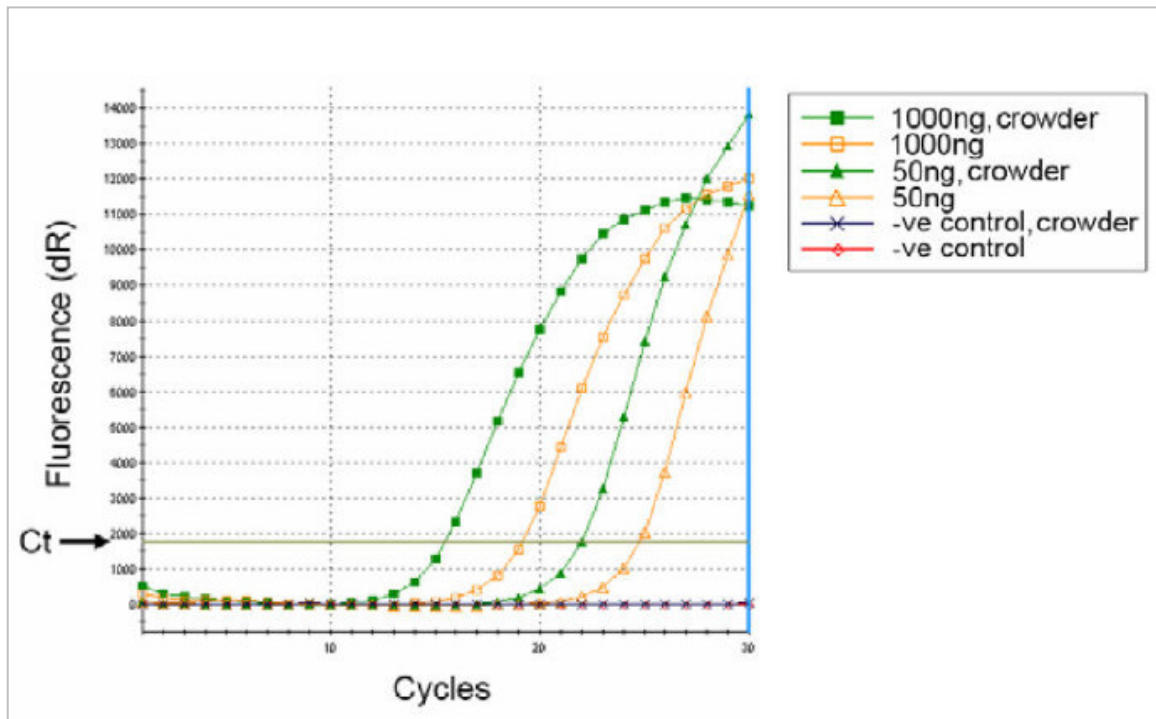


**Figure 24.** Macromolecular Crowding enhances the sensitivity of RT and PCR assays. Amplification plots of the collagen I set 1 PCR in the presence (green) and absence (orange) of Fc400 from cDNA prepared in the presence and absence of mixed crowders (Fc70 7.5 and Fc400 2.5 mg/ml), respectively. The amount of total RNA used for the RT was 1000 and 50 ng. (Lareu, Harve, Raghunath. 2007).

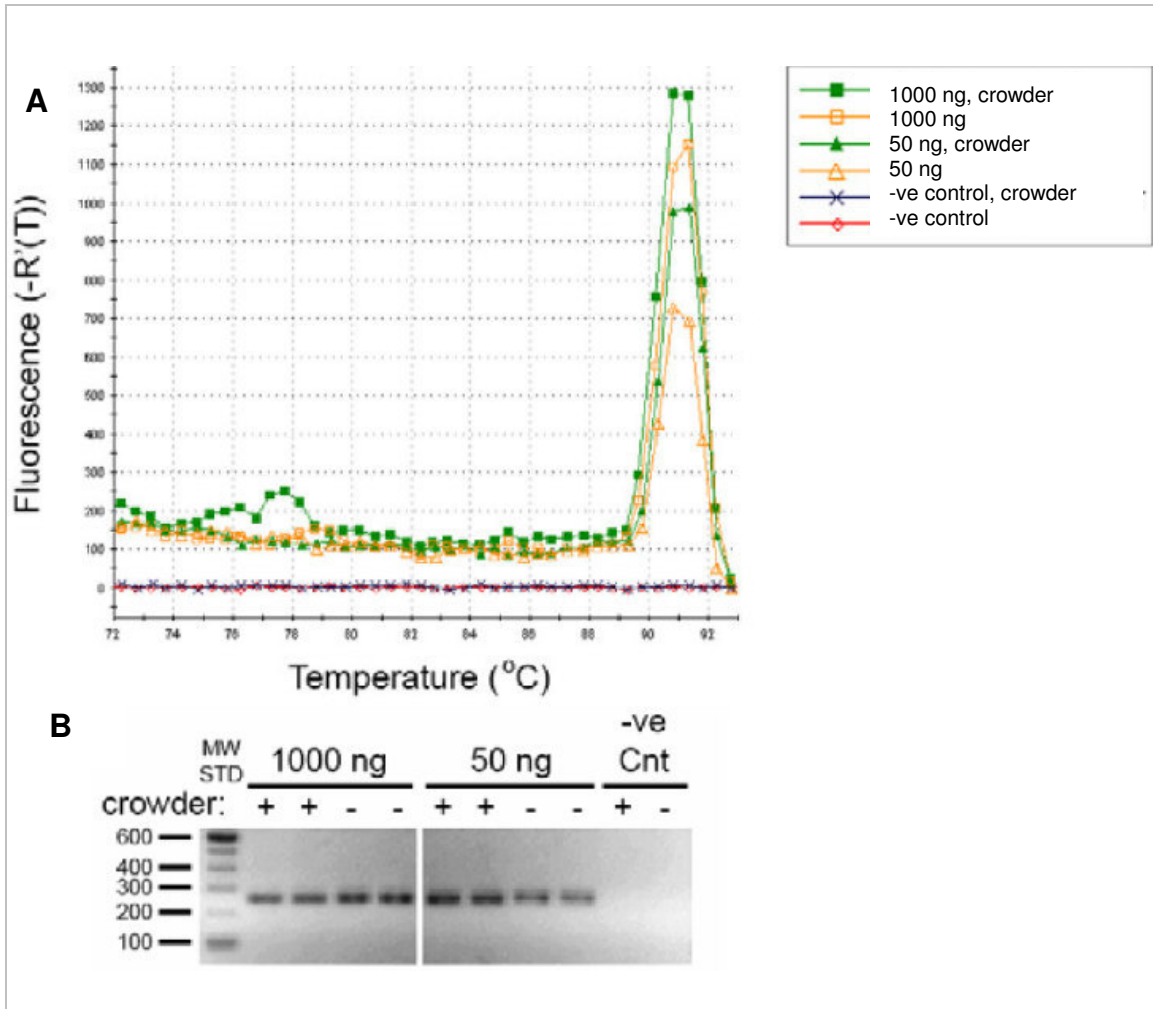


**Figure 25.** (A) Dissociation Curves of the collagen I set 1 PCR in the presence (green) and absence (orange) of Fc400 from cDNA prepared in the presence and absence of mixed crowders (Fc70 7.5 and Fc400 2.5 mg/ml), respectively. (B) An agarose gel (2%) readout of the PCR products demonstrating a specific 250 bp collagen I amplicon. (Lareu, Harve, Raghunath. 2007).



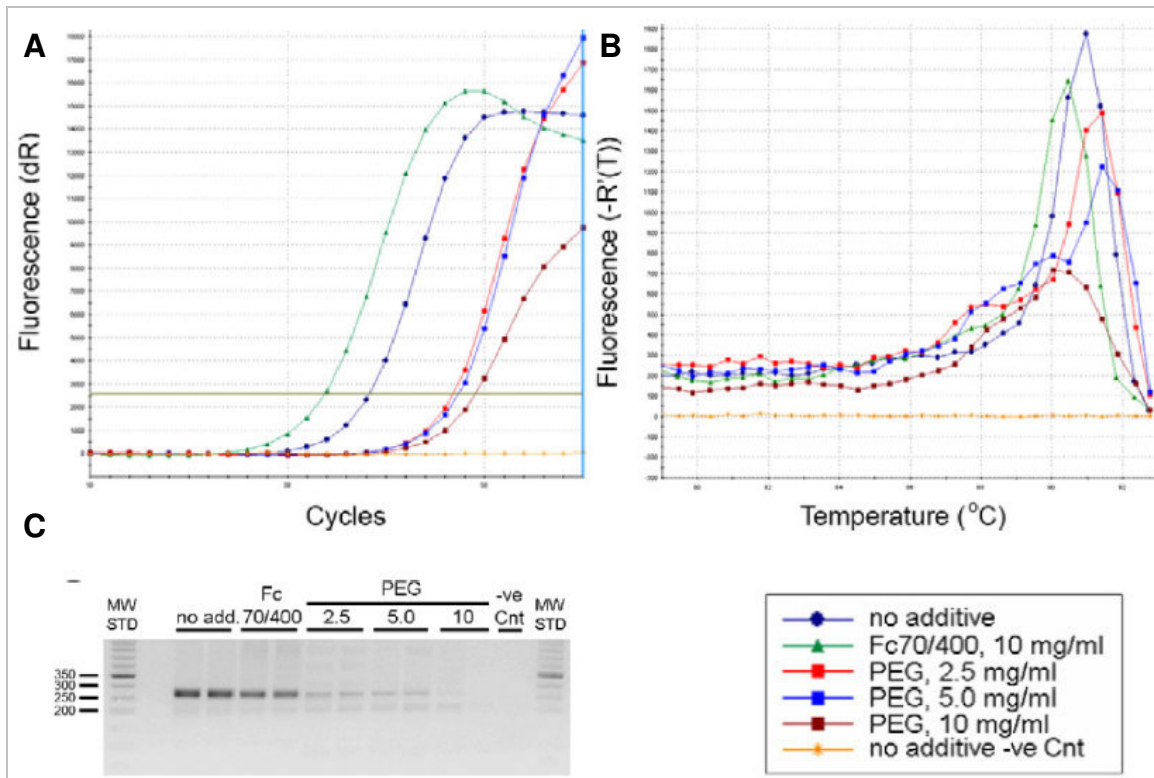


**Figure 26.** (A) Amplification plots and (B) dissociation curves of the GAPDH PCR showing the relative performance of macromolecular mixture Fc70/Fc400 (7.5/2.5 mg/ml), PEG 4 kDa at either 2.5, 5 or 10 mg/ml, and standard conditions (without additives). (C) Agarose gel (2%) demonstrating a specific 261 bp GAPDH amplicon. (Lareu, Harve, Raghunath.2007).

Dissociation run helps in identifying whether a specific product has been amplified by the PCR. The dissociation run is carried out after all the amplification cycles have been completed. Thus at the end of all amplification cycles, the reaction mix is densely populated with double-stranded DNA which are the amplified PCR products. However, when the temperature of the mix is raised from 60 to 95 °C, the double strands break up into single-strands and at a certain temperature, half the population is single-stranded. This point is the  $T_M$  of the target product and is specific for a given DNA sequence. However, the dissociation profile has to be corroborated with an Agarose gel electrophoresis to confirm the length and specificity of amplification of the PCR product.

Complementary DNA was prepared from 500 ng of total RNA under standard condition (i.e. non-crowded) and subjected to amplification with GAPDH PCR (Fig. 26 A and B) in the absence or presence of macromolecule mixture Fc70/400 (7.5/2.5 mg/ml) or PEG 4 kDa at 2.5, 5 or 10 mg/ml concentrations. Unlike the macromolecules which enhanced an already optimized PCR by 2 Ct (i.e. 4-fold increase), PEG inhibited sensitivity by greater-than 4 Ct (i.e. 16-fold decrease) which was dose dependent (Fig. 26A). In addition, the presence of PEG caused the amplification of a smaller, non-specific product, apparent by a shoulder on the left of the dissociation curves (Fig. 26B) and 200 bp band on the agarose gel (Fig. 26C).

### **9.3.2 Specificity**

It was found that amplification of a particular collagen I template target region through standard RT-PCR was difficult due to its long distance from the oligo(dT) priming site (4390 bp; NM\_000088). However, in the presence of a mixture of Fc70 and Fc400 the specific product was obtained with the lower range of primer concentrations (100-300 nM) (Fig. 27). Although higher primer concentrations resulted in high background the specific product was still present and dominated the amplicons that were generated in the presence of macromolecules. In contrast, non-crowded reactions yielded only non-specific products.

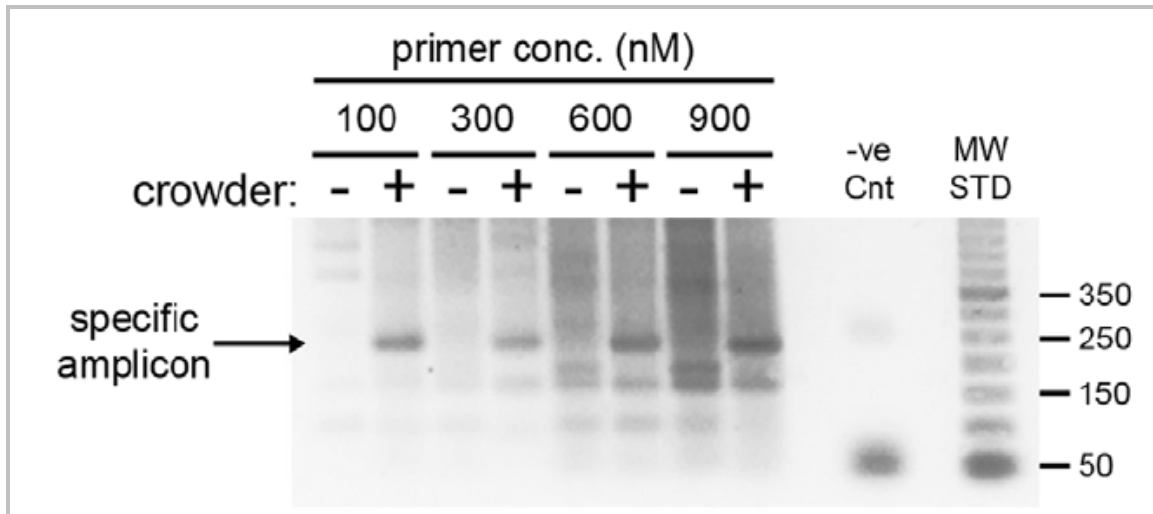


**Figure 27.** Macromolecular Crowding increased primer binding specificity. Agarose gel of RT-PCR samples amplified with the collagen I set 2 PCR in the absence or presence of the macromolecule mixture Fc70/Fc400 (15/5 mg/ml) with increasing concentrations (conc.) of primers. The specific target is indicated at 228 bp. The cDNA was prepared from 250 ng total RNA. The -ve Cnt (control) was the PCR template-free control. (Lareu, Harve, Raghunath. *BBRC* 2007)

### 9.3.3. Processivity of *Taq* Polymerase and Reverse Transcriptase

In order to assess the ability of macromolecules to enhance processivity of *Taq* DNA polymerase, we performed a classical ssM13 assay in the absence and presence of macromolecules. The presence of Fc400 resulted in longer DNA fragment lengths after 1 and 3 min of extension time (Fig. 28A) and an average increase in DNA product of 15% (Fig. 28B). Figs. 28A and B are based on the intensities and relative migration profiles of the bands from the denaturing agarose gel (Fig. 28C). The enhanced processivity induced by Crowding was tested with a long PCR assay with limited extension time of 40 s. The addition of macromolecule mixture Fc70/Fc400 enabled the amplification of the correct amplicon (1547 bp) under these limiting experimental conditions (Fig. 28D). In contrast, the reaction carried out in the absence of Crowding did not amplify the correct and long amplicon. Total RNA was used to test the effect of crowders on the processivity of reverse transcriptase.

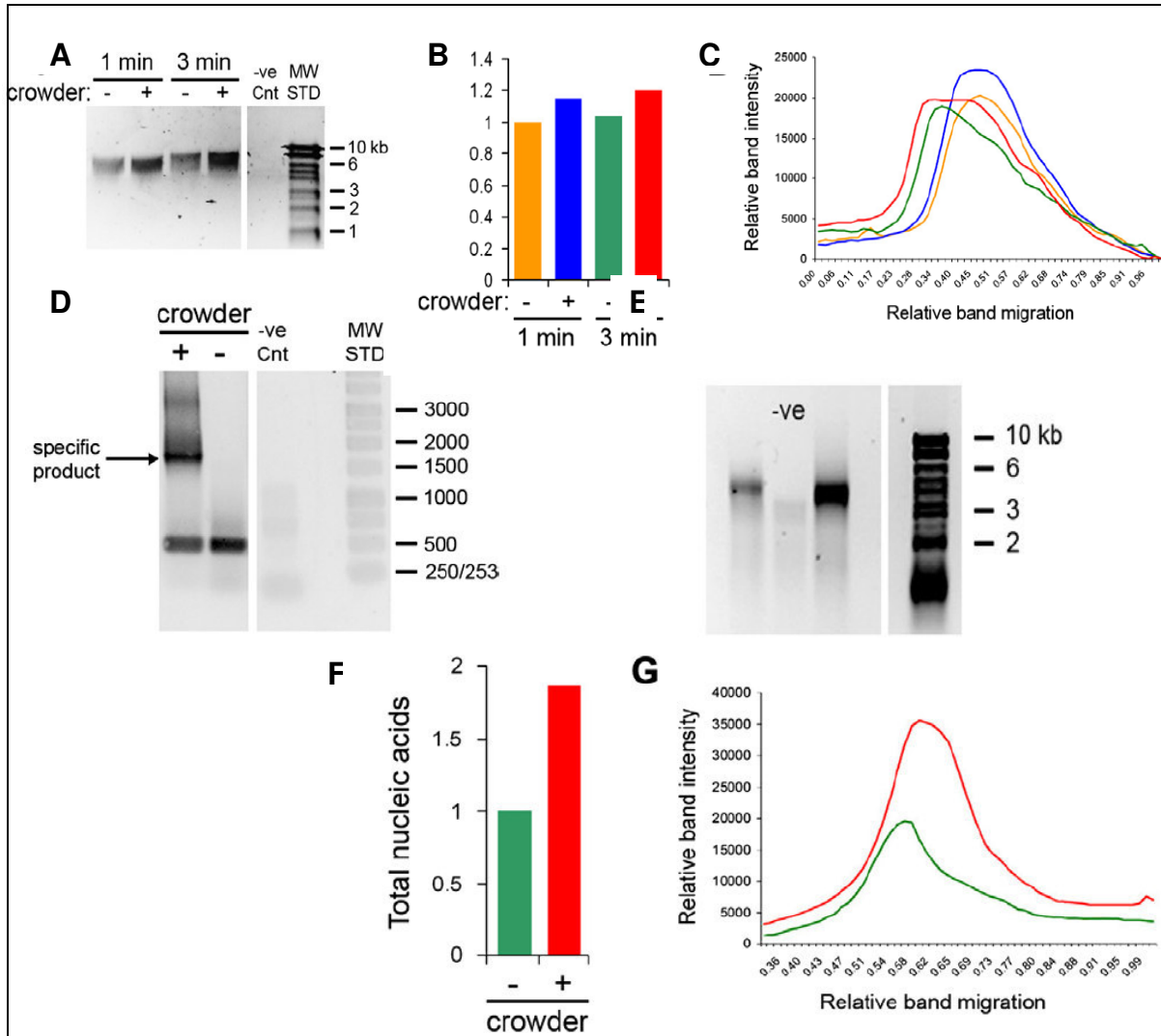


**Figure 28.** Macromolecular Crowding enhances enzyme processivity. The ssM13 processivity assay for *Taq* DNA polymerase  $\pm$  MMC (A) Densitometric analysis of the total amount of ssDNA products and (B) their relative migration through a (C) denaturing 0.6% agarose gel. The -ve Cnt was the enzyme-free negative control. (D) An agarose gel of the long M13 PCR products amplified in the absence and presence of macromolecule (mixture of Fc70 15 mg/ml and Fc400 5 mg/ml). One nanogram of ssM13 was used as target and the extension time was limited to 40 s. The -ve Cnt was without template. The arrow indicates the specific target which is 1547 bp. (E) A standard RT reaction was preformed in the absence (green) and presence (red) of Fc70/Fc400 with 500 ng of total RNA and the subsequent reaction products were separated in a denaturing 0.6% agarose gels. (F) Densitometric analysis of total reaction products and (G) their relative migration through (E). “-ve” is the enzyme negative control. Gel images are composites of the respective gels omitting irrelevant sections. (Lareu, Harve, Raghunath. *BBRC* 2007).

We carried out cDNA synthesis in the absence and presence of Crowding additives (Fc70/Fc400). Densitometry-analysis of the denaturing agarose gel of reaction products (Fig. 28E) demonstrated an increase in total cDNA of 86% (Fig. 28F) with overall longer cDNA products under crowded condition (Fig. 28G).

### **9.3.4 PCR Product Yield is enhanced under Crowded Conditions**

Decreasing amounts of Taq DNA polymerase were used to amplify a specific aP2 product from cDNA in the absence and presence of Fc400. For all Taq DNA polymerase concentrations (units of activity (U)/reaction) the presence of a Crowding agent resulted in > 2-fold yield of specific amplicon (Fig. 29C). These data were derived from integrating the area under the dissociation curves (Fig. 29B). The area under a melt curve is a measure of the total population of PCR products. This is because the dissociation-peak obtained is actually a negative derivative of the plot of decreasing fluorescence of double-stranded DNA against increasing temperature. At the melting point of duplex-DNA (50% breaking into single strands, the  $T_m$ ) there is a sudden drop in the SYBR Green I fluorescence. The real-time software then computes a negative derivative of the fluorescence at this point which is seen as a melt peak. Therefore integrating the area under such a peak mathematically yields the amount of total fluorescence at that point which quantitatively is a measure of the total population of double-stranded DNA. In order to assess the relative reaction rates in the presence and absence of macromolecular crowders, we calculated the slopes of the amplification plots at the late exponential phase for the above samples run with 1 U of enzyme (Amplification plot in Fig. 29A). The presence of Fc400 resulted in a 2-fold greater value for the slope and an additional cycle in the exponential phase demonstrating faster reaction kinetics (Fig. 29D).

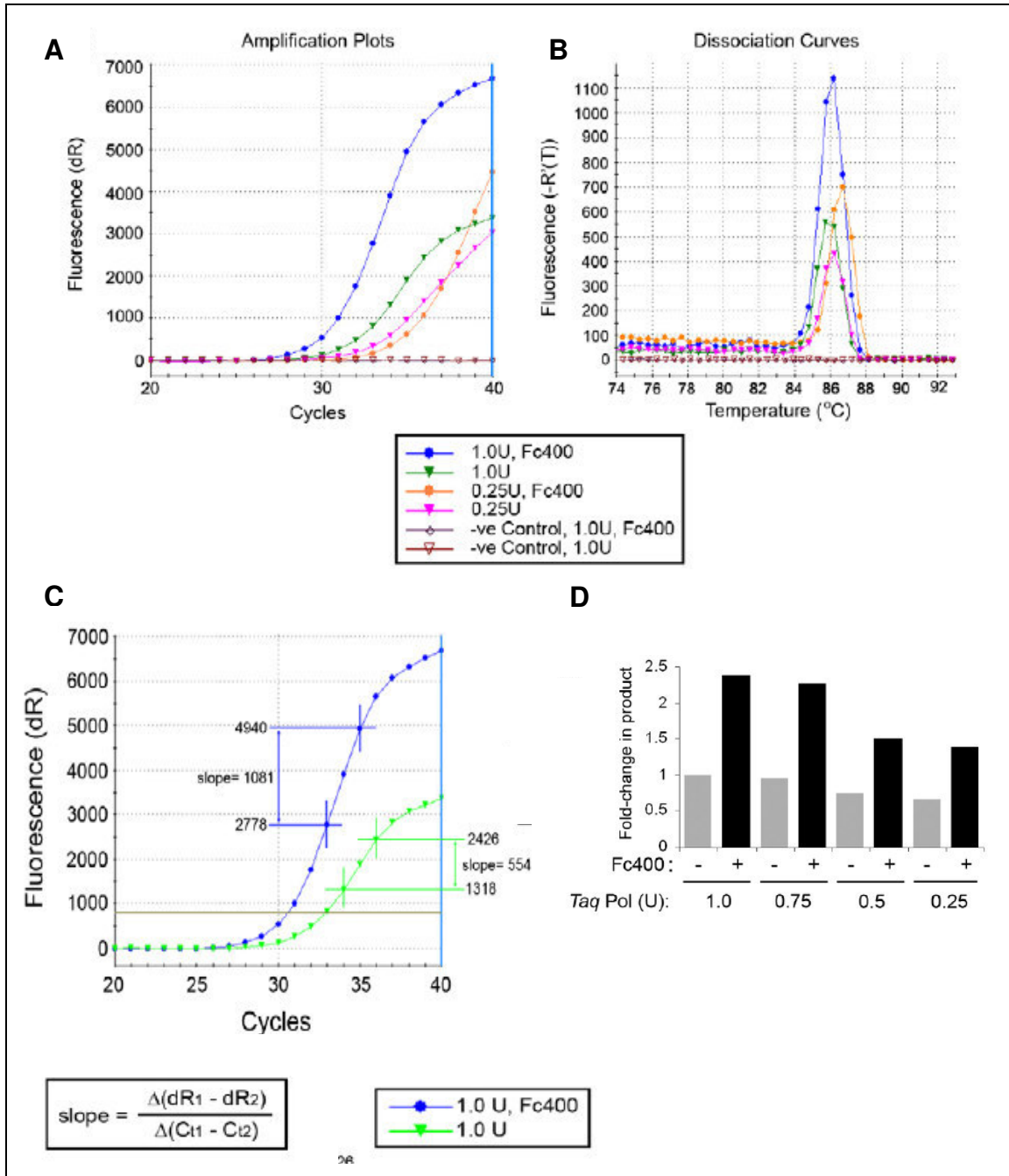


**Figure 29.** Macromolecular Crowding enhances Taq DNA polymerase activity. A range of Taq DNA polymerase concentrations (1–0.25 U/reaction) were used for aP2 PCR  $\pm$  Fc400 (2.5 mg/ml). (A) Amplification plots and (B) dissociation curves for the PCR samples performed with 1 and 0.25 U of enzyme are only shown, for display clarity. (C) The slope of the late exponential phase was calculated for the samples amplified with 1 U of enzyme above. (D) Relative comparison of the PCR product yield at different amounts of enzyme with or without Crowding (Lareu, Harve, Raghunath. *BBRC* 2007).

### 9.3.5 Crowding stabilizes Pre-stressed Enzymes against Heat

The thermal-protective property of macromolecules (i.e. Fc400) was tested for *Taq* DNA polymerase and compared against trehalose and proline, known, small molecules that have been shown to work as thermoprotectants. Ficoll PM 400 (Amersham Pharmacia; 400kDa) was dissolved in 1X PCR reaction buffer to give a final concentration of 2.5 mg/ml and 2 sets of dilutions (0.125 U/ $\mu$ l and 0.0625 U/ $\mu$ l) of *Taq* made in the PCR reaction buffer. 2 sets of Control dilutions of the enzyme were made in the PCR buffer without macromolecules. Both pairs of dilutions were subjected to heat at 95 °C for 45 minutes. After the pre-stressing, 8  $\mu$ l of each set containing 0.125 U/ $\mu$ l (referred to as A) and 0.0625 U/ $\mu$ l (referred to as B) of *Taq*, were added to a PCR reaction mix and real-time PCR was run for 40 cycles to amplify a target sequence for the *GAPDH* gene. A 2% agarose gel was then run to confirm the identity of the PCR product. Only the presence of Fc400 and trehalose preserved the *Taq* DNA polymerase's enzymatic activity (Fig. 30) but proline did not prevent the complete loss of activity.

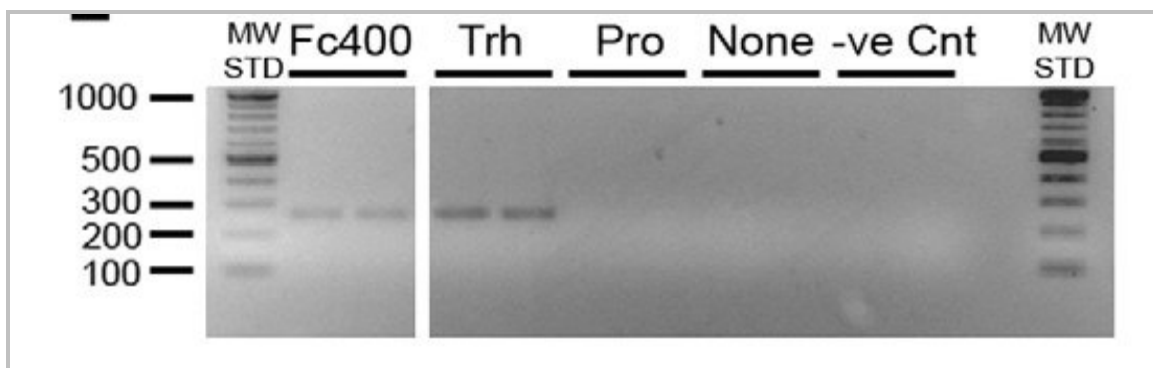


**Figure 30.** *Taq* DNA polymerase was thermally stressed in the absence (None) and presence of 2.5 mg/ml Fc400, 100 mg/ml trehalose (Trh), or 113 mg/ml proline (Pro) and then the enzyme was used to amplify *GAPDH* PCR amplicons. Two replicates per treatment are shown on a 2% agarose gel demonstrating the presence of discrete bands of the correct size, 261 bp. The -ve Cnt (control) was without template. (Lareu, Harve, Raghunath. *BBRC* 2007).

## 9.4 Discussion

Macromolecular Crowding has important thermodynamic consequences which influence reaction-kinetics and helps in bridging the void between *in vitro* and *in vivo* environmental conditions. In our current study, it was shown that reintroducing this parameter *in vitro* creates enhanced enzymatic properties expressed as dramatically more sensitive, specific and productive RT-PCR assays (Lareu, Harve & Raghunath, 2007). Using molar concentration and hydrodynamic radii of the macromolecular additives, measured by Dynamic Light Scattering (Harve *et al.* 2006) all of which are neutral and hydrophilic, we have introduced fraction volume occupancies ranging from 5% to 15% based on steric repulsion, well within the accepted range of biological Crowding (Ellis, 2001). However, the key to the success of Crowding with macromolecules at relatively low concentrations is that the actual volume exclusion would be far greater as there is a non-linear relationship between Macromolecular Crowding concentration and excluded volume, which essentially has a magnifying effect due to steric exclusion of like-sized (comparable/similar sized) molecules (Ross & Minton, 1977). Although the addition of non-reacting molecules to improve RT and PCR is not new, the addition of inert macromolecules certainly is. Other studies have either been restricted to small molecules classified as compatible solutes or small molecular size polymers, such as PEG 4 kDa, with limited success since PEG displays hydrophobic interactions with proteins (Ellis, 2001). The effects of PEG are due to improved (preferential) hydration around substrate molecules. Low molecular weight PEG has therefore not been considered an ideal Crowding agent<sup>\*\*</sup>. Preferential hydration is also the mechanism of action of trehalose (Spiess *et al.* 2004) betaine

---

<sup>\*\*</sup>Definition of macromolecule for molecular biology *in vitro* models are subject of a US patent pending, invented by Raghunath, Lareu, Harve: WO/2008/018839 METHOD FOR MOLECULAR BIOLOGY APPLICATIONS



and proline (Rajendrakumar *et al.* 1997) which are classified as compatible solutes. They are able to stabilize the structures of protein/enzymes even at high temperatures (Zimmerman & Trach, 1991). We replicated this effect of trehalose and showed that Fc400 had similar protecting effects on Taq DNA polymerase. Sensitivity and specificity are particularly crucial for diagnostic applications when the target is in low abundance (e.g. viral load in serum) or poor quality as found in archival sources. In using specific macromolecules as buffer additives we demonstrated dramatic increases in sensitivity up to 10-fold. Of note, the addition of PEG 4 kDa, in the same concentration range as macromolecules, to an optimized PCR assay was actually detrimental to the reaction with regards to sensitivity and yield.

Specificity of a PCR is determined by its ability to amplify the correct sized product. The current study was able to specifically demonstrate enhanced primer specificity under crowded conditions, which in turn would result in increased sensitivity. The usefulness of trehalose in improving sensitivity of PCR has been limited to the case of difficult cDNA templates with GC-rich regions (Spiess *et al.* 2004). Its effect is to reduce the melting temperature of these secondary structures. With regards to adding trehalose and betaine to RT reactions, an increase in the sensitivity was detected in the sub-sequent PCR but only when they were used at very high concentrations (Spiess *et al.* 2002). The increase in processivity, defined as greater product amount and length, which was attained with the addition of macromolecules would have been the direct consequence of both increased number of enzyme-nucleic acid initiation events and longer read-through of the enzymes, respectively. This is particularly significant for RT in faithfully generating enough copies of long cDNA molecules and for PCR in amplifying long amplicons. In fact, it has been shown that

a range of different molecular weight PEGs and dextrans were able to enhance the integrity and/or stability of the DNA-polymerase complex for *E. coli* T4 DNA polymerase (Jarvis *et al.* 1990). However, they were not able to attain improved processivity. It has been reported that PEG destabilizes enzymes at high temperatures due to the inherent activity of its hydrophobic nature (Lee & Lee, 1987). This may therefore hinder its application to PCR and the reason for the poor performance of PEG in our experiments and may have been responsible for the observed inability to improve processivity. In comparison to an earlier study which used compatible solutes to enhance RT reactions (Spiess *et al.* 2002), we employed high molecular weight macromolecules and attained an increase of both cDNA product and increased fragment length. However, in contrast to Spiess *et al.* 2002, increased processivity was achieved at 50 fold lower additive concentrations. At these low concentrations viscosity was close to that of water (1 centiPoise) and therefore of no concern (Harve *et al.* 2006). Conversely, the very high concentration required for compatible solutes to have an appreciable effect resulted in high viscosity to the point that it may have started acting like a “molecular brake” (Spiess *et al.* 2002) and adversely affect other parameters of the reaction mixture and could possibly interfere with subsequent downstream processing of the products. The success of the application of macromolecules to *in vitro* reactions is attributed to close emulation of the intracellular environment of cells such as bacteria whence these enzymes were derived from or naturally function in. This was clear from the overall better performance of the *Taq* DNA polymerase. Under these conditions we were able to reduce the amount of enzyme by 75% and still attained more reaction product due to faster reaction kinetics. These results could be attributed to Macromolecular Crowding of the reaction solution. The cumulative molecular and thermodynamic effects of

EVE created by Macromolecular Crowding have been explained to occur by the lowering the entropy of the reaction and thus increasing the free energy of the reactants (Zimmermann 1993). It was demonstrated that the gains we observed in Crowding of PCR mixes were a consequence of or combination of enhanced enzyme thermal stability, more primer annealing to its target and greater specificity, and enhanced enzyme-nucleic acid complex formation and stability (i.e. processivity). This improvement did not necessitate the employment of a genetically upgraded DNA polymerase, many of which are currently on the market, but by using low-cost additives. We believe this study comprehensively demonstrates the importance and potential that Macromolecular Crowding holds for *in vitro* enzymatic settings with far-reaching consequences to the fields of Biochemistry, Molecular Biology and Biotechnology in general.

## 10. Semi-Empirical Modeling of Crowding Nucleic Acid Interactions

### 10.1 Introduction

As discussed earlier, Macromolecular Crowding (MMC) is a ubiquitous feature of cellular interiors as a fundamental principle governing all biological functions *in vivo*. MMC, by excluded volume effect, helps in intra-chain folding of many polymers (Cheung *et al.*, 2005, Harve *et al.* 2006). MMC enhances thermal stability of proteins in general (Thirumalai *et al.* 2003) and *Thermus Aquaticus* (*Taq*) polymerase that catalyses the Polymerase Chain Reaction (PCR) in particular (Lareu *et al.* 2007). PCR, a DNA amplification tool, can potentially generate billions of DNA copies from a single molecule. However several hindrances inherent to the very design of the PCR significantly reduce the output from a theoretically expected magnitude. Classic routine PCR comprises of three steps: Step 1, separation of DNA double helix into single strands, step 2, annealing of primers - (20-mer oligonucleotides) to exposed single-strands to be replicated and in step 3, thermostable DNA-polymerase adds complementary nucleotides to the primer along the template. While step 1 is catalysed *in vivo* by helicases wedging themselves into double strands and breaking hydrogen bonds between bases (Bird *et al.* 1998; Johnson *et al.*, 2007), *in vitro* this is done by heating it to 94 °C and lowering to 50-55 °C for primer annealing. This re-binding is highly random, entropy-driven with reasonable hysteresis and is critical as efficiency of PCR is decided during its initial cycles (Wilhelm *et al.* 2000). Once annealing has occurred, the third step is done at a higher temperature (68-72 °C) which is optimal for thermostable polymerase but exceeds the optimal temperature for primer annealing. Therefore the primers could potentially break away from their target during the extension phase. Designing primers

with high (>50%) GC content may theoretically enable raising annealing temperature. However, this primer design modification is not general for routine (any random sequence) PCR. The PCR environment is an aqueous medium hardly reminiscent of its crowded *in vivo* counterpart. Thus, cyclic amplification of thermally unstable target-primer transition complex by a DNA polymerase at elevated temperatures in an uncrowded environment makes PCR a highly probabilistic reaction. Using high concentrations of primers, dNTPs and enzyme is one way to overcome this uncertainty of binding and polymerization. Yet, the theoretically predicted yield of amplicons is never reached in routine PCR due to the random nature of target-primer association at annealing and thermally induced primer-target dissociation during extension. These shortcomings may be remedied by creating a crowded environment during annealing and extension phases of a routine PCR. We earlier showed that MMC dramatically improves the activity of *Taq* DNA polymerase (Lareu *et al.* 2007) and partially explains why Crowding a routine PCR improves its sensitivity, specificity and efficiency. Here, we focus on the initial non-enzymatic PCR step to investigate the effects of Crowding a model DNA: DNA hybridization at cyclic temperatures typical of a routine PCR. By real time measurement of duplex DNA bound SYBR Green fluorescence and a novel *in silico* atomistic model for DNA:DNA hybridization under MMC, we enhance DNA hybridization at elevated temperatures and in so doing increase the melting temperature of the DNA duplex. By a combined *in vitro-in silico* approach, we further show the Crowding effects on other nucleic acid interactions that are key to many classical molecular biology reactions, underscoring the robustness and wide applications of MMC for molecular biology.

## **10.2 Aims and Rationale**

### **10.2.1. To determine the effects of macromolecular Crowding on the nucleic acid hybridization in a thermally stressed environment**

The earlier studies on the Crowding effects on an RT-PCR need to be further investigated to identify the critical steps in this molecular biology reaction that are sensitive to Crowding. Hence the initial step of this reaction, which is an entropy driven association of DNA (target and primer) was selected as the target to test Crowding effects in this study. The aim is to determine if Crowding could enhance DNA: DNA binding as well as maintain the duplex when subjected to heat cycles. The studies aim to determine the effects of Crowding on DNA hybrids of different lengths, sequences and conformations as well as DNA: RNA hybrids.

### **10.2.2. To investigate the mechanisms of Crowding effects on nucleic acid hybridization by means of molecular modeling**

To further investigate Crowding effects on structural stabilization of the double strands, an *in silico* model is helpful. Molecular Dynamics Simulations on single nucleic acid molecule will be explored to find out the effects of heat on DNA and RNA under crowded conditions.

## **10.3 Hypothesis**

Macromolecular Crowding stabilizes nucleic acid duplex against heat by enhancing the structural stability of individual nucleic acid strands as well as by promoting enhanced binding between the strands.

## 10.4 Materials and Methods

### 10.4.1 Real-time Measurement of DNA Hybridization

Oligo DNA with the following sequences 5'-A<sub>20</sub>-3': 5'-T<sub>20</sub>-3', 5'-A<sub>15</sub>-3': 5'-T<sub>15</sub>-3', 5'-AAT CAG TTA GTA ATT CAT TC -3': 5'- GAA TGA ATT ACT AAC TGA TT -3', 5'-T<sub>4</sub>A<sub>16</sub>-3': 5'-T<sub>16</sub>A<sub>4</sub>-3', 5'-A<sub>4</sub>T<sub>16</sub>-3': 5'-A<sub>16</sub>T<sub>4</sub>-3' (1st Base, Singapore), all at final concentrations of 1.0 $\mu$ M, were dissolved in a 10X PCR reaction buffer at final concentrations of 20mM TRIS and 50mM KCl, 3mM MgCl<sub>2</sub> and 1:500 SYBR Green I (SG I; Molecular Probes) in a 20 $\mu$ l reaction volume. Reactions were performed in duplicates. The oligomers were hybridized under PCR-typical temperatures in steps of 95 °C/30sec, 50 °C/1min, 72 °C/30sec, on a real time thermal cycler (Stratagene, USA) for 1, 4, or 40 cycles, followed by dissociation run from 50 °C  $\rightarrow$  94 °C<sup>††</sup> and fluorescence readings taken at each step. Appropriate adjustments in the thermal cycle program were made as required for different oligomer combinations. Oligomers with SNPs in their sequence 5'-A<sub>10</sub>-C-A<sub>9</sub>-3' (sequence ID:MS-1) were co-incubated with 5'-T<sub>20</sub>-3' in reaction buffer  $\pm$  MMC and real-time fluorescence monitoring to rule out non-specific binding under Crowding was done. Similar experiments were done on sequence 5'-T<sub>10</sub>-C-T<sub>9</sub>-3' (ID:MS-3) co-incubated with the sequence 5'-A<sub>20</sub>-3'. For experiments on DNA-RNA hybrids, oligo DNA 5'-T<sub>20</sub>-3': oligo RNA 5'-rA<sub>20</sub>-3' (Sigma-Aldrich) and SYBR Green I (1:500) were dissolved in water or macromolecular solution, heated at 65 °C/5' and cooled on ice as in the first step of a reverse transcription. Then the 5X first strand buffer (routinely used for cDNA synthesis) containing final concentrations of 50mM TRIS, 75mM KCl, 3mM MgCl<sub>2</sub> was added to the oligo mix kept on ice and then heated at 42 °C/5'  $\rightarrow$  70 °C/15'. Macromolecular crowders used were Ficoll 70 (Fc70;

---

<sup>††</sup> Detection of melting point of duplex nucleotides is indicated by the sudden drop in SG I fluorescence when the duplexes are heated to denaturation during the dissociation run.

Amersham; 70 kDa), Ficoll 400 (Fc400; Amersham; 400kDa) and polyvinyl pyrrolidone 360 (PVP360; Sigma; 360kDa). Fc400 as mono-crowder was used at final concentration of 40mg/ml and in combination, the final concentrations of Fc70, Fc400, PVP360 were 15mg/ml, 5mg/ml and 500 $\mu$ g/ml respectively. Area under the melt curves (AUC) were computed using the NCSS<sup>TM</sup> Software ([www.ncss.org](http://www.ncss.org)). For estimates on melting temperature, oligo Analyzer<sup>TM</sup> online software was used.

#### 10.4.2 Molecular Dynamics Simulations

MD simulations were done in the Discovery Studio<sup>TM</sup> Molecular Simulations package. CHARMM force-field was employed to simulate the dynamics cascade. Solvent (water) was simulated in an implicit solvent model (Generalized Born) that accounts for the free energy of solvation (Tsui *et al.*, 2001) with salt effects modeled by incorporating the Debye-Huckel screening parameter  $\kappa$  ( $= 0.34; \text{\AA}^{-1}$ ) for nucleic acids in physiological salt concentration (0.1M; Srinivasan *et al.*, 2000). To ensure accuracy of results a Born  $\lambda$  correction factor = 0.73 was applied on the  $\kappa$  as a scaling parameter. Initial energy minimization was done with Steepest Descent Algorithm (10,000 steps) and dynamics cascade carried out in sequential steps (1.0 femtosecond steps) of heating (target temperature: 307K; 100,000 steps), equilibration (800,000 steps) and production (NVT ensemble; 100,000 steps) for a total of 1 nanosecond. Oligo DNA simulated were the following sequences 5'-A<sub>20</sub>-3': 5'-T<sub>20</sub>-3', 5'-A<sub>15</sub>-3': 5'-T<sub>15</sub>-3', 5'- AAT CAG TTA GTA ATT CAT TC -3': 5'- GAA TGA ATT ACT AAC TGA TT -3'. Control experiments: MD simulations were carried out with single-stranded DNA to demonstrate that there was no hydrogen bond formation between single-strands and hydrogen-bonding pattern was exactly reproducing the *in vitro* picture of complementary binding of poly A and poly T



DNA strands. (2) Simulation runs at 400 ps and 800 ps were carried out and the energy profile compared. The results from these control experiments demonstrated that the energy profiles at the end of these two simulation runs were identical indicating that the system had reached equilibrium. Based on these controls, a total simulation time of 1.0 nanosecond was optimized for the test experiments under confined conditions. (3) Another set of control experiments were done to rule-out non-specific enhancement of hydrogen-bonding between mismatched DNA strands. To test this, oligomers with SNPs in their sequences 5'-A<sub>10</sub>-C-A<sub>9</sub>-3', 5'-A<sub>10</sub>-G<sub>9</sub>-3' were separately co-incubated with 5'-T<sub>20</sub>-3'. For experiments on DNA:RNA hybrids, oligo DNA 5'-T<sub>20</sub>-3': oligo RNA 5'-rA<sub>20</sub>-3' hybrids were simulated. MMC were set-up on a confinement platform by encaging the DNA in polymeric chains of alpha-D-1,6-Glucose (15 kDa). The rationale of designing the confiners is explained in results section. Stability of DNA-duplex was determined by monitoring the hydrogen bonding between the DNA-DNA or DNA-RNA strands as well as the RMSD (root-mean-squared-displacement) of the structures after the simulation runs under confined (crowded) or non-confined (uncrowded) conditions.

## 10.5 Results

### 10.5.1 Rationale of Modeling MMC as Macromolecular Confinement

In our current DNA-hybridization model, Crowding has been created by introducing neutral crowders into the reaction mix. However, the DNA 20-base-pairs, with an approximate MW of 15 kDa and are in Brownian motion in solution. The crowders although also in Brownian motion, move an order of magnitude slower than the DNA. This relative slowness of crowders vis-à-vis DNA ‘traps’ the DNA within the coiled network of the crowding macromolecule. These ‘entrapment’ effects and the deduction that within the life-time of an H-bond (~5-7 picoseconds, see Table 5), the average translation of a macromolecule is of the order ~ 0.01 nm, the mean diffusion length enable the Crowding to be considered as a case of ‘Macromolecular Confinement’.

**Table 5.** Comparing the relative diffusion coefficients of DNA and crowders

<b>Molecule/Species</b>	<b>Diffusion coefficient</b>	<b>Bond life-time</b>	<b>reference</b>
18-base ssDNA	$9.81 \times 10^{-7} \text{ cm}^2/\text{s}$	---	Nkodo <i>et al.</i> , 2001
Macromolecule(PVP360)	$7.9 \times 10^{-8} \text{ cm}^2/\text{s}$	---	Harve <i>et al.</i> , 2006
H-bond		5-7 ps	Woutersen <i>et al.</i> , 2001

The rationale of designing the confiners as capping rings (Fig. 31) at the DNA ends was as follows. Firstly, this set up a condition that prevented the “bending and untwisting” of the twisted double helix that dsDNA is. The bending event has been shown earlier (Ramstein *et al.* 1988) to be a conformational change that is correlated with the break-up of the double strand. Also we can recall that unwinding of double stranded DNA has to

take place prior to replication *in vivo* and there are specialized enzymes to carry this out. Thirdly, such carbohydrate doughnut-shaped rings have been found in nature in thermophilic bacteria (Cycloamylose; Fujii *et al.* 2005).

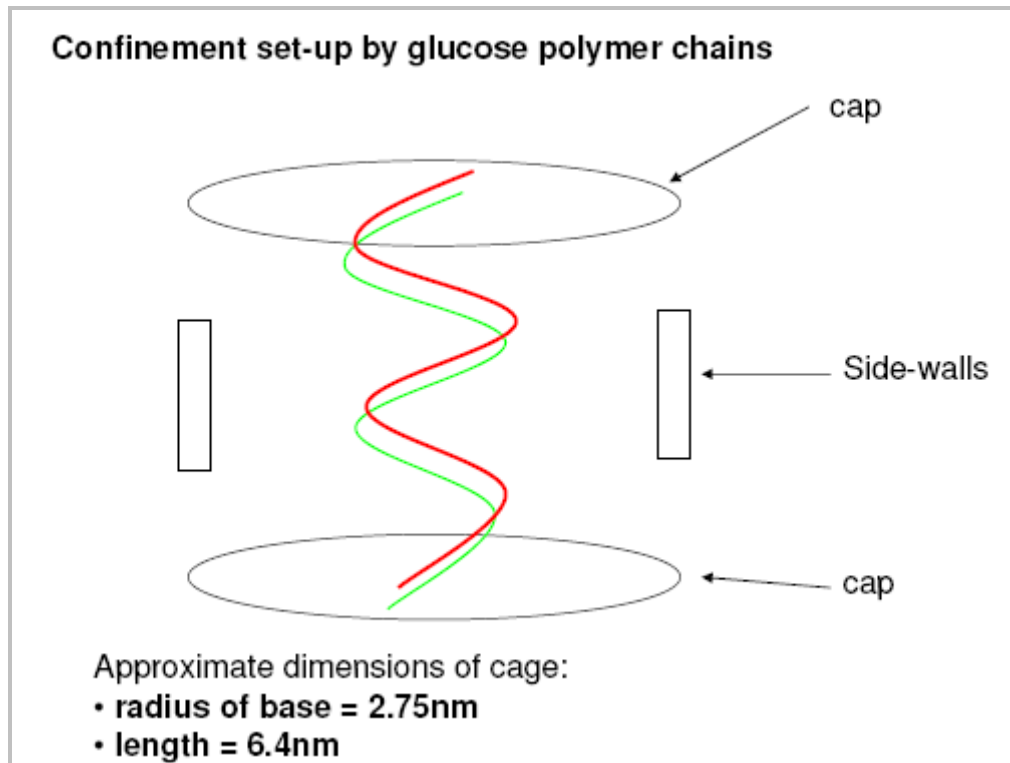


**Figure 31.** A simplified confinement model to simulate the *in vitro* DNA-hybridisation under crowded conditions.

### **10.5.2 Double-stranded DNA is stabilized at Temperature Cycles of a typical PCR under Macromolecular Crowding**

DNA-annealing involves a non-enzymatic, entropy-driven spontaneous assembly of oligonucleotides by hybridization. Real-time measurements were done at 1, 4 and 40 cycles typical of a PCR. While cycle 1 shows what the effects of Crowding would be at the onset of a typical PCR, measurement over 40 cycles demonstrates the sustainability of the Crowding effects over the entire run of a typical PCR. Results after 4 cycles (Fig 32) indicated a significant drop in fluorescence from 8,700 fluorescence units (annealing) to 3,161 units (extension) when the annealed oligomers were taken to a higher temperature.

This end-extension reading is background noise close to the value at the end-denaturation step (~ 2,400 units). In contrast, under MMC (Fc70 + Fc400 + PVP360), ~ 28,000 units were measured at end-annealing, thus a mean 3.2-fold increase in the signal over that under uncrowded conditions. At end-extension the fluorescence readings dropped but remained much above the baseline with ~ 18,000 units, a gain of 15,000 units or a 5.7-fold higher signal over the uncrowded condition (Fig. 32). Thus, at both the end-annealing and end-extension phases, the crowded condition resulted in higher fluorescence due to a greater amount of duplex DNA. A similar trend was observed at cycles 1 and 40 (Fig. 32). However the decrease in signal after 4 cycles compared to the readings after the first cycle under uncrowded conditions is interesting. Under crowded conditions, the signal does decrease from the first to the 4<sup>th</sup> cycle but there is a definite increase in the signal as we go from the 4<sup>th</sup> to the 40<sup>th</sup> cycle.

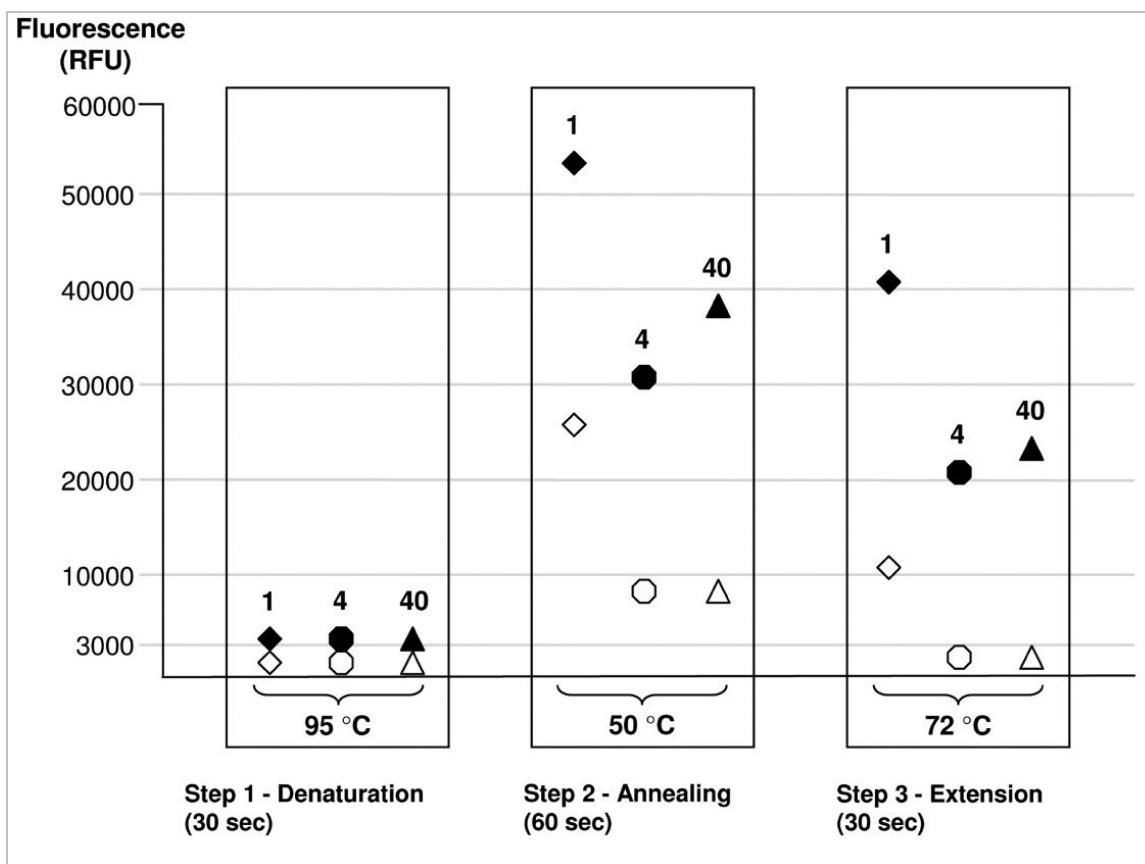


**Figure 32.** Real time readings of SG I fluorescence due to 20-mer DNA hybridization at cyclic temperatures typical of a PCR after 1, 4 and 40 cycles under uncrowded (white symbols) and MMC (black symbols). MMC yielded fluorescence signals that were up to 3-fold and 10-fold higher than the uncrowded condition at the annealing and extension phases respectively. This trend was consistent when readings were compared after 1, 4 and 40 cycles represented on the X-axis and the corresponding fluorescence readings are shown on the Y-axis. The graph is a schematic representation of the amount of duplex DNA at various temperatures typical of a PCR (not to scale).

We then compared the effects of single and binary crowder solutions with the mixed macromolecular crowder solutions mentioned above (Fig. 33). Mono-Crowding with Fc400 40 mg/ml raised the melting point by 1 °C. Crowding with a binary Ficoll mix resulted in an average 1.5 °C shift, while adding PVP360 to the Ficoll mix raised the melting point by 7-8 °C (Fig. 33). We then estimated the relative populations of dsDNA just prior to dissociation by calculating the average area under the melt curve (AUC) under non-crowded and different MMC.

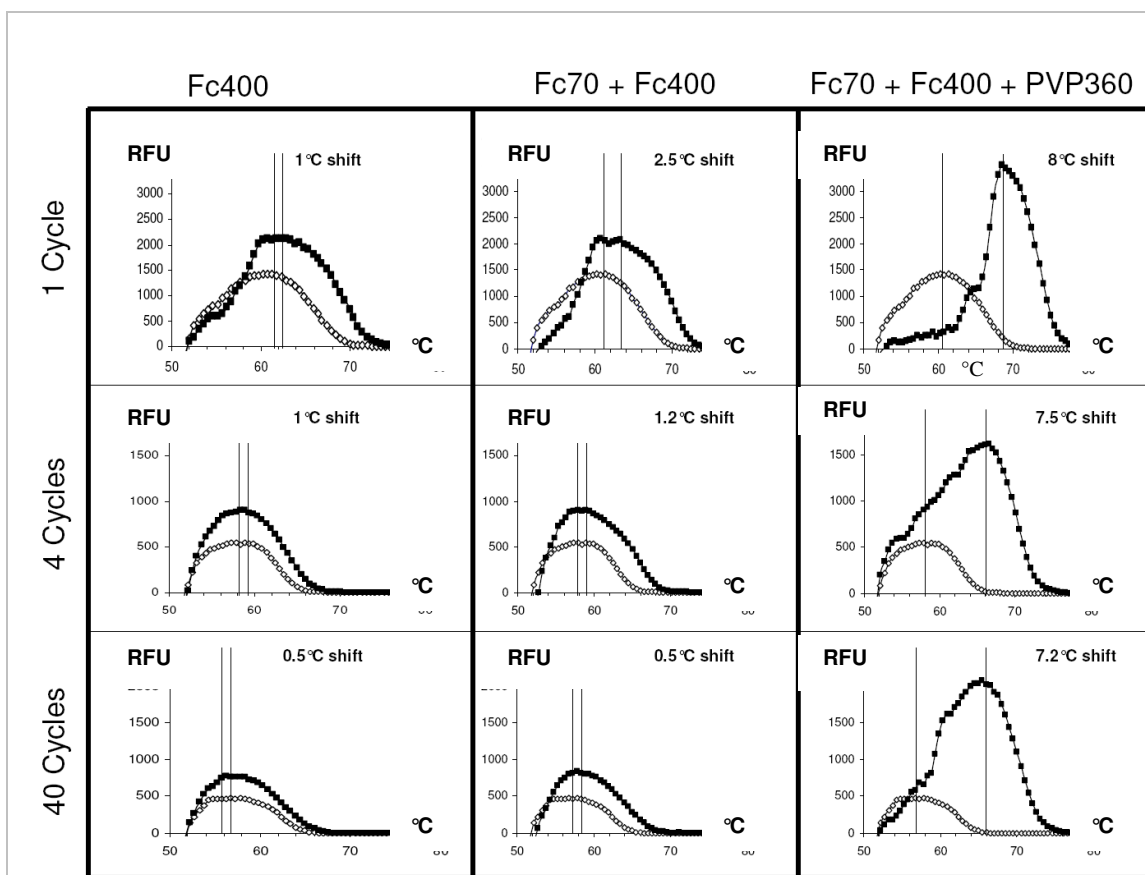


**Figure 33.** Dissociation Curves of 20-oligomer DNA-DNA hybrids under uncrowded (—□—) and crowded (—■—) conditions. MMC applied were Fc400 alone, Fc400 + Fc70 and Fc400+Fc70+PVP360 and dissociation curves obtained after 1, 4 and 40 cycles in each condition. Fc400 and the Ficoll binary mix show average shifts of 1-2.5 °C and adding PVP360 to the binary mix increased the average shift to 7-8 °C at each of the 3 cycle conditions. In each panel, graph represents the melt curve, i.e. the Y-axis shows the fluorescence (the negative derivative of fluorescence) and the X-axis the temperature (°C).

The ratio of the AUC due to crowded versus uncrowded show that mono- and binary Crowding demonstrated a 2-3 fold increase over the uncrowded duplex population, while a mixed crowder cocktail increased the duplex population by 6-fold over uncrowded control.

Control experiments to confirm that Crowding did not increase non-specific binding of mismatched oligonucleotides showed that there was no enhancement of hybridization of oligomers that had single nucleotide polymorphism in their otherwise

complementary sequences (Fig. 34). Screening simulations on mismatched DNA oligomers were done in confined and non-confined conditions and predicted that confinement conditions do not increase the stability of the mis-matched oligomers non-specifically (data not shown). Dissociation curves of DNA duplexes between mismatched oligo(20)-mers  $\pm$  MMC. When the mismatched oligomers (sequence ID MS-1) was co-incubated with 5'-T<sub>20</sub>-3', the results indicate that there is a near complete overlap of the uncrowded and crowded melt curves for the mismatches indicating that there was no non-specific enhancement of binding of these mismatched DNA under MMC. Similar experiments carried out on sequences MS-2 and 5'-T<sub>20</sub>-3', MS-3 and 5'-A<sub>20</sub>-3' and MS-4 and 5'-A<sub>20</sub>-3'. All the respective results all indicate that there was no increase in non-specific binding of the mismatched nucleotides due to Crowding.

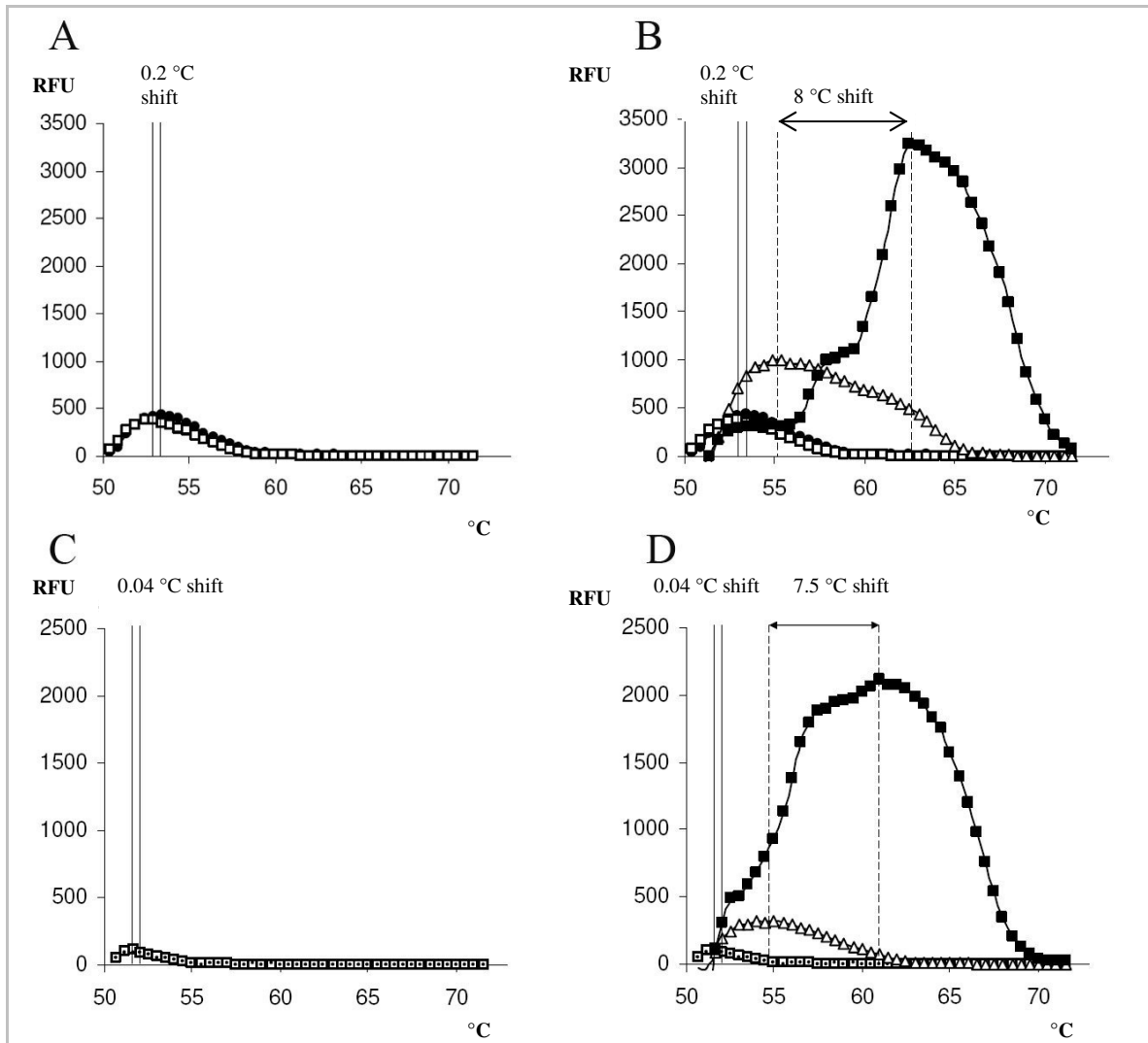


**Figure 34.** Dissociation curves of DNA duplexes between mismatched oligo(20)-mers  $\pm$  MMC. Panel A represents the melt curve when mismatched oligomers with sequence ID MS-1 was co-incubated with 5'-T<sub>20</sub>-3' under uncrowded ( $\square$ ) and MMC ( $\bullet$ ). Panel B is a result of the same experiment in which melt curves of the positive controls: the 5'-A<sub>20</sub>-3': 5'-T<sub>20</sub>-3' hybrids at uncrowded ( $\triangle$ ) and MMC ( $\blacksquare$ ) have also been shown together. Note that there is a near complete overlap of the uncrowded and crowded melt curves for the mismatches indicating that there was no non-specific enhancement of binding of these mismatched DNA under MMC. Panels C and D are results from similar experiments carried out on sequences MS-3 and 5'-A<sub>20</sub>-3' under uncrowded ( $\square$ ) and MMC ( $\bullet$ ).



### **10.5.3 *In vitro* Crowding enhances Thermal Stability of Nucleic Acids of Different Conformations**

Real-time estimation of nucleic acid thermal stability to validate the simulation results were done on short DNA fragments (15-mers), random DNA (20-mers) and DNA:RNA hybrids under uncrowded conditions and MMC. The results are summarized in Table 6. As can be appreciated from the table, the results (after 4 cycles) under uncrowded conditions indicated drop in fluorescence from mean value of 13900 units (annealing) to mean 2523 units(extension) for the 15-mers and mean value of 19570 units (annealing) to mean 2572 (extension) for random DNA. Under MMC, on average 58704 and 51760 units were measured at end-annealing for the 15-mers and random 20-mers respectively. At end-extension corresponding fluorescence readings were on average 3537 units and 5031 units, a gain of 1000 units and 2500 units respectively over uncrowded conditions. Melting temperature also increased under MMC by a mean value of 7 °C and 6.4 °C over uncrowded conditions respectively for the 15-mers and random 20-mers. Duplex population from the area under the melt curve showed a 3-fold increase due to MMC. A similar trend was observed at cycles 1 and 40 (data not shown). For DNA: RNA hybrids (Table 6), after initial heating at 65 °C/5', fluorescence was at baseline levels at both uncrowded and MMC (average 2700 units and 3100 units). Subsequent incubation of the hybrids at 42 °C/50', showed a 3-fold increase in fluorescence under MMC compared to uncrowded conditions (Table 6). Under MMC, the melting temperature was on average 53.05 °C increased by 5.4 °C compared to that under uncrowded conditions (mean value 47.7 °C). The DNA: RNA hybrid population as calculated by the AUC shows an average 3-fold increase due to MMC.

**Table 6.** Real-Time monitoring of thermal stability shows that the effects of Crowding are generic for nucleic acid hybrids of different lengths, conformations or sequence

Nucleic Acid	Mean Fluorescence (RFU)				Average Melt peak shift(°C)
	Annealing		Extension		
	UC	MMC	UC	MMC	
DNA(A <sub>15</sub> :T <sub>15</sub> )	13900	58704	2523	3537	7.0
DNA(random)	19570	51760	2572	5031	6.4
DNA:RNA	65 °C/5'		42 °C/50'		Melt shift(°C)
	2700	3100	17506	62271	5.4

#### 10.5.4 Macromolecular Confinement enhances Hydrogen Bonding to stabilize Double- stranded DNA Structure against Heat

In the current MD Simulations, solvent and salt effects have been modeled by implicit solvent methods based on a modification of the generalized Born treatment of the solvent medium as an infinite continuum. The electrostatic effects of salt were realized by introducing the Debye-Huckel parameter ( $\text{Kappa} = 0.34 \text{ \AA}^{-1}$ ) in the solvation free energy relationship. Explicit treatment of solvent by imposing periodic boundary conditions were tried to simulate denaturation of nucleic acids but were unable to simulate for greater than 100 picoseconds (ps) and hence were not pursued further. Comparison of the simulation output at the end of 400 ps with that at the end of 800 ps under both uncrowded and confined/MMC showed negligible potential energy difference suggesting that equilibrium had been reached. After initial minimization of the starting configurations of 20 base-pair oligo-DNA (A<sub>20</sub>:T<sub>20</sub>), the maximum H-bond number is 40.

The initial structures were set as reference to calculate the RMSD of the simulated structures from the initial conformations. At the end-equilibration stage, the two strands separated and displaced further during the production phase (Fig. 35a). However, under confinement conditions, the model predicts that there were still 11 of the original 40 H-bonds intact (normalized ratio of 1:4) holding the DNA strands together in double-helical conformation (Fig. 35b).

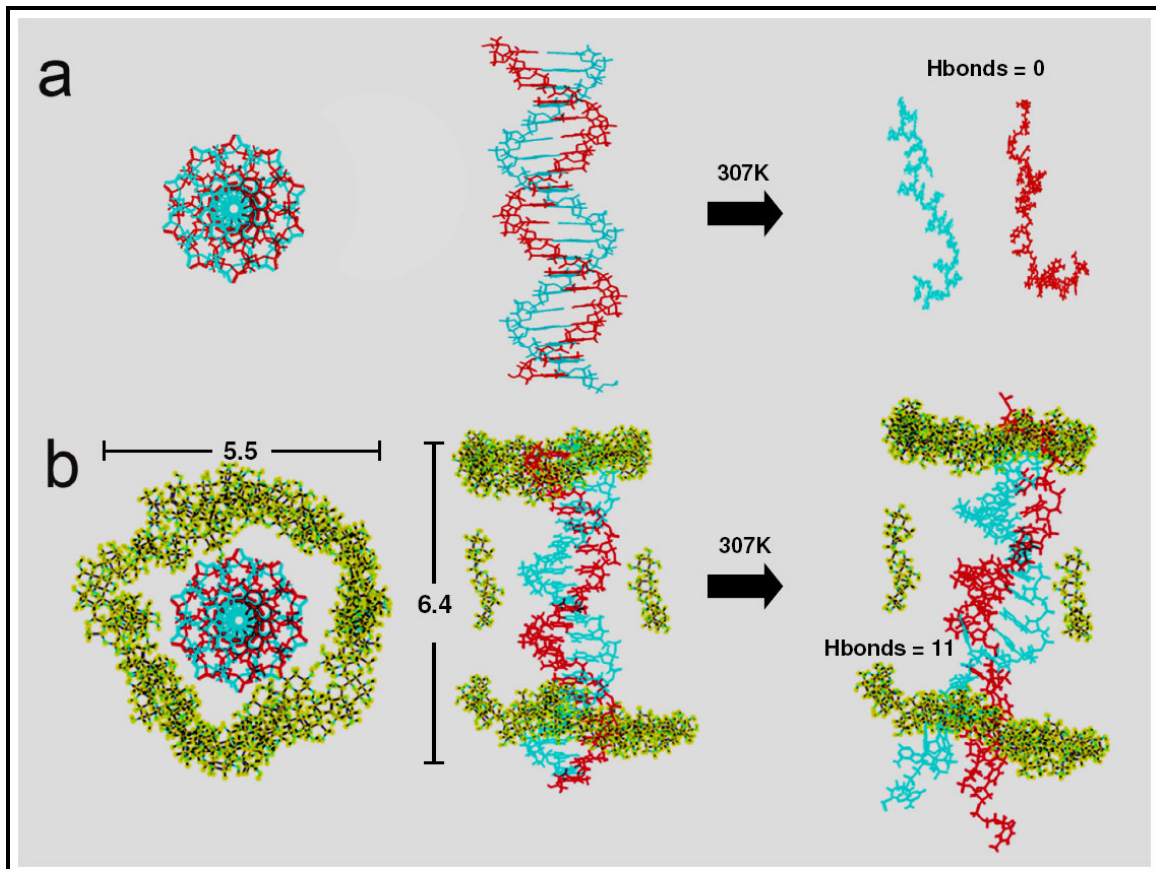


**Figure 35.** Snapshots of simulated single DNA-DNA hybrid from a Molecular Dynamics run for 1 nanosecond: (a) DNA denatured by heating to 307K breaks all the 40 H-bonds of the double helix. However, a confined environment (b) modeled as doughnut-shaped rings surrounding the DNA ends and the two chains as sidewalls, the dimensions (in nm) as shown in the figure, maintains the double helical structure by retaining 11 of the original 40 H-bonds.

RMSD values showed that under unconfined conditions, the final structure showed a mean of 21.6 nm from the initial structure. Under confinement, the RMSD was 8.325 nm,

an approximate 3-fold reduction in displacement of the final structures compared to the unconfined scenario. Therefore, simulations show that under unconfined conditions, the DNA structure is grossly disrupted.

#### **10.5.5 *In silico* Confinement Models predict Structural Stabilization of Nucleic Acids of Different Conformations at Elevated Temperatures**

We tested if the simulations could predict whether MMC can stabilize nucleic acid hybrids differing in length, sequence or conformation (Table 7). After initial minimization of the starting configurations of 15 base-pair oligo-DNA (A<sub>15</sub>:T<sub>15</sub>), the maximum number of H-Bonds is 30. At the end-equilibration stage, under confinement conditions, there were still 6 of the original 30 H-Bonds intact (normalized ratio of 1:5). The final structure showed a mean RMSD of 19.0 nm and 8.6 nm under unconfined and confined conditions respectively, from the initial structure. Thus the model predicted that confinement stabilizes shorter DNA duplexes against heat. We then tested if MMC could stabilize DNA oligomers of random sequences. At the end-equilibration stage, under confinement, there were still 10 of the original 45 H-Bonds intact (normalized ratio ~1:4). The final structure showed a mean RMSD of 20.0 nm and 9.6 nm under unconfined and confined conditions respectively, from the initial structure. The effects of confinement were then tested on DNA: RNA hybrids (20 nt). Initial simulation runs identified a target temperature of 290K as sufficient to completely break all the H-Bonds between the DNA: RNA hybrids under unconfined conditions (Table 7). At this temperature, simulated DNA:RNA hybrids under confinement show 15 of the original 40 H-Bonds (normalized ratio ~1:3) intact. Thus confinement stabilizes DNA:RNA against heat-induced denaturation.

**Table 7.** Summary of MD Simulations on nucleic acid hybrids.

Nucleic Acid type	After heat treatment					
	H-bonds		H-bond Normalized Ratio		RMSD (nm)	
	UC	MMC	UC	MMC	UC	MMC
<b>DNA:DNA(A<sub>15</sub>:T<sub>15</sub>)</b>	0	6	0	1:5	19.02	8.66
<b>DNA:DNA(random)</b>	0	10	0	1:4	20	9.6
<b>DNA:RNA(dT<sub>20</sub>:rA<sub>20</sub>)</b>	0	15	0	1: 2.5	11	8.18

### **10.5.6 MMC enhances Duplex Formation of Single-stranded Hair-pin-forming DNA Oligomers**

Oligo DNA 20-mers were designed to form hair-pin structures due to internal base-pairing between the complementary nucleotides within their sequence. When such oligomers were co-incubated with their complementary sequence nucleotides (which also similarly could form hair-pin structures) under uncrowded and MMC, we made a very significant and interesting observation. Under uncrowded conditions, the melting peaks show a very negligible fluorescence signal (Fig. 36) due to a small duplex population as indicated by the AUC (mean value of 1094 sq. units). However, under MMC, there was a clearly detectable fluorescence signal due to abundant duplex population, mean AUC = 20833 sq. units, a ~20-fold increment and with an increase in melting temperature of ~5 °C compared to the uncrowded condition. Further confirmation of the 20bp length of the hybridized products was done by a 3% Agarose gel electrophoresis (data not shown). Appropriate controls were run to visualize the SG I fluorescence when only one set of

oligomers were present in the solution without its complementary pair so that the oligomer formed a hairpin structure and no fluorescence was detectable due to absence of duplexes.

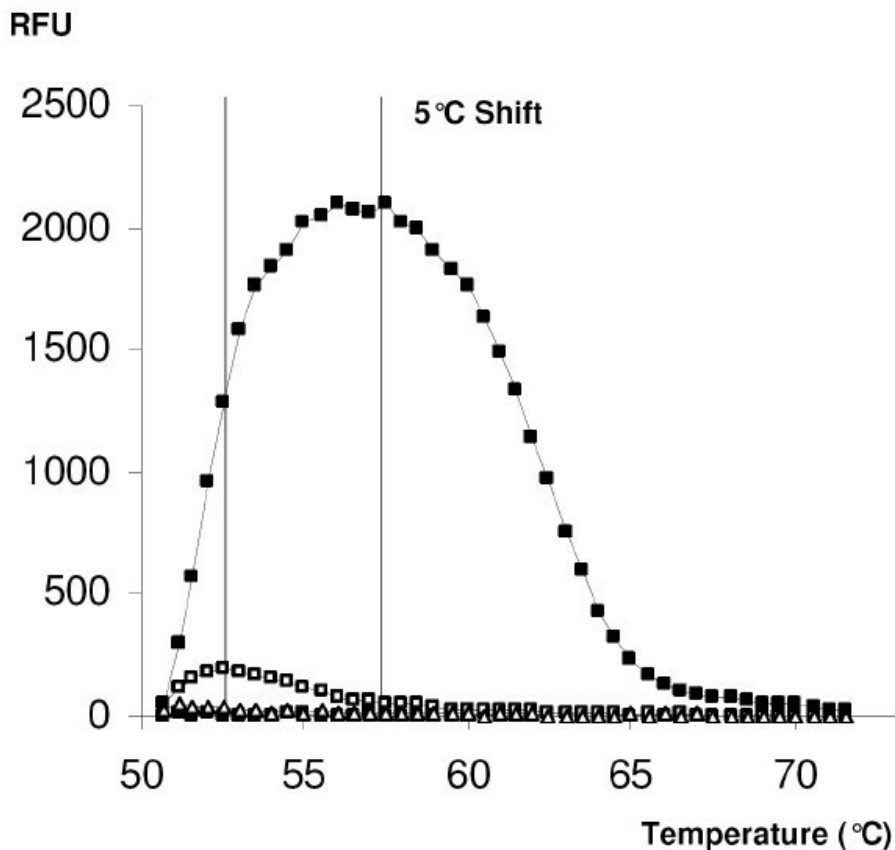


**Figure 36.** Dissociation Curves of 20-mer hair-pin DNA-DNA hybrids under uncrowded (—□—) and crowded (—■—) conditions. In each panel, x-axis represents temperature (°C) and y-axis fluorescence (RFU). MMC applied were Fc400+Fc70+PVP360 and dissociation curves obtained after 4 cycles are shown here. The uncrowded condition shows a weak fluorescence due to a sparse duplex population where as under MMC, the fluorescence is well detectable suggesting a rich duplex DNA population. Area under the melt curves were computed that showed AUC under uncrowded conditions = 1094 sq. units and that under MMC=20883 sq. units. Appropriate controls were run to visualize the SG I fluorescence when only one set of oligomers were present in the solution without its complementary pair. Thus in this case the oligomer formed a hairpin structure and no fluorescence was detectable due to absence of any duplexes (—△—).

## 10.6 Discussion

### 10.6.1 MMC drives Duplex Formation from Nucleic Acid Single Strands and stabilizes the Double-stranded State under Denaturing Conditions

The non-enzymatic step of a PCR that involves an entropy-driven association (and H-bonding) of the primer to its target is a highly probabilistic event. Hence not all targets find their complementary bases to bind. Therefore, the amount of duplex DNA formed under uncrowded conditions is rather low. This was evident from our current study when annealing of oligomers could be enhanced by up to 3-fold by introducing crowders into reaction environment. These effects of MMC could be due to enhanced association of single-stranded DNA with its complementary sequence to fold into a helix. At concentrations of the macromolecular cocktail, total fraction volume occupancy by crowders is ~22% which is in the range of biological MMC (Ellis 2001). Our three significant observations about DNA hybridization in PCR-typical temperature cycles under MMC were (i) Enhanced population of DNA-DNA hybrids at end-annealing (50 °C) (ii) stabilization of hybrids at end extension (72 °C) that is sustained over 40 cycles as in a typical PCR (iii) a dramatically increased  $T_m$  of the hybrid by ~8 °C. An interesting observation was that under uncrowded conditions, the fluorescence from SG I bound to the DNA duplexes decreases as we go from first cycle to the fourth cycle both at the annealing and extension phases and remains at the same value after 40 cycles. However, under Crowding, the signal shows a decrease after 4 cycles but then increases gradually when we follow-up to 40 cycles. The initial drop is explained by the inherent hysteresis that is associated with renaturation of DNA. The denaturation-renaturation

reaction reaches an equilibrium state by the fourth cycle and so remains stable from then on up to the 40<sup>th</sup> cycle.

If we consider a DNA association as a reaction between two single strands combining to form a double strand reaching a chemical equilibrium at an optimum (annealing) temperature, then Crowding can be seen to cause a shift in this equilibrium to the right and since formation of a double strand from a pair of single strands involves reduction in the excluded volume (and increase in available volume), this favors the formation of more double strands. If this system which is in equilibrium is perturbed by increasing the temperature, then the system tries to resist the change. Crowding reinforces this tendency of the system and thus more double strands are detected at the extension temperature than at uncrowded conditions. The effects of Crowding on DNA association have been shown to involve entropy-driven forces and also by enthalpic stabilization (Goobes *et al.* 2003). The stability of a DNA duplex is primarily dependent on the base-stacking and the H-Bond integrity.

Our simulation model explained our experimental observations and showed that under MMC modeled as confinement, the base stacks were stabilized against heat and also the H-bonds bridging single strands into a double helix. In a nutshell, the crowded/confined DNA showed greater resistance against heat and greater structural stability than under uncrowded/unconfined conditions.

#### **10.6.2 Mixed MMC greatly enhances DNA-thermal Stabilizing Effects obtained from Mono-macromolecular Solutions**

Combination of two or more different types (in terms of shape) of macromolecules in solution creates shape and size anisotropy. In our case, we used in our



cocktail, PVP360 - a random coil polymer - in combination with Ficoll, which is globular. Ficoll 70, Ficoll 400 and PVP360 have MWs of 70 kDa, 400 kDa, 360 kDa and hydrodynamic radii of 5 nm, 13 nm and 20 nm, respectively (Harve *et al.* 2006). Such a mix has the potential to result in greater volume exclusion effects than either of them alone (Zhou *et al.* 2004). In our current study, the melting temperature of DNA hybrids increased by more than 2-fold due to mixed crowders in comparison to the mono (Fc400 alone in solution) and binary combination of globular crowders (the Ficoll mix). In order to explain the mechanism of Mixed Crowding, we have earlier found that PVP360 was able to drive the multimerization of Fc70. This might result in slowing down the diffusion of crowders and enable Macromolecular Crowding to be impart a confinement effect on the faster moving DNA. In nature, the crowding element is actually derived from a heterogeneous population (proteins, nucleic acids, carbohydrates and lipids) of various sized macromolecules ranging from a few nanometers (such as small peptides) to a few hundreds of nanometers (as in DNA). Thus this is a case of a mixed crowded state. Emulating such an *in vivo* situation by Mixed Macromolecular Crowding is thus an effective strategy for maximizing the effects of Crowding *in vitro* biology.

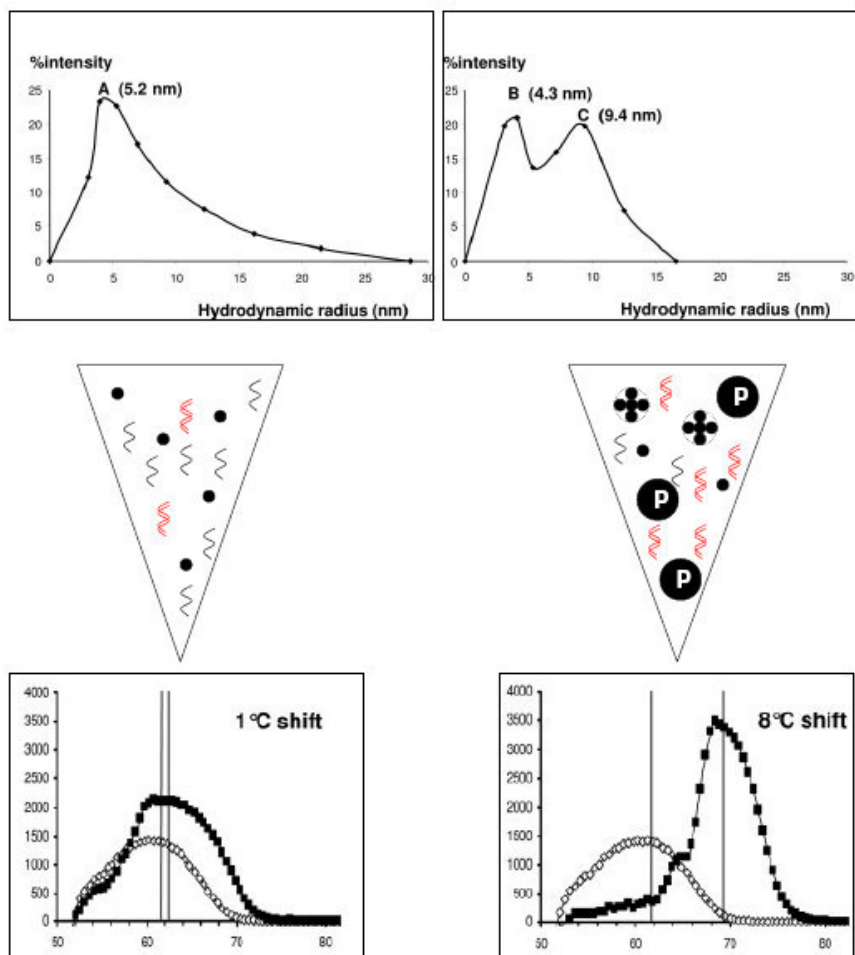


**Figure 37.** Schematic representation of Mixed Crowding effects on DNA stability.

### 10.6.3 A Combined *in vitro-in silico* Approach is a Powerful Tool to Design Optimal Crowding Conditions for Molecular Biology Reactions

Having shown that simulation models reliably predicted earlier experimental observations, we set-out to use the *in silico* tool to screen feasibility of applying MMC on other nucleic acid interactions tested for stability against heat. MMC was found to stabilize nucleic acid structure as a double helix irrespective of length, sequence or conformation *in silico*. However, these observations needed experimental proof and were aptly confirmed by real-time monitoring of thermal stability of shorter DNA, random

sequence DNA and DNA:RNA hybrids under MMC. Stabilizing effects of MMC on DNA:RNA hybrids may also partially explain its role in increasing cDNA yield of reverse transcriptase reactions by enhancing binding of oligo-dT primers to poly A sequence on mRNA independent of effects on reverse transcriptase activity. A very potent ability of MMC in enhancing specific binding of nucleic acids was evident from our study. Firstly, any non-specific promotion of nucleic acid hybridization was effectively ruled out by our experiments on oligomers containing SNPs in their sequences. Earlier studies (Goobes *et al.* 2003) have predicted that MMC enhances specificity of binding due to significant free energy differences of binding between mismatches and true matches, the latter being favored by MMC. Secondly, when oligomers which can form hair-pin structures due to complementary nucleotides within their sequences were co-incubated with their complementary oligos, MMC actually favored formation of duplexes by nucleic acid hybridization instead of hair-pin formation that was the preferred conformation under uncrowded conditions with a resultant low duplex formation. In summary, Crowding enhances specificity of nucleic acid hybridization and this effect is seen in favoring true match binding over mis-matches and also in reducing the internal base-pairing of single strands to shift the system to yield double strand formation.

#### **10.6.4 Crowding Effects by Confinement stabilize DNA-DNA against Thermal Denaturation: Evidence for *in vitro* Application of Thermostable Carbohydrates**

Our analyses and calculations suggest that in our experimental system the employed macromolecular crowders have a much slower diffusion velocity than nucleotide oligomers. Therefore, the crowders can be regarded as static in relation to

DNA-hybrids. Confinement by static crowders creates a volume exclusion effect. Several studies have shown that confinement can enhance the thermal stability of proteins such as alpha-lactalbumin in silica glass (Thirumalai *et al.*, 2003). Our simulations were carried out on single DNA molecule in confinement conditions. The results showed that in these conditions the two strands were still bound to each although much weaker than in an intact duplex DNA. At its  $T_m$ , up to half of the population of DNA would be single stranded. Therefore extrapolating our inferences from single DNA simulations to a finite number of molecules, we can predict that confinement could increase the population of intact (partial or total) duplex DNA at dissociation temperature. Hence, Macromolecular Confinement may adequately model the effects of Crowding seen in our hybridization experiments. Thermophiles and hyperthermophiles are micro-organisms that have evolutionarily survived in harsh environments with temperatures from 80-150 °C. Many factors have been suggested to influence the heat stability including “thermostable” proteins with a particular preference of certain amino acids (Karantzeni *et al.*, 2003; Sterner *et al.*, 2001), and more importantly, carbohydrate polymers such as cycloamylose (Fujii *et al.*, 2005). However, no reports are yet available to show that Crowding may also stabilize the nucleic acid material in these thermophiles. In our current study, the confining macromolecules in the simulation models resemble cycloamylose-like structures that helped in reducing the distortion of DNA structure when denatured. However, more studies need to be done in this regard. Our data demonstrate how much can be gained if a reversely bioengineered crowded environment is employed in a standard technology that is widely spread in R&D worldwide.

## **11. Macromolecular Crowding of *in vitro* Cell Culture**

### **11.1 Rationale and Aims**

Collagen biosynthesis by fibroblasts in culture is vital for matrix deposition *in vitro*. The extracellular matrix is an important constituent of tissue engineered constructs and has a role to play as a scaffold for cells to stay adherent, survive, multiply and differentiate under appropriate conditions. However, current *in vitro* culture systems are far from being crowded as was pointed out earlier in the thesis as being ‘oceans of dilution’. Therefore the ability of current culture systems to synthesize an effective extracellular matrix is poor. Therefore, this study was designed to identify potential targets for enhancement of matrix deposition in culture and also explore the possibility of speeding up matrix deposition rate *in vitro*.

#### **11.1.1 Collagen Biosynthesis**

When we study the *in vivo* biosynthesis of collagen from its precursor procollagen, as can be appreciated from the schematic shown below (Fig. 38), the first extracellular step is a proteolytic cleavage of the procollagen at its N and C termini by the respective proteinase enzymes that cleave off the N and C propeptides. Once this cleavage is completed, there is a spontaneous non-enzymatic self-assembly of the triple helices of collagen that is entropy driven. This step is followed by an enzymatic cross-linking of the collagen triple helices by another enzyme the lysyl oxidase. Finally the cross-linked collagen gets incorporated into the ECM in association with fibronectin. However, *in vitro*, the collagen deposition is very negligible. This is mainly due to the uncrowded nature of routine standard culture.

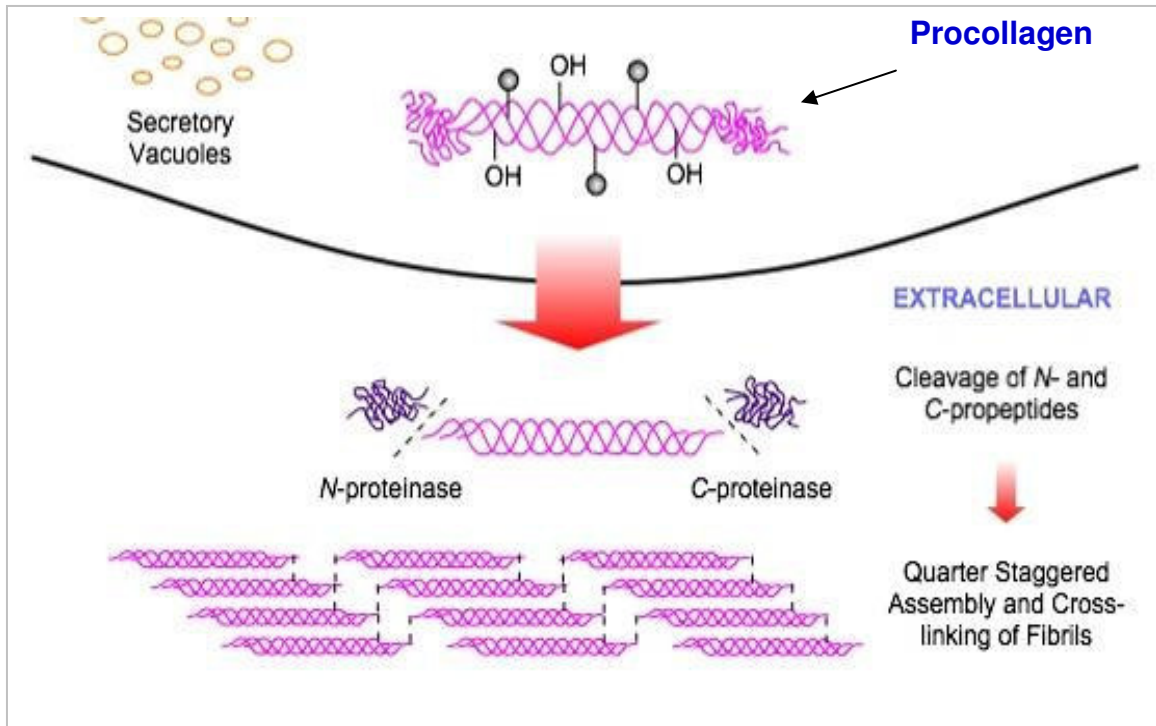


**Figure 38.** Collagen biosynthesis *in vivo*: Upon secretion of procollagen the N and C proteinase cleave the N and C propeptides leaving the triple helices to self-assemble followed up by the lysyl oxidase mediated cross-linking for final deposition into the matrix. *In vitro* the C-proteinase cleavage of procollagen is very slow due to the dilute nature of the culture medium.

The uncrowded state is particularly critical for the procollagen C proteinase and so the activity of this enzyme is extremely low and the reaction is very slow. The procollagen substrate is negatively charged under physiological conditions with a MW of ~360kDa. Hence this enzyme-substrate system involving procollagen C proteinase and procollagen is a potential target for testing the effects of Macromolecular Crowding on the extent of collagen deposition in culture. An approximate estimation of the fraction volume occupancy of macromolecules in the uncrowded culture medium turns out to be less than 1%. This estimate was made taking into account the hydrodynamic sizes of the proteinase enzymes, procollagen substrate, other secreted growth factors etc. Thus crowding the culture medium by macromolecules could enhance macromolecular association reactions.

### 11.1.2 Hypotheses

1. The *in vitro* enzymatic processing of procollagen in the extracellular space can greatly enhanced by Crowding the culture media with macromolecules thereby, greatly enhancing the amount of *in vitro* collagen deposition.
2. Since hydrodynamic radii of anionic macromolecules are greater than neutral macromolecules of similar molecular weights, Crowding effects on the negatively charged Procollagen by Dextran Sulfate (500 kDa; Fig. 39) yield greater matrix formation in fibroblast culture than neutral macromolecules (eg. Ficoll 400 kDa).
3. Since Crowding effects are maximum between like-sized macromolecules, Crowding the culture media with Dextran Sulfate (500 kDa) that is comparable to Procollagen (~360 kDa) yield greater matrix formation in fibroblast culture than relatively smaller macromolecules (eg. Dextran Sulfate 10 kDa).

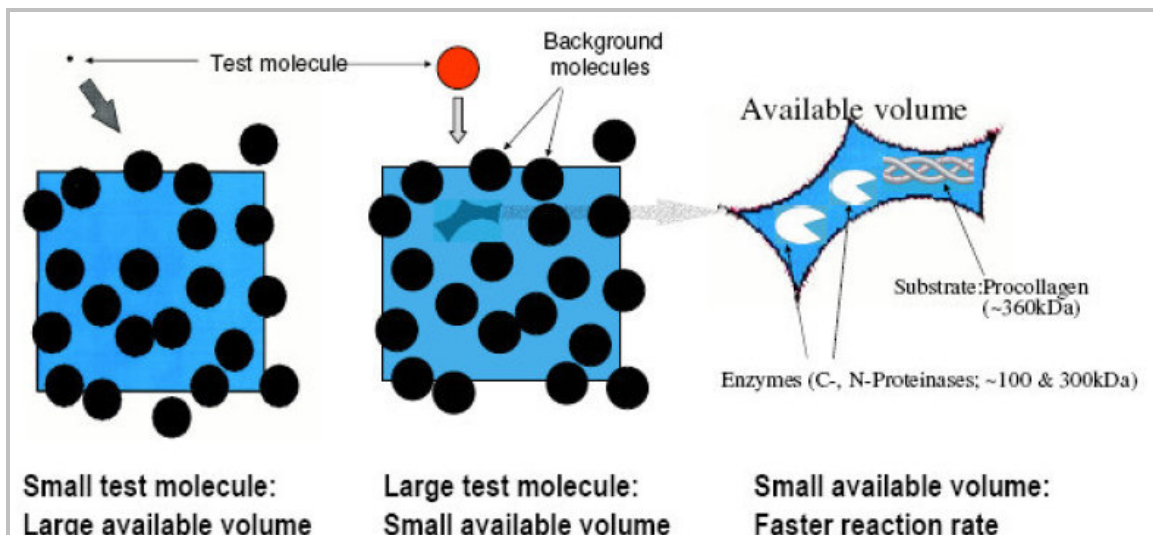


**Figure 39.** Schematic illustration of the proposed hypothesis that like-sized like charge macromolecules can accelerate the proteolytic cleavage of the substrate procollagen by the enzyme C-Proteinase.

## **11.2 Experimental Design, Readouts and Interpretation**

### **11.3 Materials and Methods**

#### **11.3.1 Tissue Culture**

Normal embryonic lung fibroblasts (WI-38; American Tissue Culture Collection, VA) were routinely cultured in Dulbecco's modified Eagle medium with 10% fetal bovine serum, 100 U/ mL of penicillin, and 100 mg/mL of streptomycin (all from GIBCO-Invitrogen, Singapore) at 37°C in a humidified atmosphere of 5% CO<sub>2</sub>. Fibroblasts were seeded at 50,000 cells/ well in 24-well plates (Nalgen Nunc International, NY) and were allowed to attach for 24 h. To induce collagen synthesis cells were supplemented with 100 mM L-ascorbic acid phosphate (Wako Pure Chemical Industries, Osaka, Japan). Macromolecular crowders were dextran sulfate (DxS) (500 kDa; pK Chemicals A/S, Koge, Denmark) and neutral dextran 670 (ND670; FlukaChemie GmbH, CH-9471, Sigma-Aldrich, Steinheim, Germany) and PSS 200(200kDa; Fluka). Crowding treatment was for full 5 days. On day 6 culture media were harvested into separate vials, whereas cell layers were washed twice with Hank's balanced salt solution (HBSS) and both culture medium and washed culture plates (without buffer) were digested with porcine gastric mucosa pepsin (2500 U/mg; Roche Diagnostics Asia Pacific, Singapore) in a final concentration of 100 mg/mL. Samples were incubated at room temperature (RT) for 2 h with gentle shaking followed by neutralization with 0.1 N NaOH.

For volume-reduction experiments, on the second day of culture, the medium was changed to DMEM supplemented with 0.5% FBS, 30µg/ml L-ascorbic phosphate magnesium salt n-hydrate (AcA, Wako) with or without 100µg/ml dextran sulfate (DxS, Amersham Biosciences) in volumes ranging from 50µl to 500µl. After 3 days of



incubation, the culture medium was collected and the cell layer was washed twice with Hank's balanced salt solution (HBSS, Gibco). Both the culture medium and cell layer were treated with 100ug/ml pepsin (200U/mg, Roche Diagnostics GmbH) derived from porcine gastric mucosa. Samples were incubated at room temperature for 2 hours with gentle shaking followed by neutralization with 0.1N NaOH.

### **11.3.2 Sodium Dodecyl Sulfate-Polyacrylamide Gel Electrophoresis (SDS-PAGE)**

Medium and cell layer samples were analyzed by SDS- PAGE under non-reducing conditions. Formats used were either small (Mini-Protean 3; Bio-Rad Laboratories, Singapore) or large (16 -18 cm; SE 600; Hoefer, San Francisco, CA). Protein bands were stained with the SilverQuest kit (Invitrogen) according to the manufacturer's protocol. Densitometric analysis of wet gels was performed on the GS-800 Calibrated Densitometer (Bio-Rad) with the Quantity One v4.5.2 image analysis software (Bio-Rad). Collagen bands were quantitated by defining each band with the rectangular tool with local background subtraction.

### **11.3.3 Immunocytochemistry**

Fibroblasts were seeded on 4-well Lab-Tek chamber slides (Nalge Nunc International) at 50,000 cells/chamber and treated with DxS as described in the preceding text. Cell layers were washed with HBSS and fixed with 2% paraformaldehyde (PFA; Sigma-Aldrich) at RT for 15 min. After washes in phosphate-buffered saline (PBS), nonspecific sites were blocked with 3% bovine serum albumin (BSA; Sigma-Aldrich) in PBS for 30 min. The cells were incubated for 90 min at RT with rabbit anti-human collagen I (AB745; Chemicon International, Temecula, CA) 1:100 in PBS. Bound antibodies were visualized using AlexaFluor488 chicken anti-rabbit in PBS (Invitrogen Molecular Probes, Carlsbad,

CA) for 30 min. Post fixation was in 2% PFA for 15 min. Cell nuclei were counterstained with 4',6'-diamidino-2-phenylindole (DAPI; Invitrogen Molecular Probes) and slides were mounted with polyvinyl alcohol mounting medium containing DABCO (Sigma-Fluka). Images were captured with an Olympus IX-71 inverted epifluorescence microscope (Olympus Corporation, Tokyo, Japan).

#### **11.3.4 Dynamic Light Scattering (DLS) and Viscosity Measurements**

Dextrans and BSA were prepared in HBSS (pH 7.4) in various concentrations. DLS runs were carried out for each of the single macromolecule solution using the DynaPro DLS instrument (DynaPro, Wyatt Technology, Santa Barbara, CA) at 20°C by loading 20 µl samples. Readings were obtained at 825.8 nm and analyzed using the Protein Solutions software (Wyatt Technology). Viscosity was measured at the corresponding concentrations via the ARES100 FRT Rheometer. Based on the viscosity values, necessary corrections were applied for calculating the hydrodynamic radii.

## 11.4 Results

### 11.4.1 Collagen Cleavage and Deposition is greatly enhanced in Crowded Environments

The peptic treatment of culture media and cell layers enabled us to get a clear picture of collagen distribution in both compartments by destroying non-collagenous proteins while leaving fibrillar collagens intact. Our SDS-PAGE conditions were tailored to analyze the presence of collagens I and V, and respective crosslink products of collagen I. Under standard (and ascorbate supplemented) conditions WI-38 fibro-blast cultures showed the majority of the collagen I to be in the medium and small amounts of it in the cell layer (Fig. 40). Densitometry showed an increase of collagen I deposition (based on  $\alpha_{1(I)}$  and  $\alpha_{2(I)}$  bands) by > 6-fold (densitometric data not shown). When the effects of DxS were tested over a concentration range, we found that at 10  $\mu\text{g/ml}$  a significant portion of collagen was still present in the medium fraction, whereas at 500  $\mu\text{g/ml}$ , collagen bands were difficult to resolve in cell layer and medium fraction. Virtually complete collagen deposition and absence of collagen from the medium occurred only in the presence of 50 and 100  $\mu\text{g/mL}$  of DxS (Fig. 41). In separate experiments, the larger neutral dextran did not show an effect from 100  $\mu\text{g/ml}$  up to 2  $\text{mg/ml}$  (Table 8).

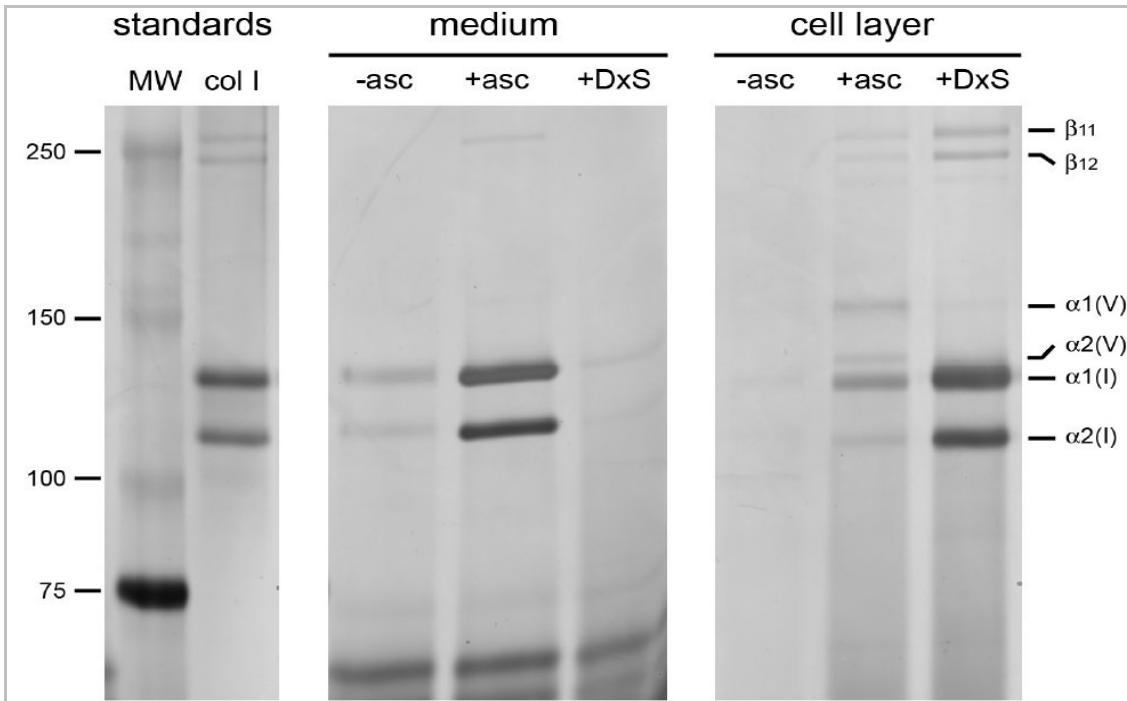


**Figure 40.** Dextran sulfate (DxS) promotes collagen deposition in cultured WI-38 fibroblasts. Silver-stained SDS-PAGE of peptic collagen extracts. DxS dramatically enhanced deposition of collagen onto the cell layer and its concurrent disappearance from the medium. Proportions of collagen V to collagen I are shifted towards collagen I under Crowding. asc, ascorbic acid; MW, molecular weight standard; col I, collagen I standard. (from Lareu *et al. Tiss. Eng.* 2007)

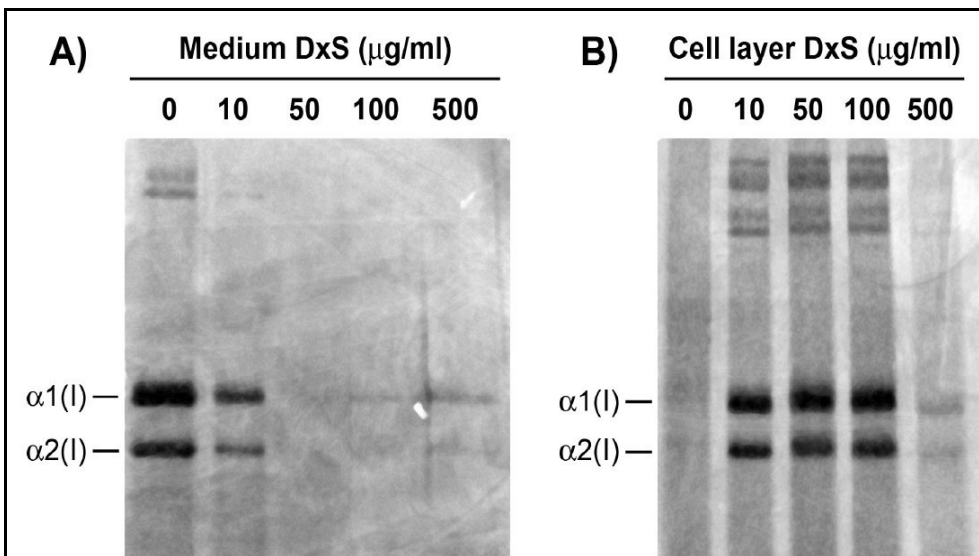


**Figure 41.** Dose-dependent stimulation of collagen deposition by DxS in WI-38 fibroblast culture. Silver-stained SDS-PAGE of peptic collagen extracts in medium (A) and cell layer (B). Maximal collagen deposition was achieved with 50 and 100 mg/mL of DxS in 5 days (Lareu *et al. Tiss. Eng.* 2007).

**Table 8.** Marginal effects of Neutral Dextran 670 on collagen deposition (Lareu *et al.* 2007)

	<i>Standard culture</i>		<i>ND670 (100 µg/mL)</i>		<i>DxS500 (100 µg/mL)</i>	
	<i>Medium</i>	<i>Cell layer</i>	<i>Medium</i>	<i>Cell layer</i>	<i>Medium</i>	<i>Cell layer</i>
	25.2	3.5	17.1	0.5	1.8	14.5
Ratio	7.2	1	34.2	1	1	8
		2 mg/mL	16.1	0.7	—	—
Ratio			23	1	—	—

The morphology of the WI-38 fibroblasts was unaltered in the presence of either dextran. The DxS results were corroborated by the immunocytochemical analysis of both WI-38 cells. In the absence of DxS hardly any deposited collagen was seen. However in the presence of DxS, granular deposits of type 1 collagen were seen around the fibroblasts in mono-layer cultures (Fig. 42).

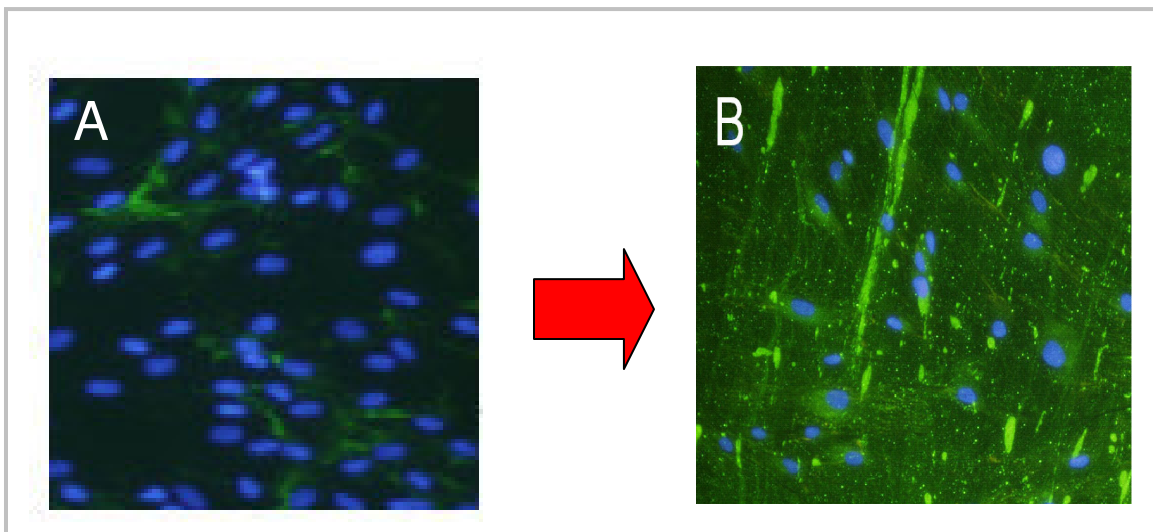


**Figure 42.** Immunocytochemical detection of deposited collagen (green) in the presence of DxS(B) compared to that in the absence of DxS(A). DxS greatly increased the presence of collagen on the cell layer. Nuclei were counterstained with DAPI (blue).

### 11.4.2 Crowding is more than just a “Concentration Effect” on Target Molecules

Macromolecules such as Dextran Sulfate have been shown to enhance matrix deposition in monolayer cultures by accelerating the proteolytic pericellular cleavage of procollagen by volume exclusion effect (EVE). Macromolecules cause volume exclusion due to size and charge effects on like-sized, like-charged ‘test’ molecules such as procollagen. EVE increases the thermodynamic activities of the reactant molecules by more than one order of magnitude (Ellis, 2001). The available volume due to ‘test’ molecules has been shown to be significantly less than the difference of the total and the excluded volumes by theoretical analysis. However, critics argue that the effects of volume exclusion might be seen by a mere reduction of the reaction volume ignoring this basic description of volume exclusion. In this study, the effects of volume exclusion were compared against volume reduction on collagen deposition in cell culture.

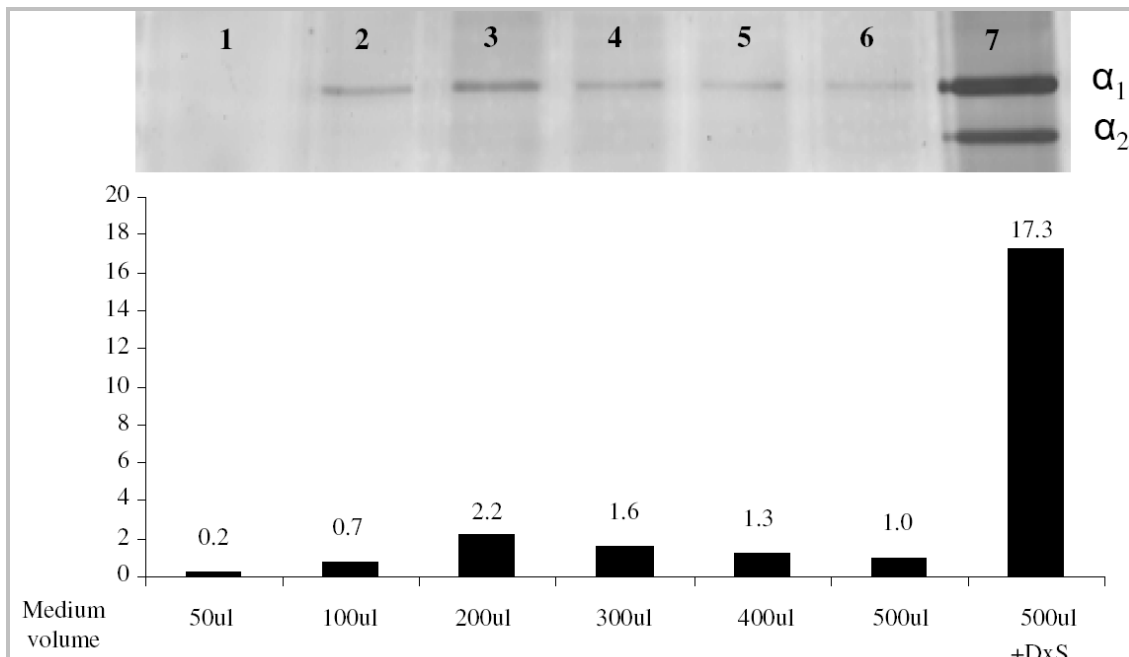


**Figure 43.** SDS-PAGE of cell fractions from cultures grown in reduced media volumes (lanes 1-6) and compared with DxS 500kDa (lane 7). Densitometry analysis of deposited collagen bands from cell fractions, the numbers on top of the bars indicate the fold increase in collagen band intensity normalized to control sample in lane 6 (Picture Courtesy: Prof. M. Raghunath, TML).

SDS-PAGE of the cell layer fractions show (lanes 1-6; Fig. 43) that the collagen bands representing the cultures grown in reduced volumes are much less dense in comparison to lane 7 that represents the DxS treated cells. Analysis of the bands by densitometry (Fig. 43) showed that the maximum yield of deposited collagen with reduced volume was 2.2 units at a volume of 200  $\mu$ l, in comparison to DxS which was 17.3 units at 100  $\mu$ g/ml. The results show clearly that mere volume reduction of even up to 10-folds is unable to enhance deposition of collagen compared to the standard DxS 500 100  $\mu$ g/ml. In fact, volumes of 50  $\mu$ l and 100  $\mu$ l have less deposited than the uncrowded control (Fig. 43).

#### **11.4.4 Charge Characterization for Crowding Potential of Anionic Macromolecules on Collagen Deposition**

It was earlier shown that PSS200 had a higher surface charge density and Zeta potential compared to DxS500. However, whether this translated into a higher volume exclusion effect had to be determined. To test this, the current experiment created crowded conditions due to DxS and PSS on *in vitro* cell culture models and compared using collagen deposition as the readout (Lareu *et al.* 2007b). The results (Fig. 44A) of SDS-PAGE show that of collagen type I deposited under crowded conditions due to PSS was greater than that under DxS500 as visualized by the density of the bands. A densitometry analysis of the bands indicated a two-fold increase in band intensity of collagen due to Crowding by PSS relative to DxS500 (Fig. 44B).

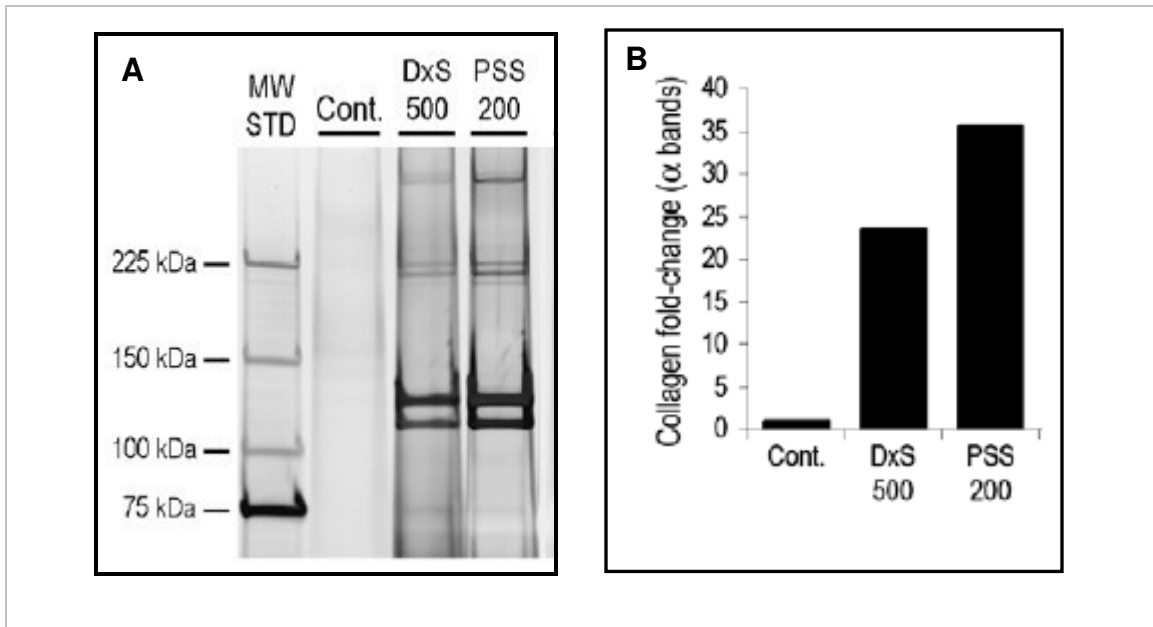


**Figure 44.** PSS is a greater volume excluder than DxS500 leading to greater collagen deposition as shown by collagen 1 bands in SDS-PAGE (A) and a densitometric analysis (B) demonstrating an approximate 2-fold greater collagen deposition than DxS (Lareu *et al.*, *FEBS lett.* 2007).

## 11.5 Discussion

Collagens are the most abundant proteins in the human body and are extremely important also in tissue engineering as adhesion and signaling matrix and creating cohesion between single cells and cell layers. Collagen self-assembles to a water insoluble matrix (fibers; Prockop *et al.* 1998). In routine fibroblast culture, an excess of procollagen in the medium and poor matrix formation results in low productivity for tissue constructs. By applying the biophysical principle of Crowding that problem can be remedied. The data suggest that Crowding of the culture medium with DxS (500 kDa) confined the space of molecules of comparable size and thus increased the interaction of the substrate (procollagen) with respective enzymes for trimming (C and N proteinase, respectively), resulting in an increase of collagen deposited in the matrix. The current



study also observed a significant increase of  $\beta$ -crosslinks with DxS. This suggests the acceleration of an additional enzyme–substrate interaction, namely collagen and lysyl oxidase. This is a copper-dependent enzyme, that catalyses the covalent crosslinking of collagen assemblies (Kagan *et al.* 2003) The current study shows here that it is possible to increase the degree of crosslinking of collagen *in vitro* just by emulating crowded conditions. Although studies have reported that dextran sulfate (500 kDa) is more efficient than PEG (Bateman & Golub, 1990), data from the current study with neutral dextran of comparable size (670 kDa) show that DxS 500 excluded greater volume than ND 670 to accelerate procollagen conversion and lysyl oxidation. Our DLS data point to the hydrodynamic radius as a critical parameter in this regard. Therefore, a negatively charged macromolecule such as DxS 500 is a superior crowder compared to a neutral polymer of similar size under physiologic conditions at similar concentrations.

The current study inferred that DxS in the culture system imposed a combined steric and electrostatic exclusion on the proteins present in the medium. Excluded-volume effect leads to increases in the net free energy of macromolecules in solution (Cheung *et al.* 2005), as well as a much stronger binding between substrates and enzymes, which in our case are procollagen, the respective proteinases and lysyl oxidase. Thus macromolecular Crowding is a useful tool to be utilized in tissue engineering applications (Lareu *et al.* 2007).

The central dogma of the excluded volume effect is that when a certain fraction of volume in a given space is occupied by Crowding macromolecules that have geometrically defined shapes (for example rigid spheres), then the volume excluded thus is always much less than the arithmetic difference of the total and the occupied volume.

As an example, a report (Takahashi *et al.* 2005) showed that when the macromolecules occupy ~30% of the total volume, then, the volume available to a macromolecule to be inserted into this space is less than 1% of the remaining volume (and not 70%!). This is due to the effect of steric repulsion imposed by the macromolecules on neighboring macromolecules. This implies that when we try to reduce the volume by a certain fraction, the thermodynamic activity does not increase appreciably and is very negligible when we compare it with the crowded situation when thermodynamic activity increases by several orders of magnitude (Ellis 2001). In our current study, although the fraction volume occupancy due to 100µg/ml DxS measures to ~5.2%, the actual volume excluded is far higher than this due to the phenomenon of steric repulsion as described above as well as the electrostatic exclusion due to the surface charge on DxS that greatly amplifies the total net volume that is ultimately excluded (Lareu *et al.* 2007). It means that, if one has to mimic the crowded situation by simply reducing the volume, then the amount to be reduced would have to be so very low that it would prohibit the survival of cells and we have observed this in our cell cultures.

Zeta Potential measurements of the anionic macromolecules were correlated with their ability to create effective EVE and thus enhance collagen fibrillogenesis through enzymatic processes (see Fig. 46). Although anionic DxS (500 kDa) and PSS200 have net negative surface charge, PSS demonstrated greater exclusion effect than DxS500 thereby enabling greater procollagen conversion *in vitro*. Earlier investigations in the current study on the surface charge density of DxS and PSS revealed that PSS had a 3 times higher surface charge density and a 3-4 fold higher  $\zeta$ -potential. This would account for the more potent volume exclusion with respect to collagen deposition for PSS even

though the percentage fraction volume occupancy for DxS (500 kDa) was 4.3-fold greater at the same concentration (Lareu *et al.* 2007b). Procollagen, a negatively charged macromolecule (pI of 5.2 at physiological pH of 7.4) would have additional volume exclusion due to electrostatic repulsion, which is a key parameter that influences EVE (Gyenge *et al.* 2003). Therefore, the potency of Crowding with negatively charged macromolecules is the combined effect of steric and electrostatic exclusion.

### **11.5.1 Difficulties of *in vitro* Cell Culture as a Model to study Crowding**

The cell culture is a complex *in vitro* system. By this we mean that the culture itself is a microcosm of a huge number of macromolecules including enzymes and their substrates, structural proteins, complex carbohydrates, signaling factors, growth factors, trace elements, co-factors and so on. While it is obvious that such an environment is an ocean of dilution, it becomes more complicated when the Crowding element is introduced into it. The introduction of Crowding may prove beneficial to many enzyme-substrate reactions, but the critical targets of Crowding depend on a whole lot of variables. In short, the culture environment is heterogeneous in terms of composition and observing the effects of the crowder on its target in isolation becomes very difficult. We can therefore appreciate that the culture environment is ill-defined and interpretation of Crowding effects on target reactions is difficult.

## 12. Final Conclusions and Outlook for the Future

Macromolecular Crowding is a critical missing link between *in vitro* and *in vivo* biology. It was therefore the primary goal of this study to recreate an *in vivo*-like physiological situation for *in vitro* biological systems and then observe the readouts to validate the hypotheses. In order to design, develop and incorporate optimum Crowding conditions to *in vitro* systems, an in-depth estimation of the biophysical parameters of Crowding quantification was done. Many interesting and fascinating phenomena about Crowding such as ‘Self-Crowding’ and ‘Mixed Crowding’ were observed and their implications on *in vitro* biology were recognized. In keeping with the fundamentals of Crowding, an optimum concentration window was identified based on the hydrodynamic radii and surface charge and Crowding applied *in vitro*. Expectedly, the *in vitro* reaction rates were enhanced by Crowding as shown by the readouts in molecular biological reactions. Although the effects of Crowding were significantly observed, more work needs to be done to understand the role of emerging concepts such as mixed macromolecular Crowding. As has been reviewed extensively in current study, life systems both intra- and extra-cellularly are crowded by a heterogeneous population of macromolecules, in essence a mixed crowded situation. However, understanding the mechanics of mixed Crowding is much harder than single-Crowding. This poses a formidable challenge to the Crowding community. Future studies need to be directed in this domain for realizing *in vivo* conditions *in vitro* more closely than current Crowding systems. Molecular modeling of Crowding by confinement models may be a plausible option to develop screening tools to predict the feasibility of applying Crowding in *in*

*in vitro* systems. The main advantages of *a priori* modeling lie in situations where Crowding of complex biological systems is required. Modeling may help explain the mechanisms of Crowding in simulation runs when understanding real-life *in vitro* biology of complex systems becomes highly difficult. The current studies showed how combined *in vitro-in silico* models of Crowding in biology can be useful in applying Crowding for practical applications.

Applications of Crowding in biology are manifold spanning from molecular biology to cell biology and experimental pharmacology to clinical medicine. Crowding effects in the field of drug discovery are yet to be realized on a large scale and this promises to be an exciting area of research in the days to come. The current study has shown how Crowding can be effectively used in molecular biology and tissue engineering applications. Enhancement of molecular biology reactions by Crowding can have immense impact on the way experiments are designed and have the potential to yield highly reliable and sensitive readouts as has been shown. Improving the sensitivity of detection can be of practical value in areas such as molecular diagnostics in clinical medicine, forensic sciences and paleontology. Application of Crowding in regenerative medicine is another exciting field of research in future days.

In summary, Macromolecular Crowding presents itself as a promising tool to realize *in vivo*-like conditions *in vitro* for a wide spectrum of biological, biotechnological and clinical applications. Current research needs to add more information to the knowledge base of macromolecular Crowding, an endeavor that we as biologists and bioengineers need to commit ourselves to.

## 13. References

1. Acerenza, L., & Grana, M. On the origins of a crowded cytoplasm. (2006). *J. Mol. Evol.*, 63, pp. 583-590.
2. Bateman, J.F., Cole, W.G., Pillow, J.J., and Ramshaw, J.A.M. Induction of procollagen processing in fibroblast cultures by neutral polymers. (1986). *J. Biol. Chem.* 261, 4198.
3. Bateman, J.F., and Golub, S.B. Assessment of procollagen processing defects by fibroblasts cultured in the presence of dextran sulfate. (1990). *Biochem. J.* 267, 573,
4. Berg, O. G. The influence of macromolecular Crowding on thermodynamic activity-solubility and dimerization constants for spherical and dumbbell-shaped molecules in a hard-sphere mixture. (1990). *Biopolymers*, 30, pp. 1027-1037.
5. Bird, L., Subramanya, H.S., Wigley, D.B., "Helicases: a unifying structural theme?", (1998). *Curr. Op. Struct. Biol.* 8 (1): 14-18.
6. Bloemendal, H., de Jong, W., Jaenicke, R., Lubsen, N. H., Slingsby, C., & Tardieu, A. Ageing and vision: Structure, stability and function of lens crystallins. (2004). *Prog. Biophys. Mol. Biol.*, 86, pp. 407-485.
7. Bray, D. Signaling complexes: Biophysical constraints on intracellular communication. (1998). *Annu. Rev. Biophys. Biomol. Struct.*, 27, pp. 59-75.
8. Cayley, S., Lewis, B. A., Guttman, H. J., & Record, M. T. Jr. Characterization of the cytoplasm of *Escherichia coli* K-12 as a function of external osmolarity: Implications for protein-DNA interactions *in vivo*. (1991). *J. Mol. Biol.*, 222, pp. 281-300.
9. Chebotareva, N. A., Kurganov, B. I., & Livanova, N. B. Biochemical effects of molecular Crowding. (2004). *Biochemistry (Moscow)*, 69(11), pp. 1239-1251.
10. Cheung, M. S., Klimov, D., & Thirumalai, D. Molecular Crowding enhances native state stability and refolding rates of globular proteins. (2005). *Proc. Natl. Acad. Sci. USA*, 102, pp. 4753-4758.
11. Colclasure, G. C., & Parker, J. C. Cytosolic protein concentration is the primary volume signal in dog red cells. (1991). *J. Gen. Physiol.*, 98, pp. 881-892.
12. Colclasure, G. C., & Parker, J. C. Cytosolic protein concentration is the primary volume signal for swelling-induced [K-Cl] cotransport in dog red cells. (1992). *J. Gen. Physiol.*, 100, pp. 1-10.

13. DePamphilis, M. L. Review: Nuclear structure and DNA replication. (2000). *J. Struct. Biol.*, 129, pp. 186-197.
14. Despa, F., Orgill, D.P., Lee, R. C. Effects of Crowding on the Thermal Stability of Heterogeneous Protein Solutions. *Ann. Biomed. Eng.*. (2005). 33, 1125-31
15. Dobson, C. M., Evans, P. A., & Radford, S. E. Understanding how proteins fold: The lysozyme story so far. (1994). *Trends Biochem. Sci.*, 19, pp. 31-37.
16. Du, F., Zhou, Z., Mo, Z.-Y., Shi, J.-Z., Chen, J., & Liang, Y. Mixed macromolecular Crowding accelerates the refolding of rabbit muscle creatine kinase: Implications for protein folding in physiological environments. (2006). *J. Mol. Biol.*, 364, pp. 469-482.
17. Ebel, C., & Zaccai, G. Crowding in extremophiles: Linkage between solvation and weak protein-protein interactions, stability and dynamics, provides insight into molecular adaptation. (2004). *J. Mol. Recognit.*, 17, pp. 382-389.
18. Eggers, D.K. & Valentine, J.S. Molecular confinement influences protein structure and enhances thermal protein stability. (2001). *Prot. Sci.*, 10, pp. 250-261.
19. Ellis, R. J., & Minton, A. P. Cell biology: Join the crowd. (2003). *Nature*, 425(6953), pp. 27-28.
20. Ellis, R. J. Macromolecular Crowding: An important but neglected aspect of the intracellular environment. (2001a). *Curr. Opinion Struct. Biol.*, 11, pp. 114-119.
21. Ellis, R. J. Macromolecular Crowding: Obvious but underappreciated. (2001b). *Trends Biochem. Sci.*, 26(10), pp. 597-604.
22. Elowitz, M., Surette, M., Wolf, P., Stock, J. & Leibler, S. Protein mobility in the cytoplasm of *Escherichia coli*. (1999). *J. Bacteriol.*, 181(1), pp. 197-203.
23. Fujii, K., Minagawa, H., Terada, Y., Takaha, T., Kuriki, T., Shimada, J and Kaneko, H. Use of Random and Saturation Mutageneses To Improve the Properties of *Thermus aquaticus* Amylomaltase for Efficient Production of Cycloamyloses. *App. Env. Microbiol.* (2005) p. 5823-5827.
24. Fulton, A. B. How crowded is the cytoplasm? (1982). *Cell*, 30, pp. 345-347.
25. Galan, A., Sot, B., Llorca, O., Carrascosa, J. L., Valpuesta, J. M., & Muga, A. Excluded volume effects on the refolding and assembly of an oligomeric protein: GroEL, a case study. (2001). *J. Biol. Chem.*, 276, 957-964.

26. García-Pérez AI, López-Beltrán EA, Klüner P, Luque J, Ballesteros P, Cerdán S. Molecular Crowding and viscosity as determinants of translational diffusion of metabolites in subcellular organelles. (1999). *Arch Biochem Biophys.* 362(2):329-38.
27. Goobes, R., Kahana, N., Cohen, O., & Minsky, A. Metabolic buffering exerted by acromolecular Crowding on DNA-DNA interactions: Origin and physiological significance. (2003). *Biochemistry*, 42, pp. 2431-2440.
28. Goodsell, D.S. The machinery of life. Springer-Verlag, 1993 with kind permission of Springer Science and Business Media.
29. Gribbon, P., Heng, B. C., Hardingham, TE. The molecular properties of hyaluronan investigated by confocal fluorescence recovery after photobleaching. (1999). *Biophys. J.* 77(4): 2210-6.
30. Guigas, G., Kalla, C. & Weiss, M. Probing the nanoscale viscoelasticity of intracellular fluids in living cells. (2007). *Biophys. J.*, 93, pp. 316-323.
31. Guigas, G., Kalla, C., & Weiss, M. The degree of macromolecular Crowding in the cytoplasm and nucleoplasm of mammalian cells is conserved. (2007a). *FEBS Letters*, 581, pp. 5094-5098.
32. Gyenge, C.C., Tenstad, O. and Wiig, H. *In vivo* determination of steric and electrostatic exclusion of albumin in rat skin and skeletal muscle. (2003) *J. Physiol.* 552, 907–916.
33. Hall, D., and Minton, A.P. Macromolecular Crowding: Qualitative and semiquantitative successes, quantitative challenges. (2003) *Biochim. Biophys. Acta* 1649, 127.
34. Hancock, R. A role for macromolecular Crowding effects in the assembly and function of compartments in the nucleus. (2004). *J. Struct. Biol.*, 146, pp. 281-290.
35. Harve, K. S., Lareu, R. R., Rajagopalan, R. & Raghunath, M. Macromolecular Crowding in biological systems: Dynamic light scattering (DLS) to quantify the excluded volume effect. (2006). *Biophys. Rev. Lett.*, 1(3), pp. 317-325.
36. Hatters D. M, Minton A. P, Howlett G. J. Macromolecular Crowding accelerates amyloid formation by human apolipoprotein C-II. (2002). *J Biol Chem.* 277(10):7824-30. Epub 2001 Dec 18.
37. Hiemenz, P. C., Rajagopalan, R. Principles of Colloid and Surface Chemistry. Edition 3; Published by CRC Press, 1997



38. Jarvis, T. C., Ring, D. M., Daube, S. S., & von Hippel, P. H. "Macromolecular Crowding": Thermodynamic consequences for protein-protein interactions within the T4 DNA replication complex. (1990). *J. Biol. Chem.*, 265, pp. 15160-15167.
39. Johnson D. S, Bai L, Smith B.Y, Patel S.S, Wang M. D. Single-molecule studies reveal dynamics of DNA unwinding by the ring-shaped T7 helicase.(2007) *Cell*. 29;129(7):1299-309.
40. Karantzeni, I., Ruiz, C., Liu, C and Licata, V. J. Comparative thermal denaturation of *Thermus aquaticus* and *Escherichia coli* type 1 DNA polymerases. (2003). *Biochem J*. 374, 785-792.
41. Kagan, H.M., and Li, W. Lysyl oxidase: Properties, specificity, and biological roles inside and outside of the cell. (2003). *J. Cell. Biochem*. 88, 660.
42. Kulkarni, S. K., Ashcroft, A. E., Carey, M., Masselos, D., Robinson, C. V. & Radford, S. E. A near-native intermediate on the slow refolding pathway of hen lysozyme. (1999). *Protein Sci.*, 8, pp. 35-44.
43. Lareu, R.R., Arsianti, I., Subramhanya, K.H., Yanxian, P., Raghunath, M. *In vitro* Enhancement of Collagen Matrix Formation and Cross-linking for Applications in Tissue Engineering: A Preliminary Study.(2007) *Tiss. Eng*. 13 (2), 385-391. doi: 10.1089/ten.2006.0224.
44. Lareu, R. R., Subramhanya, K. H., Peng, Y., Benny, P., Chen, C., Wang, Z., Rajagopalan, R., & Raghunath, M. Collagen matrix deposition is dramatically enhanced *in vitro* when crowded with charged macromolecules: The biological relevance of the excluded volume effect. (2007b). *FEBS Letters*, 581, pp. 2709-2714.
45. Lareu R. R., Harve K. S., Raghunath M. Emulating a crowded intracellular environment *in vitro* dramatically improves RT-PCR performance. (2007). *Biochem Biophys Res Commun*. 363(1):171-7. Epub 2007 Sep 5.
46. Lee, L.L., Lee, J.C. Thermal stability of proteins in the presence of poly(ethylene glycols). (1987). *Biochemistry* 26 7813-7819.
47. Li, J., Zhang, S., & Wang, C.-C. Effects of macromolecular Crowding on the refolding of glucose-6-phosphate dehydrogenase and protein disulfide isomerase. (2001). *J. Biol. Chem.*, 276, pp. 34396-34401.
48. Lindner, R., & Ralston, G. Macromolecular Crowding: Effects on actin polymerization. (1997). *Biophys. Chem.*, 66, pp 57-66.
49. Lindner, R., & Ralston, G. Effects of dextran on the self-association of human spectrin. (1995). *Biophys. Chem.*, 57, pp. 15-25.

50. Lomakin, A., Teplow, D. B., Benedek, G. B. Quasielastic Light Scattering for Protein Assembly Studies. *Methods in Molecular Biology*. (2004). 299, 153-174.
51. Matagne, A., Radford, S. E., & Dobson, C. M. Fast and slow tracks in lysozyme folding: Insight into the roles of domains in the folding process. (1997). *J. Mol. Biol.*, 267, pp. 1068-1074.
52. Minton, A. P. Protein folding: Thickening the broth. (2000a). *Curr. Biol.*, 10, pp. R97-R99.
53. Minton, A. P. Influence of macromolecular Crowding upon the stability and state of association of proteins: Predictions and observations. (2005). *J. Pharmaceutical Sci.*, 94, pp. 1668-1675.
54. Minton, A. P., & Wilf, J. Effect of macromolecular Crowding upon the structure and function of an enzyme: Glyceraldehyde-3-phosphate dehydrogenase. (1981). *Biochemistry*, 20, pp. 4821-4826.
55. Minton, A. P., Colclasure, G. C., & Parker, J. C. Model for the role of macromolecular Crowding in regulation of cellular volume. (1992). *Proc. Natl. Acad. Sci. USA*, 89, pp. 10504-10506.
56. Minton, A. P. Quantitative relations between oxygen saturation and aggregation of sickle-cell hemoglobin: Analysis of oxygen binding data. (1976). *Proc. of the Symposium on Molecular and Cellular Aspects of Sickle Cell Disease* (ed. J. I. Hercules, G. L. Cottam, M. R. Waterman and A. N. Schechter), pp. 257-273. Bethesda, MD: U.S. Department of Health, Education and Welfare.
57. Minton, A. P. The influence of macromolecular Crowding and macromolecular confinement on biochemical reactions in physiological media. (2001). *J. Biol. Chem.*, 276, pp. 10577-10580.
58. Minton, A. P. Influence of macromolecular Crowding upon the stability and state of association of proteins: Predictions and observations. (2005). *J. Pharmaceutical Sci.*, 94, pp. 1668-1675.
59. Munishkina, L. A., Cooper, E. M., Uversky, V. N., & Fink, A. L. The effect of macromolecular Crowding on protein aggregation and amyloid fibril formation. (2004). *J. Mol. Recognit.*, 17, pp. 1-9.
60. Owczarzy R, Vallone, P. M., Gallo, F.J., Paner, T. M, Lane, M. J., Benight, A. S. Predicting sequence-dependent melting stability of short duplex DNA oligomers. (1997). *Biopolymers*. 44(3); 217-39.

61. Partikian, A. Iveczky, B. O'. Swaminathan, R Li, Y.. Verkman, A.S. Rapid diffusion of green fluorescent protein in the mitochondrial matrix. (1998). *J. Cell Biol.* 140 821–829.
62. Prockop, D.J., Sieron, A.L., and Li, S.W. Procollagen N-proteinase and procollagen C-proteinase: Two unusual metalloproteinases that are essential for procollagen processing probably have important roles in development and cell signaling. (1998).*Matrix Biol.* 16, 399,
63. Purohit, P. K. ´ Kondev, J., and Rob Phillips. Mechanics of DNA packaging in viruses. (2003). *PNAS.* 100, 6: 3173–3178
64. Radford, S. E., Dobson, C. M., & Evans, P. A. The folding of hen lysozyme involves partially structured intermediates and multiple pathways. (1992). *Nature*, 358, pp. 302-307.
65. Rajendrakumar, C.S., Suryanarayana, T., Reddy, A.R. DNA helix destabilization by proline and betaine: possible role in the salinity tolerance process. (1997). *FEBS Lett.* 410, 201–205.
66. Ralston, G. B. Effects of Crowding in protein solutions. (1990).*J. Chem. Educ.*, 10, pp. 857-860.
67. Ramstein, J., Lavery, R.. Energetic coupling between DNA bending and base-pair opening. (1988). *PNAS.* Vol. 85, 7231-7235.
68. Rasmussen, R., Morrison, T., Hermann, M., Wittwer, C. Quantitative PCR by continuous fluorescence monitoring of a double strand DNA specific binding dye. (1998) *Biochemica.* 2, 8–11.
69. Record, M. T. Jr., Courtenay, E. S., Cayley, S., & Guttman, H. J. Biophysical compensation mechanisms buffering E. coli protein-nucleic acid interactions against changing environments. (1998). *Trends Biochem. Sci.*, 23, pp. 190-194.
70. Ren, G., Lin, Z., Tsou, C.-L., & Wang, C.-C. Effects of macromolecular Crowding on the unfolding and the refolding of D-glyceraldehyde-3-phosphate dehydrogenase. (2003). *J. Prot. Chem.*, 22, pp. 431-439.
71. Rivas, G., Ferrone, F., & Herzfeld, J. (2004). Life in a crowded world: Workshop on the biological implications of macromolecular Crowding. *EMBO reports*, 5, pp. 23-27.
72. Rivas, G., Fernandez, J. A., & Minton, A. P. Direct observation of the self-association of dilute proteins in the presence of inert macromolecules at high concentration via tracer sedimentation equilibrium: Theory, experiment, and biological significance. (1999). *Biochemistry*, 38, pp. 9379-9388.

73. Rivas, G., Fernandez, J. A., & Minton, A. P. Direct observation of the enhancement of noncooperative protein self-assembly by macromolecular Crowding: Indefinite linear self-association of bacterial cell division protein FtsZ. (2001). *Proc. Natl. Acad. Sci. USA*, 98(6), pp. 3150-3155.
74. Rivas, G., Fernandez, J. A., & Minton, A. P. Direct observation of the enhancement of noncooperative protein self-assembly by macromolecular Crowding: Indefinite linear self-association of bacterial cell division protein FtsZ. (2001). *Proc. Natl. Acad. Sci. USA*, 98(6), pp. 3150-3155.
75. Rohwer, J. M., Postma, P. W., Kholodenko, B. N., & Westerhoff, H. V. Implications of macromolecular Crowding for signal transduction and metabolite channeling. (1998). *Proc. Natl. Acad. Sci. USA*, 95, pp. 10547-10552.
76. Ross, P.D A.P. Minton, Analysis of nonideal behaviour in concentrated haemoglobin solutions. (1977). *J. Mol. Biol.* 112 437–452.
77. SantaLucia, J. Jr., Allawi, H.T., Seneviratne P.A. Improved nearest-neighbor parameters for predicting DNA duplex stability. (1996). *Biochem.* 35(11); 3555-62.
78. Sikorav, J.-L., & Church, G. M. Complementary recognition in condensed DNA: Accelerated DNA renaturation. (1991). *J. Mol. Biol.*, 222, pp. 1085-1108.
79. Snoussi K, Halle B. Protein self-association induced by macromolecular Crowding: a quantitative analysis by magnetic relaxation dispersion. (2005) *Biophys J.* 88 (4):2855-66. Epub 2005 Jan 21.
80. Somalinga, B. R., & Roy, R. P. Volume exclusion effect as a driving force for reverse proteolysis: Implications for polypeptide assemblage in a macromolecular crowded milieu. (2002). *J. Biol. Chem.*, 277, pp. 43253-43261.
81. Somero, G. N. Environmental adaptation of proteins: strategies for the conservation of critical functional and structural traits. (1983). *Comp Biochem Physiol A.* 76(3):621-33.
82. Spiess, A.N.. Mueller, N Ivell, R. Trehalose is a potent PCR enhancer: lowering of DNA melting temperature and thermal stabilization of Taq polymerase by the disaccharide trehalose. (2004). *Clin. Chem.* 50, 1256–1259.
83. Spiess, A.N.. Ivell, R.A. Highly efficient method for long-chain cDNA synthesis using trehalose and betaine. (2002). *Anal. Biochem.* 301, 168–174.

84. SpineUniverse.com. (1999-2007). Back pain, neck pain, sciatica – symptoms exercises treatments causes. Retrieved November 21, 2007, from SpineUniverse.com Web site: <http://www.spineuniverse.com/>
85. Steadman, B. L., Trautman, P. A., Lawson, E. Q., Raymond, M. J., Mood, D. A., Thomson, J. A., & Middaugh, C. R. A differential scanning calorimetric study of the bovine lens crystallins. (1989). *Biochemistry*, 28, pp. 9653-9658.
86. Sterner, R. and Liebl, W. Thermophilic adaptation of proteins. (2001) *Crit. Rev. Biochem. Mol. Biol.* 36, 39–106.
87. Thirumalai, D., Klimov, D. K., & Lorimer, G. H. Caging helps proteins fold. (2003). *Proc. Natl. Acad. Sci. USA*, 100, pp. 11195-11197.
88. Tokuriki N, Kinjo M, Negi S, Hoshino M, Goto Y, Urabe I, Yomo T. Protein folding by the effects of macromolecular Crowding. (2004). *Protein Sci.* Jan;13(1):125-33.
89. van den Berg, B., Chung, E. W., Robinson, C. V., Mateo, P. L., & Dobson, C. M. The oxidative refolding of hen lysozyme and its catalysis by protein disulfide isomerase. (1999b). *EMBO J.*, 18, pp. 4794-4803.
90. van den Berg, B., Wain, R., Dobson, C. M., & Ellis, R. J. Macromolecular Crowding perturbs protein refolding kinetics: Implications for folding inside the cell. (2000). *The EMBO J.*, 19(15), pp. 3870-3875.
91. Verkman, A. S. Solute and macromolecule diffusion in cellular aqueous compartments. (2002). *Trends Biochem. Sci.* 27:27–33.
92. Walter, J., Sun, L., & Newport, J. Regulated chromosomal DNA replication in the absence of a nucleus. (1998). *Mol. Cell*, 1, pp. 519-529.
93. Watson, J. D., Hopkins, N. H., Roberts, J. W., Steitz, J. A., & Weiner, A. M. (1987). *Molecular Biology of the Gene*, Vol. 1. Menlo Park, CA: Benjamin Cummings. 4th ed.
94. Weiss, M., Elsner, M., Kartberg, F. & Nilsson, T. Anomalous subdiffusion is a measure for cytoplasmic Crowding in living cells. (2004). *Biophys. J.*, 87(5), pp. 3518-3524.
95. Wenner, J. R, Bloomfield, V. A. Crowding effects on EcoRV kinetics and binding. (1999). *Biophys J.* 77(6):3234-41.

96. Wilf, J., & Minton, A. P. Evidence for protein self-association induced by excluded volume myoglobin in the presence of globular proteins. (1981). *Biochim. Biophys. Acta*, 670, pp. 316-322.
97. Wilhelm, J. Hahn, M and Pingoud, A. Influence of DNA. Target Melting Behavior on Real-Time PCR Quantification. (2000). *Clin chem.* 46(11). Pp 1738-43.
98. Zimmerman, S. B., & Minton, A. P. Macromolecular Crowding: Biochemical, biophysical, and physiological consequences. (1993). *Annu. Rev. Biophys. Biomol. Struct.*, 22, pp. 27-65.
99. Zimmerman, S. B. Macromolecular Crowding effects on macromolecular interactions: Some implications for genome structure and function. (1993). *Biochim. Biophys. Acta*, 1216, pp. 175-185.
100. Zimmerman, S. B., & Murphy, L. D. Macromolecular Crowding and the mandatory condensation of DNA in bacteria. (1996). *FEBS Letters*, 390, pp. 245-248.
101. Zimmerman, S. B., & Harrison, B. Macromolecular Crowding increases binding of DNA polymerase to DNA: An adaptive effect. (1987). *Biochem.*, 84, pp. 1871-1875.
102. Zimmerman, S. B., & Trach, S. O. Macromolecular Crowding extends the range of conditions under which DNA polymerase is functional. (1988a). *Biochim. Biophys. Acta*, 949, pp. 297-304.
100. Zimmerman, S. B., & Trach, S. O. Effects of macromolecular Crowding on the association of *E.coli* ribosomal particles. (1988b). *Nucleic Acids Res.*, 16(14), 6309-6326.
101. Zimmerman, S.B., & Trach, S. O. Estimation of macromolecule concentrations and excluded volume effects for the cytoplasm of *Escherichia coli*. (1991). *J. Mol. Biol.*, 222, 599-620.
102. Zhou, B. R., Liang, Y., Du, F., Zhou, Z. Chen, J. Mixed macromolecular Crowding accelerates the oxidative refolding of reduced, denatured lysozyme: Implications for protein folding in intracellular environments. (2004). *J.Biol.Chem.*, 279, 55109-55116.

# Appendix

---

# BIOPHYSICAL

## Reviews and Letters

Vol. 1 • No. 3 • July 2006

Macromolecular Crowding in Biological  
Systems: Dynamic Light Scattering  
(DLS) to Quantify the Excluded Volume  
Effect (EVE)

K. S. Harve, M. Raghunath, R. R. Lareu and R. Rajagopalan



## MACROMOLECULAR CROWDING IN BIOLOGICAL SYSTEMS: DYNAMIC LIGHT SCATTERING (DLS) TO QUANTIFY THE EXCLUDED VOLUME EFFECT (EVE)\*

KARTHIK S. HARVE and MICHAEL RAGHUNATH†

*Tissue Modulation Laboratory, Division of Bioengineering  
National University of Singapore, Singapore*  
†bierm@nus.edu.sg

RICKY R. LAREU

*Tissue Modulation Laboratory, NUS Tissue Engineering Program  
National University of Singapore, Singapore*  
and  
*Department of Orthopaedic Surgery, Yong Loo Lin School of Medicine  
National University of Singapore, Singapore*

RAJ RAJAGOPALAN

*Department of Chemical and Biomolecular Engineering  
National University of Singapore, Singapore*

Received 30 May 2006

Revised 27 June 2006

Macromolecules crowd defined spaces, thereby excluding other like-sized molecules from the volume they occupy. These excluded-volume effect(s) (EVE) are well characterized for intracellular and partially for extracellular compartments such as blood plasma. We showed that EVE in fibroblast culture leads to faster enzymatic procollagen conversion and matrix deposition. Apparently, EVE can be applied to emulate *in vivo* conditions in an *in vitro* setting. Thus, we attempted to quantitatively capture the crowding potential of various macromolecules using dynamic light scattering under physiological conditions. We found that charged macromolecules like dextran sulfate (negative, 500 kDa) have a hydrodynamic radii of  $46.4 \pm 0.3$  nm i.e.  $\sim 4$  fold larger than that of neutral macromolecules like Ficoll (neutral, 400 kDa) and thus show greater EVE potential. At biologically effective concentrations viscosity was not increased. Unexpectedly, we observed a dramatic drop of hydrodynamic radii of all macromolecules tested above a threshold concentration. This suggested a hyper-crowding state in which the crowders compacted themselves mutually. We will use this hyper-crowding threshold to determine retrogradely rules that allow to predict the conditions for optimum crowding effects (such

\*Paper presented at the Asia and Pacific Workshop on Biological Physics, 3–5 July 2006, National University of Singapore.

†Joint appointment with Department of Biochemistry, Yong Loo Lin School of Medicine, National University of Singapore, Singapore 117576.

as the half-hyper-crowding concentration) in biological systems. We propose Dynamic Light Scattering (DLS) as a potential tool to estimate EVE in biotechnical applications.

**Keywords:** Crowding; excluded-volume effect; hydrodynamic radius; Dynamic Light Scattering.

## 1. Introduction

Volume exclusion is a phenomenon that results from the physical occupation of a finite volume by a population of a given macromolecular species making that space unavailable to other molecule(s). The excluded-volume effect (EVE) of macromolecules in biological systems is referred to as Macromolecular crowding.<sup>1</sup> Crowding is an inevitable phenomenon that results from the large size and shape properties of the macromolecules that exclude volume they occupy, thus denying that space for other molecules.<sup>2</sup> The degree of volume excluded to any molecule sensitively depends on the size of the crowding molecules that are already occupying the available volume (Fig. 1). The term "crowding molecule" here implies that these species do not take part in the "test" reaction in question. A "test" molecule of size very much less compared to the crowding molecules, could spontaneously diffuse and distribute itself in the available volume. However, a test molecule of a size close to that of the crowding molecules has a much reduced available volume (refer to the shaded area shown by grey arrow in Fig. 1).<sup>3</sup>

This reduction of available volume is a consequence of the steric repulsion between the crowding and test macromolecules. The mutual impenetrability between the two species results from the geometric constraints of the individual molecules. Macromolecular crowding influences macromolecular interactions principally by EVE. The earliest work that observed the effects of macromolecular crowding showed exclusion effects of hyaluronic acid on albumin across a dialyzing membrane that was permeable to the smaller albumin but not to hyaluronic acid.<sup>4</sup>

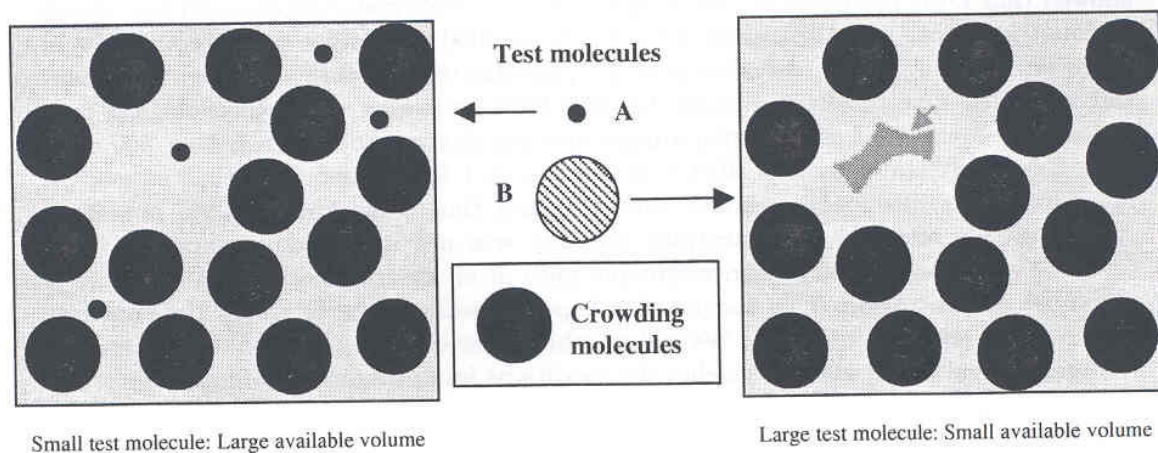


Fig. 1. EVE is determined by the size of test molecules as compared to the crowding molecules in aqueous media. The shaded area (see grey arrow) represents the volume available to the centre of mass of "test" molecule B in presence of crowding molecules.

Because of volume exclusion, albumin was displaced across the membrane partitioning it from hyaluronic acid. This seminal work showed that steric repulsion is an important factor in causing volume exclusion effects. However, at higher concentrations, other factors like viscosity of the solution become significantly high to oppose the effects due to EVE on the macromolecular reaction rates. This maps out a bimodal characteristic of the relationship between the rate constant of a macromolecular reaction and the concentration of the crowder molecule, with an optimum concentration for the rate maximum. This optimum point depends on the size and shape of the macromolecule, the fractional volume occupancy due to the macromolecules and the viscosity of the solution.<sup>5</sup>

The mechanisms of EVE have been explained to be due to lowering of the configurational and conformational entropy of the "test" molecules (reacting molecules of a macromolecular reaction) in a crowded environment (see Fig. 2). The resultant increase in free energy of the system drives the "test" molecules into association. EVE influences macromolecular reaction rates and equilibria by stabilizing the transition-state-complexes which ultimately result in products.<sup>6</sup> Examples of such transition-states are the enzyme-substrate complexes. EVE also drives the protein structures into more compact states, thus stabilizing the native structures and hence improving their function.<sup>7</sup>

Biological systems function in highly crowded environments both at intra- and extra-cellular levels. Crowding, a highly conserved phenomenon in evolution, is found in all life forms, from prokaryotes to multi-cellular organisms.<sup>8</sup> Macromolecules such as DNA and proteins are main crowdors inside the cell, whilst, in the extracellular space, proteins (collagen) and glycosaminoglycans crowd the space.<sup>9</sup> EVE has been appreciated to have manifold effects in biology and there have been excellent reviews to this effect.<sup>10,11</sup> The crowded environment helps in speeding up biological reaction rates, volume-sensing for cellular integrity, DNA structure and function and so on.

Qualitative effects of crowding have been noticed in fibroblast cultures that synthesize collagen and other extracellular matrix proteins *in vitro*. Adding a

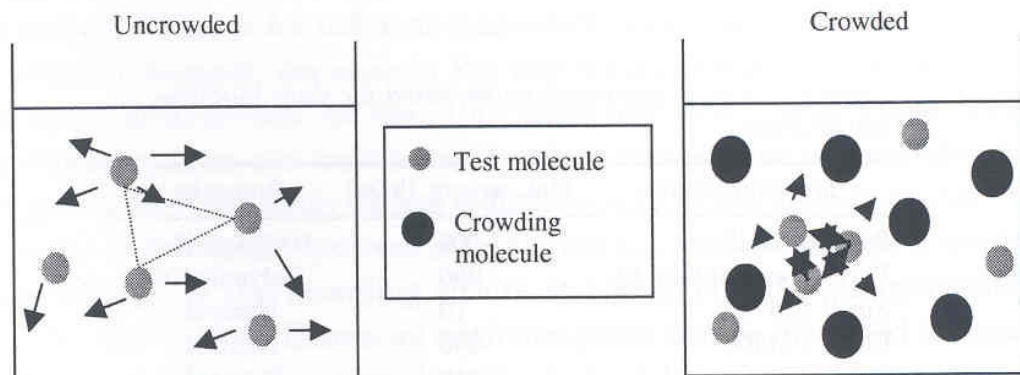


Fig. 2. EVE lowers configurational and conformational entropy of test molecules in the presence of crowding molecules in aqueous media.

crowding macromolecule such as dextran sulfate or polyethylene glycol into the culture medium promotes the processing of secreted procollagen into collagen.<sup>12,13</sup> However, there are quantitative challenges in defining the degree of this "crowdedness". It would greatly benefit biologists if a ready-to-apply relationship between the amount of crowding agent to be added to the reaction medium and the magnitude of excluded volume and hence the biological effects, could be developed. A sound biophysical approach would enable us to determine these parameters and hence predict the optimum crowding concentration.

The current study explores the utility of a biophysical tool, based on light scattering to determine the biophysical profile of the macromolecule solutions which help in understanding the diffusion behavior of macromolecule species and hydrodynamic radii when present at such concentrations that crowd the solution.

## 2. Materials and Methods

### 2.1. Sample preparation

Solutions of macromolecules (see Table 1) covering a series of concentrations were prepared in Hanks Balanced Salt Solution (HBSS) to mimic physiologic conditions of electrolyte concentration and pH.

### 2.2. Dynamic Light Scattering (DLS) methods

Dynamic light scattering experiments were performed at an incident laser wavelength of 8258 Å. Scattering from a 20  $\mu$ l sample of macromolecular solution (20°C) was detected by a photomultiplier tube at 90° and processed by a Flex-99-adn digital correlator. From each run 20 readings were obtained and average values for the hydrodynamic radius determined.

### 2.3. Viscosity measurements

Viscosities of macromolecular solutions at different concentrations were estimated using the *ARES100 FRT Rheometer*.

Table 1. List of macromolecules tested for their biophysical profiles.

Macromolecule	Mol. weight (kDa)	Remarks
Dextran Sulfate	500	Polyanionic
Polystyrene Sulfonate	200	Polyanionic
Ficoll PM70	70	Neutral
Ficoll PM400	400	Neutral
Dextran	410	Neutral
Dextran	670	Neutral

Table 2. Charged macromolecules are larger than neutral macromolecules of similar molecular weight in physiological solutions at concentrations of 100  $\mu\text{g}/\text{ml}$ .

Macromolecule	MW (kDa)	Charge	$R_H$ (nm)
Dextran sulfate	500	Polyanionic	$46.4 \pm 0.3$
Polystyrene Sulfonate	200	Polyanionic	$21.6 \pm 2$
Ficoll PM400	400	Neutral	$13.6 \pm 0.3$
Dextran	670	Neutral	$21 \pm 0.2$

### 3. Results

#### 3.1. *Charged macromolecules have significantly larger hydrodynamic radii compared to neutral macromolecules of similar molecular weights under physiologic conditions*

Dextran sulfate (DxS, polyanionic; 500 kDa) was dissolved in HBSS at increasing concentrations from 100  $\mu\text{g}/\text{ml}$  to 10 mg/ml. Diffusion coefficients and hydrodynamic radii ( $R_H$ ) were determined at each concentration. The mean hydrodynamic radius for DxS is  $\sim 46.4 \pm 0.3$  nm at a concentration of 100  $\mu\text{g}/\text{ml}$  (Table 2). Ficoll PM400 (Fc400, neutral; 400 kDa) was dissolved in HBSS and DLS measured an  $R_H$  of  $\sim 13.6 \pm 0.3$  nm at 100  $\mu\text{g}/\text{ml}$ . Polystyrene Sulfonate, a polyanionic molecule of half the molecular weight of Ficoll 400, still was approximately twice as large as the neutral Ficoll (see Table 2).

#### 3.2. *A concentration-dependent decrease in hydrodynamic radii of crowding macromolecules under physiologic conditions*

As shown in Fig. 3, with increasing concentrations of the crowding agent, at a particular concentration (e.g. 1 mg/ml for DxS), the  $R_H$  dramatically decreases and at 10 mg/ml, there is a three-fold decrease in the  $R_H$ . Similar observations were made for other macromolecules (Fig. 3). The hydrodynamic radii showed a decreasing trend with increasing concentration. The concentration range for this observation was different for different macromolecules. The threshold concentration beyond which a dramatic decrease in  $R_H$  was observed was at 1 mg/ml for DxS500 which is more obvious than for the other three macromolecules tested. Therefore, at these concentrations, the mutual interactions between the macromolecules seem to be triggering an intra-chain folding transition within the macromolecule, thereby increasing the self-diffusion between neighboring macromolecules. As a result, there is an "off-setting" of the crowding effects at higher crowder concentrations (the "hyper-crowding" range). Hence, an optimum point can be identified for maximum EVE without significant viscosity changes at physiologic conditions as shown later in the current study.

## Hydrodynamic radius (nm)

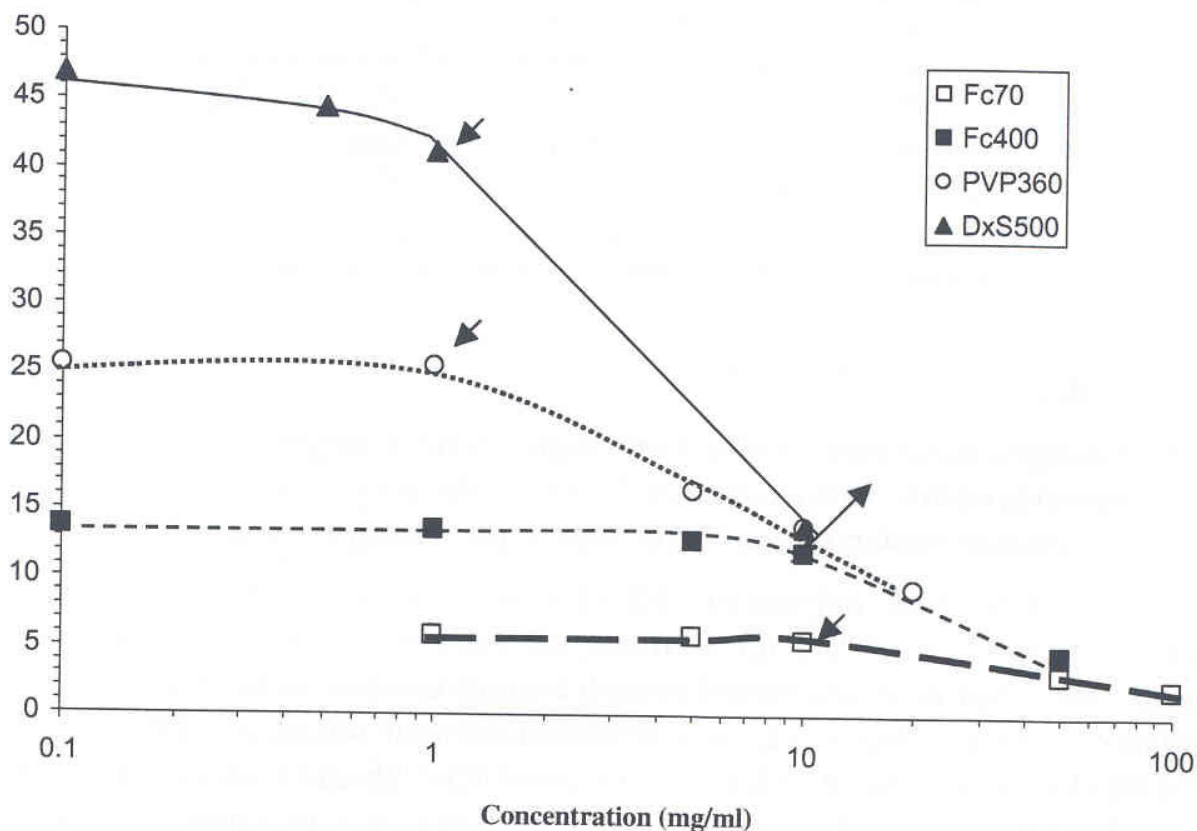


Fig. 3. Concentration dependent decrease in hydrodynamic radii beyond a threshold observed for all the tested macromolecules. The observed thresholds (arrows) were seen at 1 mg/ml for DxS500 and PVP360;  $\sim 10$  mg/ml for Fc400; 12.5 mg/ml for Fc70. Each value is an average of three independent experiments at 20 readings/trial. Threshold for DxS500 and PVP360 is more conspicuous than for the other two macromolecules tested.

### 3.3. A retrograde approach from the "hyper-crowding point" identifies onset-of-crowding concentrations of macromolecule in physiological solutions

From our previous results (Fig. 3), it could be inferred that actual crowding onset might be occurring at much lower concentrations from the "hyper-crowding" point. To validate this hypothesis, another series of concentrations of Ficoll PM70 were made in HBSS in the range 1 mg/ml to 2.5 mg/ml (as shown in Fig. 4). Interestingly, the hydrodynamic radius shows a slight but significant increase while going from 1 to 1.5 mg/ml and stabilizes between 1.5 to 2 mg/ml. It then falls off at concentrations  $> 2$  mg/ml. In case of DxS500, there is an increase of  $R_H$  going from 50 to 100  $\mu\text{g/ml}$ . It then decreases at 200  $\mu\text{g/ml}$  and further reduces at higher concentrations as shown earlier, these higher concentrations marking the thresholds beyond which this decrease in  $R_H$  becomes more apparent. Similar observations were made for Fc400 also (between 200  $\mu\text{g/ml}$  to 300  $\mu\text{g/ml}$ ; graph not shown). PVP 360 is yet to be tested for this behavior.

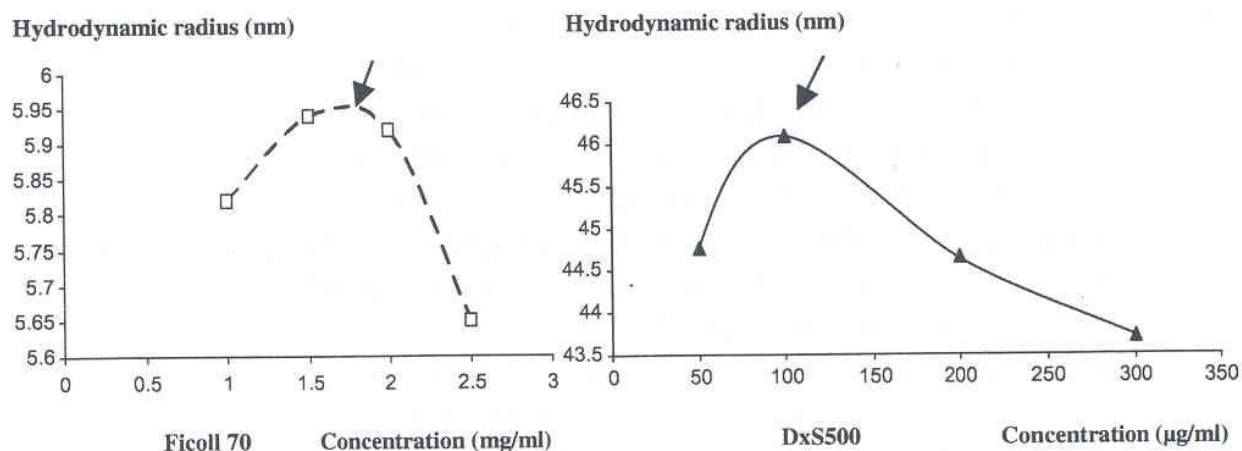


Fig. 4. Points of maxima (arrow) can be observed due to an apparent increase in hydrodynamic radius resulting from slowing of diffusion in the concentration range 1 mg/ml to 2.5 mg/ml of Fc70 and 100  $\mu\text{g/ml}$  to 200  $\mu\text{g/ml}$  of DxS500 in HBSS. Such a behavior was also observed for Fc400 at  $\sim 200 \mu\text{g/ml}$  to 300  $\mu\text{g/ml}$  (graph not shown) and yet to be tested for PVP360.

#### 4. Discussion

Our current study suggests that the application of macromolecules as crowding agents has to consider the structural flexibility of these molecules for determining the concentrations, that they may be used at in biology (e.g., in culture media). Comparing DxS500 and Fc400 with MW close to each other (500 & 400 kDa respectively), it is appreciated that charge screening effects of HBSS on DxS notwithstanding, there is still more than three-fold difference in  $R_H$  of DxS compared to Fc400. This tells us that, a charged macromolecule such as DxS could be a better crowder compared to a neutral polymer of similar size under physiologic conditions for similar concentrations. In other words, this implies that for the same volume occupancy, far less DxS molecules are required than that for Fc400 and hence a lower concentration of the charged macromolecule compared to a neutral molecule for similar crowding effects. This might be advantageous, because at high concentrations macromolecular solutions tend to be more viscous which is undesirable.

An interesting observation was made, when a concentration series of the macromolecules in physiological solutions was subjected to DLS. With increasing concentrations of the crowding agent, beyond a particular concentration (e.g. 1 mg/ml for DxS), the  $R_H$  dramatically decreases. These observations can be explained by the "hyper-crowding" effect. By this term, we mean that, as the concentration of the macromolecules increases, individual molecules begin to interact with each other and this triggers an intra-chain-folding-transition within the macromolecules since they are not rigid hard spheres. Such observations have been made in earlier studies.<sup>14,15</sup> Therefore, it is important to determine the point at which there is a large decrease in hydrodynamic size (hyper-crowding) and then work back in a retrograde manner from this point to identify an optimum crowding concentration (for example, at the half-point maximum of hyper-crowding). This is determined by

the size and the number density (to estimate fractional volume occupancy) of the macromolecules. This compaction effect of individual molecules on neighbouring molecules suggests that within this concentration range of the crowder in solution, crowding is forcing the structural folding of the macromolecular chain. If the macromolecules were rigid hard spheres, then the effects of crowding would have been to reduce the diffusion of molecules rather than size reduction. However, the concentration range at which the structural changes are seen suggest that the system is a crowded environment in this range. The other inference from our studies is that since molecular flexibility probably counters the mutual interactions and in doing so, offsets the crowding itself, it is important to know at what point and beyond this happens, so that unnecessarily high concentrations of the crowders in solution need not be used. But it has to be noted here that these observations pertain to a single macromolecular species system, which, in the present case, is a physiologic (HBSS) solution of the crowder. It has to be seen whether a system of two or more different species of macromolecules mixed in solution ("Mixed Macromolecular crowding")<sup>16</sup> also demonstrates a similar behavior.

The hydrodynamic radius of Ficoll 70 shows an increase while going from 1 to 1.5 mg/ml and stabilizes between 1.5 to 2 mg/ml. It then falls off at concentrations  $> 2$  mg/ml. This marks out a "maximum point" of the value of the hydrodynamic radius at the concentration 1.5–2 mg/ml as a result of decrease in diffusion of the molecules which are at mutual interactions with each other just below this concentration point ( $< 1.5$  mg/ml). This hints at possible onset of crowding at this point (see arrow in Fig. 4). Similarly, for DxS500, a peak in  $R_H$  is observed between 100–200  $\mu$ g/ml in HBSS. In the case of Fc400, such a maxima for the  $R_H$  was observed in the range 200–300  $\mu$ g/ml. PVP360 will be tested for this behavior as well. Further studies to confirm this phenomenon for mixed macromolecular solutions are due. However, a corollary that can be inferred from this observation is that in this concentration window, (where viscosity was marginally higher than 1cP, which is very close to that of water), the slowing of diffusion that was observed could be attributed solely to EVE with no contribution from any viscosity changes. This agrees with theory that the effects of crowding on diffusion is determined by EVE that predominates at lower concentrations, whereas at higher concentrations the opposing effects of viscosity become dominant.<sup>17</sup>

An earlier study on molecular crowding in intracellular compartments demonstrated that diffusion depends on EVE independently of viscosity.<sup>18</sup> Therefore, by studying diffusion behavior of solutions at concentrations which have viscosities close to water would help us in determining the contribution of EVE alone in decreasing the diffusion of the macromolecules. Hence, the concentrations at the maxima of hydrodynamic radius could well mark the neighborhood for the range of crowding concentrations for Fc70, Fc400 and DxS500. A combined knowledge of the hydrodynamic radius-maxima and the hyper-crowding points would therefore enable tailoring an appropriate crowding concentration range for a given single macrosolute in solution.



## Acknowledgments

The following grants and funding are gratefully acknowledged: NUS Tissue Engineering Program, Start-up grants R-397-000-604-101(Provost), R-397-000-604-712 (Office of Life Sciences). KH is a recipient of a PhD scholarship from the Division of Bioengineering, NUS. Special thanks to Mr. Jobichen Chacko, PhD scholar, and Assistant Professor J. Sivaraman, Department of Biological Sciences, NUS, for their kind support and help in carrying out the light scattering experiments.

## References

1. N. A. Chebotareva, B. I. Kurganov and N. B. Livanova, *Biochemistry* **69**, 1239 (2004).
2. D. Hall and A. P. Minton, *Biochem. Biophys. Acta* **1649**, 127 (2003).
3. A. P. Minton, *J. Biol. Chem.* **276**, 10577 (2001).
4. A. G. Ogston and C. F. Phelps, *Biochem. J.* **78**, 827 (1960).
5. R. J. Ellis, *Trends Biochem. Sci.* **26**, 597 (2001).
6. S. Schnell and T. E. Turner, *Progress in Biophysics & Molecular Biology* **85**, 235 (2004).
7. M. S. Cheung, D. Klimov and D. Thirumalai, *Proc. Natl. Acad. Sci. USA* **102**, 4753 (2005).
8. R. Goobes, N. Kahana, O. Cohen and A. Minsky, *Biochemistry* **42**, 2431 (2003).
9. R. J. Ellis, *Curr. Op. Struct. Biol.* **11**, 114 (2001).
10. S. B. Zimmerman and A. P. Minton, *Ann. Rev. Biophys. Biomol. Struct.* **22**, 27 (1993).
11. A. P. Minton, *Curr. Biol.* **10**, R97 (2000).
12. J. F. Bateman, W. G. Cole, J. J. Pillow and J. A. Ramshaw, *J. Biol. Chem.* **261**, 4198 (1986).
13. I. Arsianti, R. R. Lareu, K. Harve, S. Joshi and M. Raghunath, *Proc. Int. Federation for Medical and Biol. Engng.* **12**, 105 (2005).
14. J. R. Wenner and V. A. Bloomfield, *Biophys. J.* **77**, 3234 (1999).
15. N. Tokuriki, M. Kinjo, S. Negi, M. Hoshino, Y. Goto, I. Urabe and T. Yomo, *Prot. Sci.* **13**, 125 (2004).
16. B. R. Zhou, Y. Liang, F. Du, Z. Zhou and J. Chen, *J. Biol. Chem.* **279**, 55109 (2004).
17. L. A. Munishkina, E. M. Cooper, V. N. Uversky and A. L. Fink, *J. Mol. Recognit.* **17**, 1 (2004).
18. A. I. Garcia-Perez, E. A. Lopez-Beltran, P. Kluner, J. Luque, P. Ballesteros and S. Cerdan, *Arch. Biochem. Biophys.* **362**, 329 (1999).

# *In Vitro* Enhancement of Collagen Matrix Formation and Crosslinking for Applications in Tissue Engineering: A Preliminary Study

RICKY R. LAREU, Ph.D.,<sup>1,2</sup> IRMA ARSIANTI,<sup>1</sup> HARVE KARTHIK SUBRAMHANYA, M.D.,<sup>1</sup> PENG YANXIAN,<sup>1</sup> and MICHAEL RAGHUNATH, Ph.D., M.D.<sup>1,3</sup>

## ABSTRACT

The construction of stable engineered tissue depends on the formation of a functional connective tissue produced by cells locally. A major component of connective tissue is collagen. Its deposition into a stable matrix depends on the enzymatic extracellular conversion of procollagen to collagen. This step is very slow *in vitro* and we hypothesized that this is due to a lack of crowdedness and insufficient excluded volume effect (EVE) in culture media. We used neutral (670 kDa) and negatively charged dextran sulfate (DxS, 500 kDa) to create EVE in cell cultures and to enhance *in vitro* matrix formation by accelerating procollagen conversion. Biochemical analyses in 2 human fibroblast lines revealed mostly unprocessed procollagen in uncrowded culture medium, whereas in the presence of DxS, procollagen conversion occurred and most of the collagen was associated with the cell layer. Immunocytochemistry confirmed DxS-related collagen deposition that colocalized with fibronectin. The large neutral dextran showed, in identical concentration ranges, no effects that correlated well with its smaller hydrodynamic radius as determined by dynamic light scattering. This predicted a 10 times bigger crowding power of DxS and benchmarks it as a potentially promising crowding agent facilitating the formation of extracellular matrix *in vitro*.

## INTRODUCTION

THE DEPOSITION OF A COLLAGEN MATRIX depends on the conversion of de novo synthesized procollagen to collagen in the extracellular space or immediately before its release into the same.<sup>1</sup> This limiting step for collagen matrix deposition is very slow *in vitro* both in monolayer cultures and in 3D scaffolds.<sup>2,3</sup> Surprisingly, this knowledge is not widespread in the tissue engineering field, and many research groups measure the amount of collagen I in culture media, where it actually does not belong.<sup>4</sup> Obviously, this culture artifact represents a serious bottleneck in the creation of coherent and stable tissue structures before implantation or

for *in vitro* systems (e.g., in drug discovery). We hypothesized that this *in vitro* deficit stems from a deficiency in crowding of standard culture media. It is well known that biological systems function as highly crowded intra- and extracellular environments. Crowding is an inevitable phenomenon that results from the large size and shape properties of the macromolecules that exclude volume they occupy, thus making that space unavailable for other molecules.<sup>5</sup> Macromolecular crowding causes the excluded-volume effect (EVE) that has been appreciated to have manifold effects in biology.<sup>6</sup> It has been mostly characterized for the interior of cells, but this principle works also in the extracellular environment. Cells are embedded in the extracellular

<sup>1</sup>Tissue Modulation Laboratory, Division of Bioengineering, Faculty of Engineering, National University of Singapore, Singapore.

<sup>2</sup>NUS Tissue Engineering Program, Department of Orthopedic Surgery, Yong Loo Lin School of Medicine, National University of Singapore, Singapore.

<sup>3</sup>Department of Biochemistry, Yong Loo Lin School of Medicine, National University of Singapore, Singapore.

matrix (ECM), which consists of the largest macromolecules present in the human body.<sup>7</sup> Cells isolated from tissues are in a totally different environment in standard cell culture. Derived from a highly complex and dense ECM, they are now bathed in large volumes of aqueous medium and have little associated ECM. The only exogenous source of macromolecules in cell culture is fetal calf serum, a crucial additive for cell survival and continued replication. It contains ca. 80 g/L of protein, a concentration that can cause significant crowding effects.<sup>8</sup> However, used at 10% (v/v) in routine cell culture the final protein concentration reaches only ca. 8 g/L. Clearly, standard routine culture media are far from being crowded.

Scarce literature had indicated earlier that the addition of midsized neutral polymers such as dextran T-40 (40 kDa) and small polyethylene glycol (3.35 kDa) accelerated the processing of procollagen and its deposition.<sup>9</sup> The negatively charged dextran sulfate (DxS; 500 kDa) was later described to be more efficient in comparison to the above very much smaller neutral crowders.<sup>10</sup> These data were never followed up for biotechnical applications. Our preliminary study with 2 fibrogenic human cell lines significantly extend these data with regard to quantitation and immunocytochemical localization of collagen. In addition, we show for the first time dynamic light scattering data that explain the dramatic differences in the crowding potential of 2 differently charged but comparably sized macromolecular dextrans in our read-out system, collagen deposition.

## MATERIALS AND METHODS

### *Tissue culture*

Normal embryonic lung fibroblasts (WI-38; American Tissue Culture Collection, VA) and adult hypertrophic scar fibroblasts (HSF) were routinely cultured in Dulbecco's modified Eagle medium with 10% fetal bovine serum, 100 U/mL of penicillin, and 100 µg/mL of streptomycin (all from GIBCO-Invitrogen, Singapore) at 37°C in a humidified atmosphere of 5% CO<sub>2</sub>. Fibroblasts were seeded at 50,000 cells/well in 24-well plates (Nalgen Nunc International, NY) and were allowed to attach for 24 h. To induce collagen synthesis cells were supplemented with 100 µM L-ascorbic acid phosphate (Wako Pure Chemical Industries, Osaka, Japan). Macromolecular crowders were dextran sulfate (DxS) (500 kDa; pK Chemicals A/S, Koge, Denmark) and neutral dextran 670 (ND670; FlukaChemie GmbH, CH-9471, Sigma-Aldrich, Steinheim, Germany). In selected experiments the lysyl oxidase inhibitor β-aminopropionitrile (BAPN; Sigma-Aldrich, St. Louis, MI) was included. Crowding treatment was for full 5 days. On day 6 culture media were harvested into separate vials, whereas cell layers were washed twice with Hank's balanced salt solution (HBSS) and both culture medium and washed culture plates (without buffer) were digested with porcine gastric mucosa pepsin (2500 U/mg;

Roche Diagnostics Asia Pacific, Singapore) in a final concentration of 100 µg/mL. Samples were incubated at room temperature (RT) for 2 h with gentle shaking followed by neutralization with 0.1 N NaOH.

### *Sodium dodecyl sulfate-polyacrylamide gel electrophoresis (SDS-PAGE)*

Medium and cell layer samples were analyzed by SDS-PAGE under nonreducing conditions as described earlier (T = 5%, C 2.66%).<sup>11</sup> Formats used were either small (Mini-Protean 3; Bio-Rad Laboratories, Singapore) or large (16×18 cm; SE 600; Hoefer, San Francisco, CA). Protein bands were stained with the SilverQuest™ kit (Invitrogen) according to the manufacturer's protocol. Densitometric analysis of wet gels was performed on the GS-800™ Calibrated Densitometer (Bio-Rad) with the Quantity One v4.5.2 image analysis software (Bio-Rad). Collagen bands were quantitated by defining each band with the rectangular tool with local background subtraction.

### *Protein extraction and Western blotting*

Medium was harvested and washed cell layers were extracted with a buffer containing 150 mM NaCl, 50 mM Tris (pH 7.5), 5 mM EDTA (pH 8.0), 1% Triton-X100, and Protease Inhibitor Cocktail tablets (Roche Diagnostics Asia Pacific, Singapore). Subsequently, 20 µL of protein extract (even cell numbers) for each sample were mixed with 1×Laemmli buffer and 2 µL of β-mercaptoethanol and subjected to small format SDS-PAGE as described in the preceding text. Proteins were then electroblotted onto a nitrocellulose membrane (Bio-Rad) with the Mini Trans-Blot® transfer cell (Bio-Rad) according to the manufacturer's protocol. Membranes were blocked with 5% nonfat milk (Bio-Rad) in TBST pH 8 (20 mM Tris-base–150 mM NaCl–0.05% Tween-20) for 1 h at RT. Subsequently, the primary antibody (mouse anti-human collagen I; Monosan, Uden, The Netherlands) at a 1:500 dilution with 1% nonfat milk in TBST was incubated for 1 h at RT. Bound primary antibody was detected with goat anti-mouse HRP (Pierce Biotechnology, Rockford, IL) diluted 1:1000 in 1% nonfat milk in TBST for 1 h at RT. The membrane was then incubated with Super Signal® West Dura substrate (Pierce Biotechnology) and chemiluminescence was captured via an LAS-1000 Luminescent Image Analyzer (Fuji Photo Film, Tokyo, Japan).

### *Immunocytochemistry*

Fibroblasts were seeded on 4-well Lab-Tek™ chamber slides (Nalge Nunc International) at 50,000 cells/chamber and treated with DxS as described in the preceding text. Cell layers were washed with HBSS and fixed with 2% paraformaldehyde (PFA; Sigma-Aldrich) at RT for 15 min. After washes in phosphate-buffered saline (PBS), nonspecific sites were blocked with 3% bovine serum albumin (BSA; Sigma-

Aldrich) in PBS for 30 min. The cells were incubated for 90 min at RT simultaneously with rabbit anti-human collagen I (AB745; Chemicon International, Temecula, CA). 1:100 in PBS and mouse anti-human fibronectin (F7387; Sigma-Aldrich) 1:200 for 90 min. Bound antibodies were visualized using AlexaFluor488 chicken anti-rabbit and AlexaFluor546 goat anti-mouse 1:400 in PBS (Invitrogen Molecular Probes, Carlsbad, CA) for 30 min. Postfixation was in 2% PFA for 15 min. Cell nuclei were counterstained with 4',6-diamidino-2-phenylindole (DAPI; Invitrogen Molecular Probes) and slides were mounted with polyvinyl alcohol mounting medium containing DABCO (Sigma-Fluka). Images were captured with an Olympus IX-71 inverted epifluorescence microscope (Olympus Corporation, Tokyo, Japan).

### Cell enumeration

WI-38 fibroblasts were seeded on optically clear 24-well Lumox™ plates (Greiner Bio-One, Frickenhausen, Germany) and treated with DxS as described. In parallel and to ensure linearity of the assay 5000–200,000 cells/well were seeded in triplicate to generate calibration points. The cells on the calibration plate were washed in HBSS and fixed in prechilled (–20°C) methanol for 10 min, air dried, and stored at 4°C, whereas the DxS cultures were fixed on day 6 as described earlier. Fixed cell layers on calibration plate and treatment plate were then stained in parallel with DAPI in PBS (1 µg/mL) 30 min to stain nuclei. After 3 PBS washes, the cells were kept in a minimal volume of PBS. Blank wells containing unstained cells served as background for read-out with a PHERAstar microplate reader (BMG LABTECH, VIC, Australia) with excitation/emission wavelengths of 340/460 nm.

### Dynamic light scattering (DLS) and viscosity measurements

Dextrans and BSA were prepared in HBSS (pH 7.4) in various concentrations. DLS runs were carried out for each of the single macromolecule solution using the DynaPro DLS instrument (DynaPro™, Wyatt Technology, Santa Barbara, CA) at 20°C by loading 20-µL samples. Readings were obtained at 8258 Å and analyzed using the Protein Solutions™ software (Wyatt Technology). Viscosity was measured at the corresponding concentrations via the ARES100 FRT Rheometer. Based on the viscosity values, necessary corrections were applied for calculating the hydrodynamic radii.

## RESULTS

### Dextran sulfate promotes collagen deposition in vitro

The peptic treatment of culture media and cell layers enabled us to get a clear picture of collagen distribution in both compartments by destroying noncollagenous proteins while

leaving fibrillar collagens intact. Our SDS-PAGE conditions were tailored to analyze the presence of collagens I and V, and respective crosslink products of collagen I. Collagen III is in fibroblast culture of low abundance and better visualized using metabolic (radioactive) labeling.<sup>12</sup> Under standard (and ascorbate supplemented) conditions WI-38 and HSF fibroblast cultures showed the majority of the collagen I to be in the medium and small amounts of it in the cell layer (Fig. 1). Densitometry showed an increase of collagen I deposition (based on  $\alpha_{1(I)} + \alpha_{2(I)}$  bands) by > 6-fold for WI-38 and > 11-fold for HSF (not shown) (Fig. 1, densitometric data not shown). When we tested the effects of DxS over a concentration range, we found that at 10 µg/mL a significant portion of collagen was still present in the medium fraction, whereas at 500 µg/mL, collagen bands were difficult to resolve in cell layer and medium fraction. Virtually complete collagen deposition and absence of collagen from the medium occurred only in the presence of 50 and 100 µg/mL of DxS (Fig. 2). In separate experiments, the larger neutral dextran did not show an effect from 100 µg/mL up to 2 mg/mL (Table 1). The morphology of the WI-38 fibroblasts was unaltered in the presence of either dextran.

The DxS results were corroborated by the immunocytochemical analysis of both HSF (Fig. 3) and WI-38 cells (data not shown). In standard culture double-staining immunofluorescence revealed strong reticular fibronectin signal on the cell layer (Fig. 3c) with scant and wispy collagen I staining almost at background levels (Fig. 3b). In the presence of DxS, the fibronectin meshwork was coarser (Fig. 3f). Collagen I was present on the cell layer in the form of small and large aggregates (Fig. 3e) and now gave a strong signal and major colocalization with fibronectin.

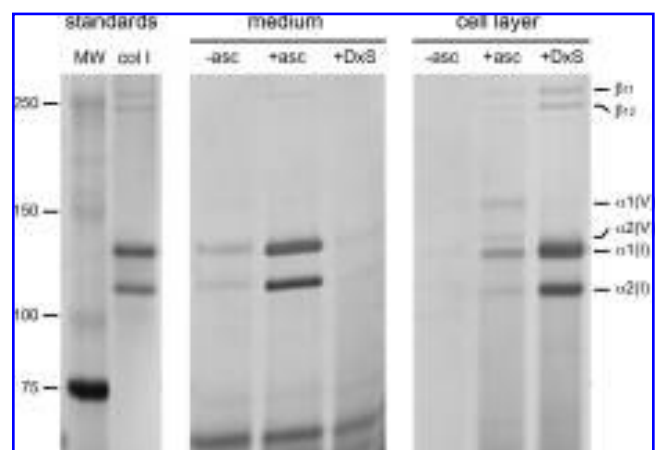


**FIG. 1.** Dextran sulfate (DxS) promotes collagen deposition in cultured WI-38 fibroblasts. Silver-stained SDS-PAGE of peptic collagen extracts. DxS dramatically enhanced deposition of collagen onto the cell layer and its concurrent disappearance from the medium. Proportions of collagen V to collagen I are shifted towards collagen I under crowding. asc, ascorbic acid; MW, molecular weight standard; col I, collagen I standard.

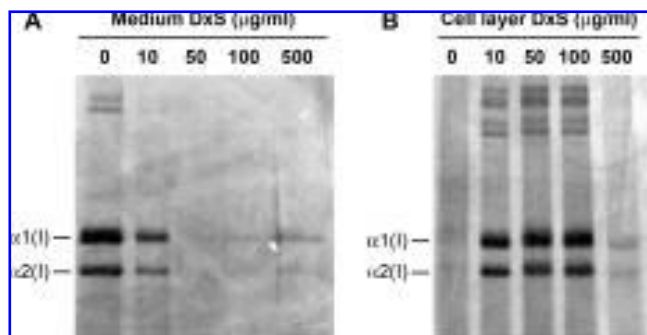


**FIG. 2.** Dose-dependent stimulation of collagen deposition by Dxs in WI-38 fibroblast culture. Silver-stained SDS-PAGE of peptic collagen extracts in medium (A) and cell layer (B). Maximal collagen deposition was achieved with 50 and 100  $\mu\text{g}/\text{mL}$  of Dxs in 5 days.

#### Assessment of effects of Dxs on fibroblast proliferation

Adherent cytometry using DAPI and a microplate reader was highly linear and accurate over the cell density range (not shown) and showed that Dxs slightly reduced proliferation at the optimum concentration for procollagen conversion (50 and 100  $\mu\text{g}/\text{mL}$ ) but more pronounced at 500  $\mu\text{g}/\text{mL}$  (Fig. 4).

#### Dextran sulfate increases collagen-related enzymatic processes in vitro

To demonstrate that the increased collagen deposition in the presence of Dxs is due to correct enzymatic processing, total proteins from culture medium and cell layer fractions were analyzed by immunoblotting using a collagen antibody that recognizes the central portion of the molecule.

**TABLE 1.** MARGINAL EFFECTS OF NEUTRAL DEXTRAN 670

	Standard culture		ND670 (100 $\mu\text{g}/\text{mL}$ )		Dxs500 (100 $\mu\text{g}/\text{mL}$ )	
	Medium	Cell layer	Medium	Cell layer	Medium	Cell layer
Ratio	25.2	3.5	17.1	0.5	1.8	14.5
	7.2	1	34.2	1	1	8
		2 mg/mL	16.1	0.7	—	—
Ratio			23	1	—	—

Densitometric adjusted volume values of collagen ( $\alpha_{1(I)} + \alpha_{2(I)}$  bands) of silver-stained SDS-PAGE minigels of peptic collagen extracts from WI-38 fibroblasts. Note the inversion of the medium/cell layer ratio in the presence of Dxs 500 whereas ND670 not only failed to increase collagen deposition but also appeared to interfere with baseline deposition seen in standard culture.

Standard cultures contained collagen only in the form of procollagen in the medium, no procollagen or collagen was detectable in the cell layer (Fig. 5). In the presence of Dxs, only converted collagen was detected in the cell layer; the medium was devoid of either procollagen or collagen. This could only have been the result of specific activity of procollagen C and N proteinases. Increased lysyl oxidase activity in the presence of Dxs which produces large molecular weight dimers known as  $\beta$ -dimers, specifically  $\beta_{11}$  and  $\beta_{12}$  was evident and could be reduced by up to 60% by BAPN (Fig. 6A). This calculation was based on the ratio of the total intensity of  $\beta$ -dimers ( $\beta_{11}$  and  $\beta_{12}$ ) and that of  $\alpha$ -chains ( $\alpha_1(I)$  and  $\alpha_2(I)$ ) (Fig. 6B).

#### Hydrodynamic radius and viscosity measurements

DLS is a method of estimating the diffusion of macromolecules that are in brownian motion in solution and hence their hydrodynamic radii by measuring the change in inten-

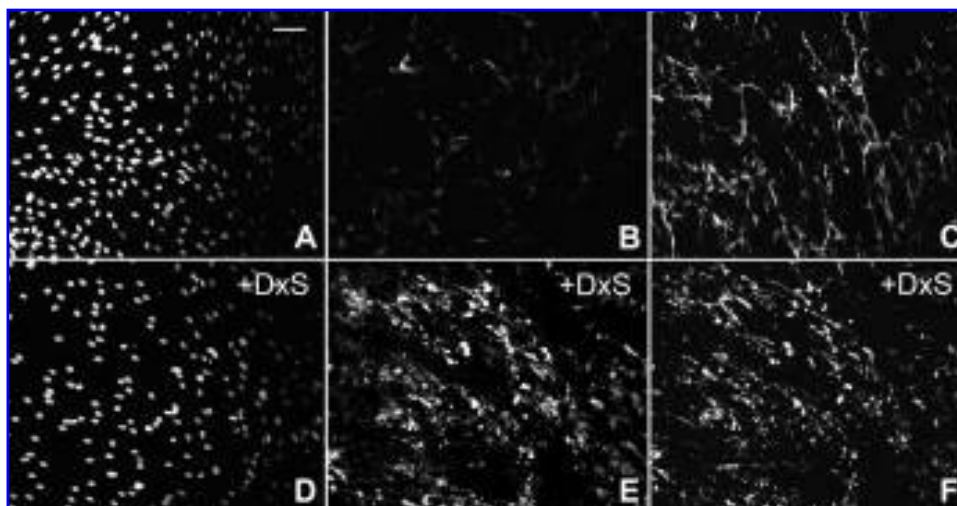


**FIG. 3.** Immunocytochemical detection of deposited collagen in the presence of Dxs. Fibronectin (C, F) and collagen I (B, E) as detected by double immunofluorescence in HSF cultures. Dxs (+Dxs) greatly increased the presence of collagen on the cell layer. Nuclei were counterstained with DAPI (A, D). Magnification,  $\times 10$ ; scale bar in (a) = 50  $\mu\text{m}$ .

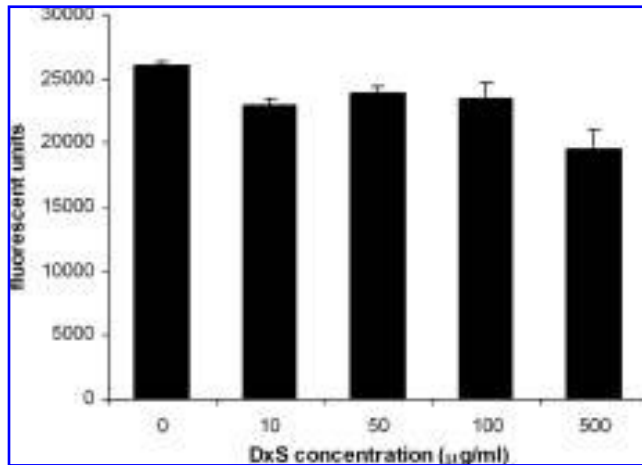


**FIG. 4.** Fluorescent adherent cytometry in the presence of DxS. DxS reduced the proliferation of WI-38 fibroblasts over 5 days significantly but to a small degree. More conspicuous reduction observed with DxS concentration of 500 µg/mL.

sity of scattered light over time.<sup>13</sup> In physiological salt solution and at concentration of 100 µg/mL the hydrodynamic radii were  $46.4 \pm 0.3$  nm (DxS 500),  $21 \pm 0.2$  nm (ND670), and  $4.24 \pm 0.05$  nm (BSA, 67 kDa). Viscosity of solutions were ca. 1 cP in all cases, equaling that of water. The data demonstrate that a negatively charged macromolecule has a much larger hydrodynamic radius than a neutral macromolecule of comparable size. This suggests a stronger crowding efficiency as EVE due to DXS is a combination of both steric repulsion and electrostatic repulsion, compared to only steric repulsion by neutral molecules.<sup>14</sup>

**DISCUSSION**

Collagens are the most abundant proteins in the human body and are extremely important also in tissue engineering

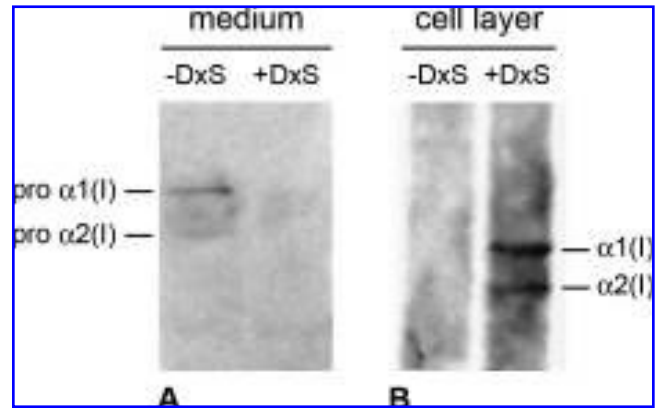


**FIG. 5.** Procollagen conversion is induced by DxS *in vitro*. Western blotting analysis of collagen type I in HSF culture. In the absence of DxS, unprocessed procollagen was observed in the medium fraction (A) and in the presence of DxS collagen was observed in the cell layer (B) indicating increased C and N proteinase activity.

as adhesion and signaling matrix and creating cohesion between single cells and cell layers.<sup>15</sup> The bulk of collagen is represented by the fibrillar collagen I. It is synthesized by mesenchymal cells and exported into the extracellular space as water-soluble procollagen. The subsequent proteolytic removal of the C- and N-terminal propeptide converts procollagen to collagen. Only collagen can self-assemble to a water insoluble matrix (fibers).<sup>16</sup> A low procollagen conversion rate is the default state of cell culture systems, which means an excess of procollagen in the culture medium and poor collagen matrix formation resulting in low productivity for tissue building. We demonstrate here by applying the biophysical principle of EVE that this cell culture-intrinsic problem can be overcome. The data suggest that crowding of the culture medium with DxS (500 kDa) confined the space of molecules of comparable size and thus increased the interaction of the substrate

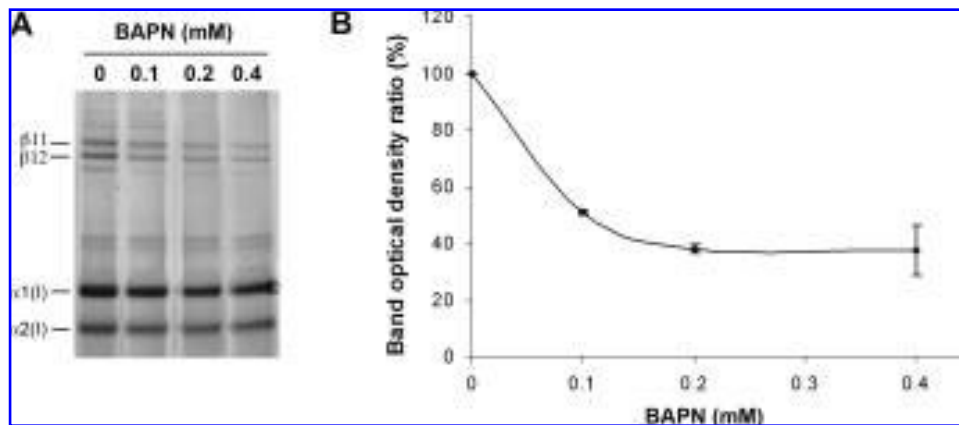


**FIG. 6.** Augmented lysyl oxidase activity in the presence of DxS. Silver-stained SDS-PAGE. (A) Clear occurrence of crosslinked collagen α-chain dimers (β<sub>11</sub> and β<sub>12</sub>) (B) Dimer formation was reduced by BAPN to 40% (densitometry) based on the ratio of β<sub>(11+2)</sub> to α<sub>(1+2)</sub> bands.

(procollagen) with respective enzymes for trimming (C and N proteinase, respectively), resulting in an increase of collagen deposited in the matrix and a massive decrease of procollagen in culture medium. We also observed a significant increase of  $\beta$  crosslinks with DxS. This suggests the acceleration of an additional enzyme–substrate interaction, namely collagen and lysyl oxidase. This is a copper-dependent enzyme, that catalyses the covalent crosslinking of collagen assemblies.<sup>17</sup> Recent attempts were made to accelerate this enzymatic activity in blood vessel tissue engineering by adding more copper ions to culture media.<sup>18</sup> This led to an increased crosslinking of collagen; however, it took several weeks after an initial lag phase. We show here that it is possible to increase dramatically the crosslinking status of collagen *in vitro* just by emulating crowded conditions within a matter of days without the needs of further supplements.

Interestingly, EVE appeared also to influence the ratios between collagen types deposited into the collagen matrix. Ascorbate supplemented fibroblasts under standard conditions showed basal deposition of collagen I and V, suggesting the presence of heterotypic fibrils with substantial collagen V content. However, in the presence of DxS collagen V was hardly detectable and collagen I become the dominant collagen type. Immunohistochemistry revealed that the typically seen reticular pattern of deposited fibronectin<sup>19</sup> not only changed under crowding but also that there was a major colocalization of collagen and fibronectin. In fact, fibronectin deposition has been described as a prerequisite to collagen deposition (on fibronectin).<sup>1</sup> Thus, we have reason to assume that we have created more physiological conditions in our system by macromolecular crowding.

Initially, the increased conversion of procollagen in metabolically labeled fibroblast cultures was shown in the presence of mid-sized dextran T-40 and small polyethylene glycol (3.35 kDa).<sup>9</sup> Although later studies suggested the very much larger dextran sulfate (500 kDa) to be more efficient than the originally introduced crowders,<sup>10</sup> no data with similarly sized neutral dextran were generated up to now. In our direct comparison, DxS 500 outperformed ND 670 dramatically in its ability to accelerate procollagen conversion and lysyl oxidation. Our DLS data point to the hydrodynamic radius as a key figure to explain this phenomenon. At 100  $\mu\text{g}/\text{mL}$  DxS showed a 2.21-fold larger  $R_h$  than ND670, which translates into a 10.8-fold larger volume due to charge effects and hydration. Therefore, a negatively charged macromolecule such as DxS 500 is a superior crowder compared to a neutral polymer of similar size under physiologic conditions at similar concentrations. This implies that for the same volume occupancy, far fewer DxS molecules are required than that for ND670 and thus lower concentrations. We would deem this advantageous because at high concentrations macromolecular solutions tend to be undesirably viscous. Looking into serum proteins as potential crowding agents, we studied serum albumin (67 kDa), representing roughly 60% of serum proteins. In standard (10% FCS) culture conditions its

predicted concentration would be 5 mg/mL. According to its hydrodynamic radius its volume would be 1300 times smaller than that of DxS 500, and to achieve the same crowding effect as DxS 500 it would have to be present at a concentration as high as 130 mg/mL, up to almost 3 times higher than to be found in pure serum.

For the concentration that showed optimal procollagen conversion, we calculated an occupied volume of 5% for 100  $\mu\text{g}/\text{mL}$  DxS by (1) calculating the volume of the sphere of each DxS molecule from the hydrodynamic radius and (2) based on the number of DxS molecules present at the given concentration and the molar weight of each DxS molecule. Obviously, this volume occupancy was sufficient to accelerate at least 3 enzymatic steps for collagen deposition and stabilization. We speculate that DxS in our system imposed a steric exclusion effect on the proteins present in the medium, resulting in their spatial confinement. This would lead to the increase in the total free energy of macromolecules in solution, as well as a much higher strength of interaction between substrates and enzymes, in this case procollagen, the respective proteinases and lysyl oxidase.

We conclude that EVE is a valuable factor to be included in tissue engineering applications and that negatively charged macromolecular crowders such as DxS will have an important role to play in the construction of tissues.

## ACKNOWLEDGMENTS

The authors thank Dr. Phan Toan Thang (Department of Surgery, Yong Loo Lin School of Medicine, NUS) for the kind donation of HSF. M.R. acknowledges support by the NUS Tissue Engineering Program (NUSTEP) and the Office of Life Sciences. This work was supported by grants from the National Medical Research Council of Singapore (NMRC grant CPG/003/2004), the Faculty of Engineering, Office of Research FRC grant R-397-000-017-112, and a start-up grant from the Office of Life Science (R-397-000-604-712) and the Provost of NUS (R-397-000-604-101). I.A. was a recipient of a graduate research scholarship from the Graduate Program in Bioengineering and the Division of Bioengineering, NUS.

## REFERENCES

1. Canty, E.G., and Kadler, K.E. Procollagen trafficking, processing and fibrillogenesis. *J. Cell Sci.* **118**, 1341, 2005.
2. Goldberg, B., and Sherr, C.J. Secretion and extracellular processing of procollagen by cultured human fibroblasts. *Proc. Natl. Acad. Sci. USA* **70**, 361, 1973.
3. Nusgens, B., Merrill, C., Lapiere, C., and Bell, E. Collagen biosynthesis by cells in a tissue equivalent matrix *in vitro*. *Collagen Rel. Res.* **4**, 351, 1984.
4. Lareu, R.R., Joshi, S., Lim B., and Raghunath, M. Essential pre-treatment of tissue culture medium for the accurate

- quantitation of collagen for tissue engineering: Pitfalls and solutions for the usage of the colorimetric Sircol Collagen Assay. *Tissue Eng.* Submitted.
5. Hall, D., and Minton, A.P. Macromolecular crowding: Qualitative and semiquantitative successes, quantitative challenges. *Biochim. Biophys. Acta* **1649**, 127, 2003.
  6. Minton, A.P. Protein folding. Thickening the broth. *Curr. Biol.* **10**, R97, 2000.
  7. Laurent, T.C. An early look at macromolecular crowding. *Biophys. Chem.* **57**, 7, 1995.
  8. Ellis, R.J. Macromolecular crowding: obvious but underappreciated. *TIBS* **26**, 597, 2001.
  9. Bateman, J.F., Cole, W.G., Pillow, J.J., and Ramshaw, J.A.M. Induction of procollagen processing in fibroblast cultures by neutral polymers. *J. Biol. Chem.* **261**, 4198, 1986.
  10. Bateman, J.F., and Golub, S.B. Assessment of procollagen processing defects by fibroblasts cultured in the presence of dextran sulfate. *Biochem. J.* **267**, 573, 1990.
  11. Raghunath, M., Steinmann, B., DeLozier-Blanchet, C., Extermann, P., and Superti-Furga, A. Prenatal diagnosis of collagen disorders by direct biochemical analysis of chorionic villus biopsies. *Pediatr. Res.* **36**, 441, 1994.
  12. Mackay, K., Raghunath, M., Superti-Furga, A., Steinmann, B., and Dalgleish, R. Ehlers-Danlos syndrome type IV caused by Gly400Glu, Gly595Cys and Gly1003Asp substitutions in collagen III: Clinical features, biochemical screening, and molecular confirmation. *Clin. Genet.* **49**, 286, 1996.
  13. Schurr, J.M. Dynamic light scattering of biopolymers and biocolloids. *CRC Crit. Rev. Biochem.* **4**, 371, 1977.
  14. Harve, K.S., Lareu, R.R., Rajagopalan, R., and Raghunath, M. Macromolecular crowding in biological systems: dynamic light scattering (DLS) to quantify the excluded volume effect (Eve). *Biophys. Rev. Lett.* 2006, in press.
  15. Lanza, R.P., Langer, R., and Vacanti, J. *Principles of Tissue Engineering*, 2nd ed. San Diego, London: Academic Press, 2000.
  16. Prockop, D.J., Sieron, A.L., and Li, S.W. Procollagen N-proteinase and procollagen C-proteinase: Two unusual metalloproteinases that are essential for procollagen processing probably have important roles in development and cell signaling. *Matrix Biol.* **16**, 399, 1998.
  17. Kagan, H.M., and Li, W. Lysyl oxidase: Properties, specificity, and biological roles inside and outside of the cell. *J. Cell. Biochem.* **88**, 660, 2003.
  18. Dahl, S.L., Rucker, R.B., and Niklason, L.E. Effects of copper and cross-linking on the extracellular matrix of tissue-engineered arteries. *Cell Transplant.* **14**, 367, 2005.
  19. Raghunath, M., Tschödrich-Rotter, M., Sasaki, T., Chu, M.-L., Meuli, M., and Timpl, R. Confocal scanning analysis of the association of fibulin-2 with elastic microfibrils in normal and regenerating skin. *J. Invest. Dermatol.* **112**, 97, 1999.

Address reprint requests to:

*Michael Raghunath, M.D., Ph.D.*

*Division of Bioengineering, Faculty of Engineering*

*and Department of Biochemistry*

*Yong Loo Lin School of Medicine*

*Division Office Block EA 03-12*

*9 Engineering Dr. 1*

*Singapore 117576*

*E-mail: bierm@nus.edu.sg*





# Collagen matrix deposition is dramatically enhanced *in vitro* when crowded with charged macromolecules: The biological relevance of the excluded volume effect

Ricky R. Lareu<sup>a,b</sup>, Karthik Harve Subramhanya<sup>a</sup>, Yanxian Peng<sup>a</sup>, Paula Benny<sup>a</sup>, Clarice Chen<sup>a</sup>, Zhibo Wang<sup>a</sup>, Raj Rajagopalan<sup>c</sup>, Michael Raghunath<sup>a,d,\*</sup>

<sup>a</sup> Tissue Modulation Laboratory, Division of Bioengineering, Faculty of Engineering, National University of Singapore, Singapore

<sup>b</sup> NUS Tissue Engineering Program, Department of Orthopedic Surgery, Yong Loo Lin School of Medicine, National University of Singapore, Singapore

<sup>c</sup> Department of Chemical and Biomolecular Engineering, Faculty of Engineering, National University of Singapore, Singapore

<sup>d</sup> Department of Biochemistry, Yong Loo Lin School of Medicine, National University of Singapore, Division Office Block EA# 03-12, 9 Engineering Dr. 1, Singapore 117576, Singapore

Received 23 February 2007; revised 4 April 2007; accepted 8 May 2007

Available online 21 May 2007

Edited by Felix Wieland

**Abstract** The excluded volume effect (EVE) rules all life processes. It is created by macromolecules that occupy a given volume thereby confining other molecules to the remaining space with large consequences on reaction kinetics and molecular assembly. Implementing EVE in fibroblast culture accelerated conversion of procollagen to collagen by procollagen C-proteinase (PCP/BMP-1) and proteolytic modification of its allosteric regulator, PCOLCE1. This led to a 20–30- and 3–6-fold increased collagen deposition in two- and three-dimensional cultures, respectively, and creation of crosslinked collagen footprints beneath cells. Important parameters correlating with accelerated deposition were hydrodynamic radius of macromolecules and their negative charge density.

© 2007 Published by Elsevier B.V. on behalf of the Federation of European Biochemical Societies.

**Keywords:** Excluded volume effect; Macromolecular crowding; Extracellular matrix; Collagen deposition; Procollagen C-proteinase

## 1. Introduction

Tissue engineering combines cell biology and materials science to provide therapeutic strategies for the generation of tissues *in vitro* and/or *in vivo* when situations result in complete

organ failure or ineffectual natural or augmented repair processes. As with every cell culture, be it two- or three-dimensional, cells are isolated from preexisting tissue. They are either terminally differentiated or show various degrees of “stemness” e.g. adult bone marrow-derived and embryos. The isolation and seeding process removes the harvested cells from a context of highly complex and dense arrays of macromolecules, the extracellular matrix (ECM), and places them abruptly onto a naked or thinly-coated tissue culture plastic while being bathed in large volumes of non-crowded aqueous medium. This situation is far from physiological given the fact that the total concentration of protein and RNA inside pro- and eukaryotic cells is in the range of 300–400 g/l [1–3] and that the extracellular space is usually dominated by dense arrays of ECM macromolecules. Even blood has a solute concentration of 80 g/l [4]. The addition of fetal calf serum in routine culture media, however, fails to create a crowded environment [5]. As the cells are confronted with an environment devoid of ECM they start to rebuild their environment by producing their own ECM. While fibronectin is deposited rapidly *in vitro* [6], the deposition of a collagen matrix, the primary structural biological material in all tissues and organs, is enzymatically rate-limited. As the current culturing practices are characterized by a lack of macromolecular crowding and hence excluded volume effect (EVE), the procollagen conversion and as a consequence, collagen matrix deposition, is notoriously slow *in vitro* [5]. Many weeks are needed to create cohesive tissue sheets that contain sufficient ECM [7]. This represents a major bottle-neck in tissue engineering and impedes the studies of ECM formation *in vitro*. In order to overcome this obstacle we tested a series of polymeric macromolecules for their ability to exclude volume and speed-up specific enzymatic steps required for collagen deposition *in vitro*.

## 2. Materials and methods

### 2.1. Tissue culture

Low passage (3–8) normal primary embryonic lung fibroblasts (WI-38; American Tissue Culture Collection, VA, USA) were routinely cultured as outlined in Lareu et al. [5]. Fibroblasts were seeded on 24-well plates at 50000/well and the following day the media was

\*Corresponding author. Address: Division of Bioengineering, Faculty of Engineering and Department of Biochemistry, Yong Loo Lin School of Medicine, National University of Singapore, Division Office Block EA# 03-12, 9 Engineering Dr. 1, Singapore 117576, Singapore. Fax: +65 6872 3069.

E-mail address: bierm@nus.edu.sg (M. Raghunath).

URL: [www.tissuemodulation.com](http://www.tissuemodulation.com)

**Abbreviations:** EVE, excluded volume effect; PCP, procollagen C-proteinase; ECM, extracellular matrix; DxS, dextran sulfate; PSS, polysodium-4-styrene sulfonate; Fc, Ficoll™; PLLA, poly L-lactic acid; PCOLCE1, PCP enhancer protein 1; DAPI, 4',6-diamidino-2-phenylindole; DLS, dynamic light scattering; MMP2, matrix metalloproteinase 2

replaced with 0.5% FBS, 100  $\mu$ M of L-ascorbic acid with or without macromolecules. The macromolecules employed were 500 kDa dextran sulfate (DxS) and 10 kDa DxS at 100  $\mu$ g/ml (pK Chemicals A/S, Koge, Denmark), 200 kDa polysodium-4-styrene sulfonate (PSS) at 100  $\mu$ g/ml (Sigma–Aldrich, Singapore), 400 kDa Ficolll™ (Fc) and 70 kDa Fc at 50 mg/ml (Amersham Pharmacia, Uppsala, Sweden). The medium and cell layer fractions were harvested separately. Collagen from medium, cell layer and footprints was extracted with pepsin under acidic conditions [5]. For footprint analysis, cell layers were washed twice with HBSS and solubilized three times with 0.5% sodium deoxycholate (Sigma–Aldrich) on ice for 10 min as outlined in [8].

### 2.2. Three-dimensional (D) culture and bioreactors

250 000 WI-38 fibroblasts were seeded onto either Biobrane® (3.5 cm diameter) (Bertek Pharmaceuticals Inc, WV, USA) or poly L-lactic acid ( $25 \times 50 \times 3$  mm) (PLLA, 0410-2  $\times$  45; Transome Inc., FL, USA) felt scaffolds in 6 well plates and cultured routinely in 10% FBS for 1 and 2 days, respectively. For static treatment, ascorbic acid and with or without 100  $\mu$ g/ml of DxS 500 kDa were supplemented and incubated for 3 and 5 days, respectively. The PLLA scaffolds were placed in modular parallel-plate bioreactors design according to Gemmiti and Guldberg [9] and incubated initially as for static culture following transfer to the bioreactor modules for 5 days. Treatments were as for

static culture. Bioreactor flow rate was 0.2 ml/min. After culture treatments, the scaffolds were removed from the bioreactor modules and pepsin-treated for deposited collagen as above.

### 2.3. Sodium dodecylsulfate–polyacrylamide gel electrophoresis (SDS–PAGE)

Protein samples were separated under non-reducing conditions either using pre-cast gradient NuPage 3–8% Tris-acetate polyacrylamide gels (Invitrogen, Singapore) or 5% resolving/3% stacking polyacrylamide gels as outlined in [10]. Protein standards used were the Precision Plus Dual Color and Prestained Broad Range (Bio-Rad, Singapore), and collagen type I (Koken Co., Tokyo, Japan). Protein bands were stained with the SilverQuest™ kit (Invitrogen) and densitometric analysis was performed on the collagen  $\alpha$ -bands with a GS-800™ Calibrated Densitometer (Bio-Rad).

### 2.4. Western immunoblotting

Proteins were extracted from the cell layer, subjected to reducing SDS–PAGE (NuPage 3–8% Tris-acetate gels) and immunoblotted [5]. Primary antibodies for procollagen C-proteinase (PCP; rabbit anti-human BMP-1, AB81031; Chemicon International, CA, USA) and PCP enhancer protein 1 (PCOLCE1; rabbit anti-human PCOLCE1, CL1PCOLE1; Cedarlane Laboratories Ltd, Ontario, Canada) were used at 1/2500 dilutions. The signal was detected with chemilumines-

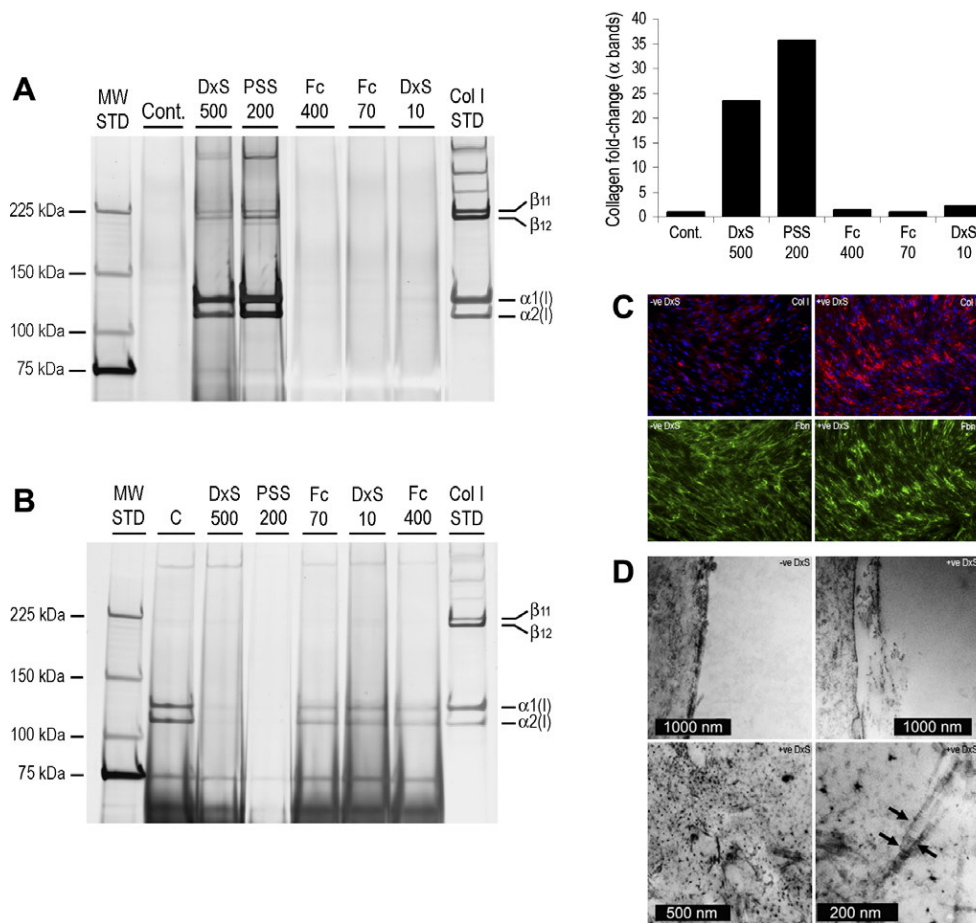


Fig. 1. EVE enhanced collagen deposition. (A) SDS–PAGE (NuPage) and densitometric analysis of collagen deposition (fold-change relative to Cnt) onto the cell layer after 48 h in absence and presence of different macromolecules. (B) SDS–PAGE (NuPage) analysis of collagen from the medium fraction of the above treatments. Each lane contains three pooled individual samples. (C) Double immunofluorescence staining of collagen (red; nuclei counterstained with DAPI) and fibronectin (green) in the ECM in the absence and presence of DxS 500 kDa (100  $\mu$ g/ml). All magnifications at 10 $\times$ . (D) Transmission electron micrograph of the pericellular matrix in the absence and presence of DxS 500 kDa (100  $\mu$ g/ml). Arrows indicate collagen-typical fibrillar formations in the presence of EVE. *Abbreviations*: Col I, collagen type I; Cnt, control; Fbn, fibronectin; MW STD, molecular weight standards.

cence (Super Signal® West Dura kit; Pierce Biotechnology Inc., IL, USA) and captured with a VersaDoc Imaging System model 5000 (Bio-Rad).

### 2.5. Immunocytochemistry

Cell layers or footprints were fixed with 2% paraformaldehyde (Sigma–Aldrich) and double-immunofluorescence was carried-out in PBS with 3% BSA. Primary antibodies used were mouse anti-human collagen I at 1:100 (AB745; Chemicon International) and rabbit anti-human fibronectin at 1:200 (F7387; Sigma–Aldrich). Secondary antibodies were goat anti-mouse AlexaFluor594 (Molecular Probes, OR, USA) and chicken anti-rabbit AlexaFluor488 at 1/400 dilutions, respectively. Cell nuclei were counterstained with DAPI (4',6-diamidino-2-phenylindole; Molecular Probes). Images were captured with an Eclipse TE2000-E inverted epifluorescence microscope (Nikon, Singapore). All digital images were background-subtracted based on conjugate control.

### 2.6. Transmission electron microscopy

3.4 million fibroblasts were seeded in 35 mm dishes and were allowed to attach for 16 h after which they were treated with ascorbate in the presence or absence of DxS for 48 h as described above. Cultures were then washed in PBS and fixed in 2.5% glutaraldehyde in PBS, pH 7.4, for 16 h at 4 °C. Cell layers were scraped, pelleted and embedded in 0.5% agarose. Agarose cylinders containing cell pellets were then processed for electron microscopy (osmication, dehydration, infiltration, araldite embedding). Thin sections were viewed in a JEOL 1220 (Tokyo, Japan) electron microscope. Digital images were taken with a ES 500 DDC camera (Gatan GmbH, Munich, Germany) using Digital Micrograph software.

### 2.7. Biophysical measurements

Dynamic light scattering (DLS) measurements on macromolecules were performed in HBSS, pH 7.4, and corrected for viscosities according to Harve et al. [11]. For zeta ( $\zeta$ )-potential measurements, macromolecules were dissolved in water and measured using a ZetaPlus analyzer (Brookhaven Instruments Corporation, NY, USA) at 25 °C.  $\zeta$ -potential was expressed as the mean of 10 readings and tabulated with the standard error of mean.

## 3. Results and discussion

### 3.1. EVE enhances collagen deposition

Only the large negatively charged polymeric macromolecules induced collagen deposition above control levels (Fig. 1A). As described previously [5], the benchmarked polymer DxS 500 kDa resulted in enhanced collagen deposition (23-fold). More remarkably, PSS (200 kDa), a sulfonated anionic polymer, caused an even greater collagen deposition (36-fold). PSS enabled virtually the complete conversion of procollagen into collagen. This was apparent by its complete absence from the medium fraction (Fig. 1B). Neither DxS 10 kDa nor the Fc range caused substantial collagen deposition above control. Immunocytochemistry of extracellular collagen deposition in the presence of DxS (500 kDa) corroborated the quantitative biochemical data above (Fig. 1C). In contrast, the fibronectin pattern and staining intensity were not significantly enhanced. In the absence of EVE, collagen staining was wispy and strictly colocalized with fibronectin, whereas under EVE both the collagen and fibronectin deposition patterns become more granular and not always showed complete colocalization. Furthermore, preliminary ultrastructural studies confirmed the presence of fibrillar pericellular matrix in crowded versus not crowded cultures (Fig. 1D). On several occasions, aggregates of a width of 25–80 nm with collagen-typical cross-striation were observed.

### 3.2. Biophysical characterization of macromolecules

Biophysical characterization of the macromolecules was studied to establish correlates with their ability to create effective EVE and thus enhance collagen fibrillogenesis through enzymatic processes (see below). Molecular size in solution and net surface charge density were the key parameters. The hydrodynamic radius describes the effective size of a macromolecule in a physiological, aqueous environment. It combines the physical size with the space its hydration shell(s) occupies. Although anionic DxS (500 kDa) and neutral Fc 400 have comparable molecular weights, DxS had a larger hydrodynamic radius, and hence greater percentage fraction volume occupancy (Fig. 2A). Astonishingly, this was at 500 times lower concentration. These data corroborate the findings in [5], where comparison between anionic and neutral dextrans (500 and 670 kDa, respectively) demonstrated a greater-than 2-fold hydrodynamic radius for the smaller but negatively-charged dextran, enabling dramatically greater procollagen conversion *in vitro*. An investigation into the surface charge density of

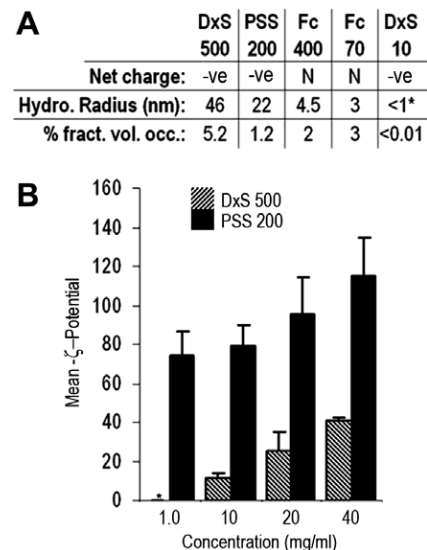


Fig. 2. Biophysical properties of the macromolecules. (A) Net charge, hydrodynamic (Hydro.) radius and percentage fraction volume occupancy (% fract. vol. occ.) are shown for the macromolecules. (B)  $\zeta$ -potential values of DxS 500 kDa and PSS 200 kDa at various concentrations measuring surface charge density. \* indicates below sensitivity of instrument. Abbreviations: N, neutral; -ve, negative.

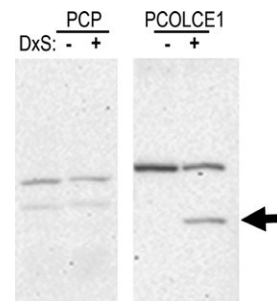


Fig. 3. Western immunoblot of PCP and PCOLCE1 proteins after 48 h of culturing in 10% FBS in the absence or presence of DxS 500 kDa (100  $\mu$ g/ml). Arrow indicates the 34–36 kDa C-terminus activated form of PCOLCE1.

DxS and PSS revealed that PSS had a 3–4 times higher  $\zeta$ -potential (Fig. 2B). This would account for the more potent volume exclusion with respect to collagen deposition for PSS even though the percentage fraction volume occupancy for DxS (500 kDa) was 4.3-fold greater at the same concentration. Procollagen, a negatively charged macromolecule (pI of 5.2 at physiological pH of 7.4) would have additional volume exclusion due to electrostatic repulsion, which is a key parameter that influences EVE [12]. Therefore, the potency of EVE in our system, with negatively charged macromolecules, is the combined effect of steric and electrostatic repulsion. The latter property, which is appreciably stronger for PSS, would

explain the enhanced procollagen conversion of PSS over DxS 500 kDa.

### 3.3. Enhanced extracellular enzymatic activity

Although increased procollagen conversion and subsequent collagen deposition due to the establishment of EVE in tissue culture is a definitive functional assay for PCP activity, Western immunoblotting for the PCP protein did not detect a quantitative difference in the presence of EVE (DxS 500 kDa, 100  $\mu$ g/ml) (Fig. 3). However, although PCP has many extracellular target proteins, an allosteric enhancer of PCP-procollagen-specific activity, PCOLCE1, has been shown

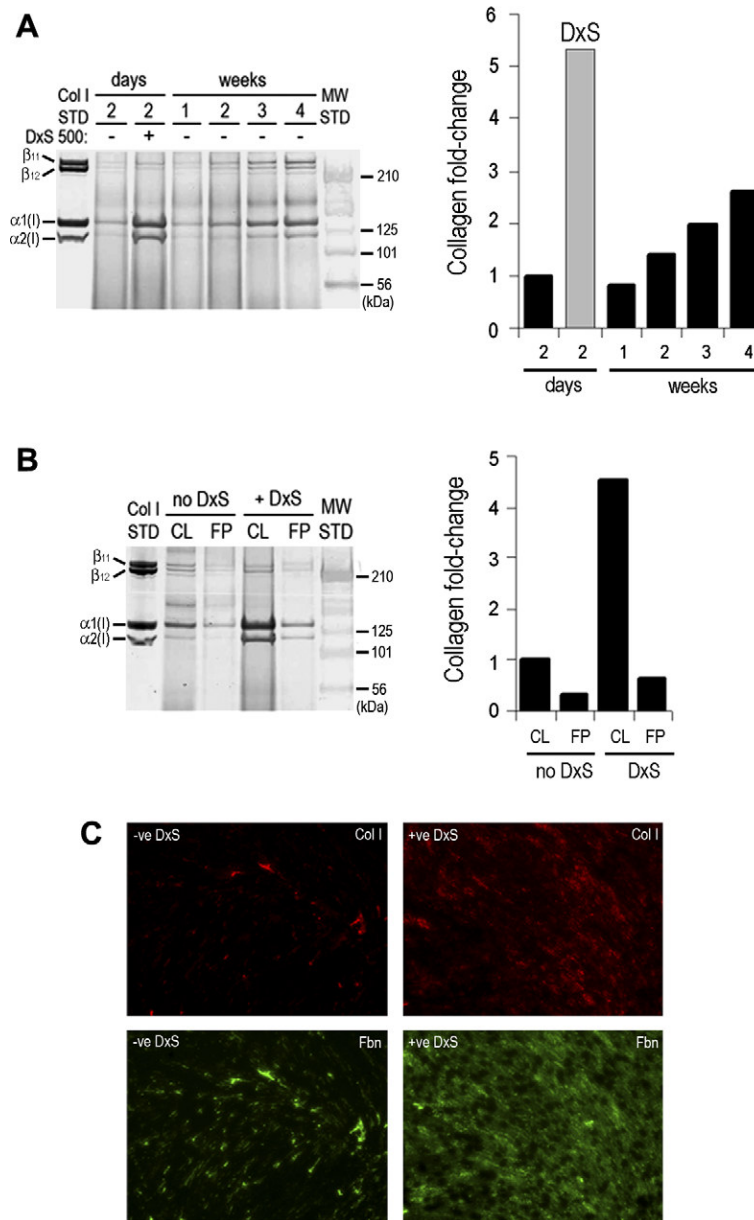


Fig. 4. EVE enhanced the rate of collagen deposition on the supporting material. (A) SDS-PAGE (NuPage) and densitometric analysis of collagen deposition after 2 days culturing in the presence of DxS 500 kDa (100  $\mu$ g/ml; grey column) and in its absence for 2 days and up to 4 weeks. Fold-change values are relative to 2 days culturing in the absence of DxS. (B) SDS-PAGE (NuPage) and densitometric analysis of 2 days for total collagen deposition (CL) and footprints (FP; after cell solubilization with detergent) in the absence (reference) and presence of DxS 500 kDa (100  $\mu$ g/ml). (C) Double immunofluorescence staining of collagen (red) and fibronectin (green) of the footprints in the absence and presence of DxS 500 kDa. All magnifications at 10 $\times$ . All lanes contain three pooled individual samples.

to enhance PCP activity 10-fold [13–15]. Only in the presence of crowding did we detect a 36 kDa active form of this PCP enhancer protein (Fig. 3). Furthermore, the PCOLCE1 C-terminus, a fragment with an apparent MW of 16.5 kDa, has been shown to inhibit matrix metalloproteinase 2 (MMP2) with greater efficiency than tissue inhibitor of MMP2 [16]. Therefore, by introducing EVE, we not only accelerated PCP enzymatic activity but also the proteolytic conversion of PCOLCE1 into a PCP-enhancing element and an additional strong metalloproteinase inhibitor. This would complement the matrix deposition process by inhibiting proteins that destroy the ECM. Finally, the ECM forming process is augmented under EVE with an increased lysyl oxidase activity resulting in an enhanced presence of collagen beta crosslinks [5].

### 3.4. EVE enhances collagen deposition onto the supporting material

Although several studies have been continuously hinting at the potential of EVE [17,18] it has not been exploited for applications in biological *in vitro* systems. We were able to dramatically enhance collagen deposition quantitatively and temporally in the presence of DxS 500 kDa. In the presence of EVE, 48 h of culturing resulted in greater-than 5- and 2-fold collagen deposition compared to the control cultures (without EVE) for 1 and 4 weeks, respectively (Fig. 4A). In addition, the amount of ECM, with respect to collagen and fibronectin, was also enhanced on the tissue culture plastic. Both quantitative (SDS-PAGE; Fig. 4B) and immunostaining (Fig. 4C) of ECM footprints after detergent removal of the cellular layer revealed substantial amounts of collagen and fibronectin deposited directly on the culture plate when cultured in the presence of DxS. There was an almost complete fine granular confluent coverage of the supporting surface, which was contrasted by the small amounts of patchy coverage in its absence. Therefore, the application of EVE is an important tool in creating greater and more confluent ECM coverage of the supporting material. This is particularly important for the 3-D bioreactor setting, where flow rates and scaffold design can generate strong local shear forces which detach cells [19,20]. To attain suitable seeding rates onto scaffolds, incubations are usually first performed under static culture conditions for several days [21,22]. Therefore, speeding up the matrix formation within scaffolds would greatly enhance cell adhesion, survival, migration and biological functionality. We investigated the enhanced deposition of collagen onto 3-D scaffolds through the addition of DxS 500 kDa (100 µg/ml) in the media. Under static culture, the presence of DxS resulted in more than 6-fold increased collagen incorporation into both Biobrane (Fig. 5A) and PLLA scaffolds (Fig. 5B). Under bioreactor conditions, there was a 3-fold increase in collagen matrix formation on the PLLA scaffold compared to the control (Fig. 5B). Of note, although the bioreactor experiments were neither optimized for cell seeding density or flow rate, the beneficial effects of EVE were immediately evident.

### 3.5. Mechanism of EVE

The successful application of EVE in our *in vitro* system can be explained by a spectrum of thermodynamic effects [17] such as driving optimal folding of proteins enhancing their function [23], enhancing enzyme catalytic activity [24], specifically creating substrate–enzyme complexes with longer half-lives [25],

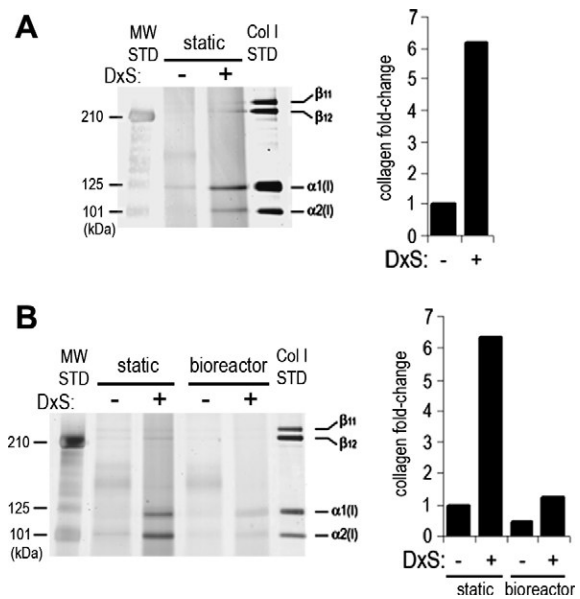


Fig. 5. EVE enhanced matrix deposition onto 3-D scaffolds. (A) Biobrane and (B) PLLA 3-D scaffolds analyzed by SDS-PAGE (in-house) and densitometry of collagen deposition in the absence and presence of DxS 500 kDa (100 µg/m). Biobrane was cultured for 3 days under static conditions whereas PLLA was used under both static (5 days) and bioreactor (5 days) conditions. Fold-change values are relative to static cultures in the absence of DxS.

and enhancing protein aggregation and specific polymerization of monomers into greater order structures [26]. Accordingly, we propose that in our system EVE (1) shifted the enzymatic reaction equilibrium towards procollagen conversion by stabilizing the PCP-procollagen transition complex, (2) caused a tighter or more frequent binding of the enhancer protein (PCOLCE1) to PCP increasing its activity by allosteric regulation, (3) induced proteolytic conversion of PCOLCE1 into a PCP-enhancing fragment and a MMP inhibiting fragment, and (4) promoted self-assembly of the collagen triplehelices into insoluble fibers. Supporting evidence for point 4 comes from groups that have shown that collagen in solution self-assembles faster in the presence of macromolecules [27–29]. However, further work needs to be done to address these issues in more detail.

In conclusion, EVE is an indispensable component of intra- and extracellular biochemistry and can be regarded, in its various forms, as a creator and keeper of organic life through biochemistry. Authorities in the field state that many estimates of reaction rates and equilibria made with uncrowded solutions in the test tube differ by orders of magnitude from those of the same reactions operating under crowded conditions within cells or the extracellular compartment [1,30]. Along this line, our data show that when EVE is applied to a biological system with living cells, its effects are striking and from a biotechnological point of view, highly promising for providing solutions to advanced tissue engineering and certainly any other biological processes that are emulated *in vitro*.

**Acknowledgments:** The authors thank Dr. Phan Toan Thang (Dept. of Surgery, National University of Singapore (NUS)) and Dr. Dietmar W. Huttmacher (Division of Bioengineering, NUS) for their in-kind gifts of the Biobrane and PLLA scaffolds, respectively. We are also grateful for the expert technical help of Mrs. Mary Chu (Dept. of

Pathology, NUS/NUH) and the NUS Tissue Engineering Programme for strong support. M.R. acknowledges funding by a start-up grant from Provost and the Office of Life Sciences of NUS (R-397-000-604-101; R-397-000-604-712), the Faculty of Engineering (FRC) (R-397-000-017-112) and the National Medical Research Council (R397-000-018-213).

## References

- [1] Zimmerman, S.B. and Minton, A.P. (1993) Macromolecular crowding: biochemical, biophysical, and physiological consequences. *Annu. Rev. Biophys. Biomol. Struct.* 22, 27–65.
- [2] Ellis, R.J. (2001) Macromolecular crowding: an important but neglected aspect of the intracellular environment. *Curr. Opin. Struct. Biol.* 11, 114–119.
- [3] Partikian, A., Ölveczky, B., Swaminathan, R., Li, Y. and Verkman, A.S. (1998) Rapid diffusion of green fluorescent protein in the mitochondrial matrix. *J. Cell Biol.* 140, 821–829.
- [4] Ellis, R.J. (2001) Macromolecular crowding: obvious but underappreciated. *Trends Biochem. Sci.* 26, 597–604.
- [5] Lareu, R.R., Arsianti, I., Subramhanya, K.H., Peng, Y.X. and Raghunath, M. (2007) In vitro enhancement of collagen matrix formation and crosslinking for applications in tissue engineering – a preliminary study. *Tissue Eng.* 13, 385–391.
- [6] Mao, J. and Schwarzbauer, J.E. (2005) Fibronectin fibrillogenesis, a cell-mediated matrix assembly process. *Matrix Biol.* 24, 389–399.
- [7] Auger, F.A., Berthod, F., Moulin, V., Pouliot, R. and Germain, L. (2004) Tissue-engineered skin substitutes: from in vitro constructs to in vivo applications. *Biotechnol. Appl. Biochem.* 39, 263–275.
- [8] Raghunath, M. et al. (1999) Carboxy-terminal conversion of profibrillin to fibrillin at a basic site by PACE/furin-like activity required for incorporation in the matrix. *J. Cell. Sci.* 112, 1093–1100.
- [9] Gemmiti, C.V. and Guldberg, R.E. (2006) Fluid flow increases type II collagen deposition and tensile mechanical properties in bioreactor-grown tissue-engineering cartilage. *Tissue Eng.* 12, 469–479.
- [10] Raghunath, M., Steinmann, B., DeLozier-Blanchet, C., Extermann, P. and Superti-Furga, A. (1994) Prenatal diagnosis of collagen disorders by direct biochemical analysis of chorionic villus biopsies. *Pediatr. Res.* 36, 441–448.
- [11] Harve, K.S., Lareu, R.R., Rajagopalan, R. and Raghunath, M. (2006) Macromolecular crowding in biological systems: dynamic light scattering (DLS) to quantify the excluded volume effect (EVE). *Biophys. Rev. Lett.* 1, 317–325.
- [12] Gyenge, C.C., Tenstad, O. and Wiig, H. (2003) *In vivo* determination of steric and electrostatic exclusion of albumin in rat skin and skeletal muscle. *J. Physiol.* 552, 907–916.
- [13] Adar, R., Kessler, E. and Goldberg, B. (1986) Evidence for a protein that enhances the activity of type I procollagen C-proteinase. *Coll. Relat. Res.* 6, 267–277.
- [14] Kessler, E. and Adar, R. (1989) Type I procollagen C-proteinase from mouse fibroblasts. Purification and demonstration of a 55-kDa enhancer glycoprotein. *Eur. J. Biochem.* 186, 115–121.
- [15] Takahara, K. et al. (1994) Type I procollagen COOH-terminal proteinase enhancer protein: identification, primary structure, and chromosomal localization of the cognate human gene (PCOLCE). *J. Biol. Chem.* 269, 26280–26285.
- [16] Mott, J.D. et al. (2000) Post-translational proteolytic processing of procollagen C-terminal proteinase enhancer releases a metalloproteinase inhibitor. *J. Biol. Chem.* 275, 1384–1390.
- [17] Hall, D. and Minton, A.P. (2003) Macromolecular crowding: qualitative and semiquantitative successes, quantitative challenges. *Biochim. Biophys. Acta* 127, 1649–1656.
- [18] Sasahara, K., McPhie, P. and Minton, A.P. (2003) Effect of dextran on protein stability and conformation attributed to macromolecular crowding. *J. Mol. Biol.* 326, 1227–1237.
- [19] Millward, H.R. et al. (1994) Mammalian cell damage in a novel membrane bioreactor. *Biotechnol. Bioeng.* 43, 899–906.
- [20] Sikavitsas, V.I., Bancroft, G.N. and Antonios, M.G. (2002) Formation of three-dimensional cell/polymer constructs for bone tissue engineering in a spinner flask and a rotating wall vessel bioreactor. *J. Biomed. Mater. Res.* 62, 136–148.
- [21] Goldstein, A.S., Juarez, T.M., Helmke, C.D., Gustin, M.C. and Mikos, A.G. (2001) Effect of convection on osteoblastic cell growth and function in biodegradable polymer foam scaffolds. *Biomaterials* 22, 1279–1288.
- [22] Yu, X., Botchwey, E.A., Levine, E.M., Pollack, S.R. and Laurencin, C.T. (2004) Bioreactor-based bone tissue engineering: the influence of dynamic flow on osteoblast phenotypic expression and matrix mineralization. *Proc. Natl. Acad. Sci. USA* 101, 11203–11208.
- [23] Cheung, M.S., Klimov, D. and Thirumalai, D. (2005) Molecular crowding enhances native state stability and refolding rates of globular proteins. *Proc. Natl. Acad. Sci. USA* 102, 4753–4758.
- [24] Moran-Zorzano, M.T., Viale, A.M., Munoz, F.J., Alonso-Casajus, N., Eydallin, G.G., Zugasti, B., Baroja-Fernandez, E. and Pozueta-Romero, J. (2007) *Escherichia coli* AspP activity is enhanced by macromolecular crowding and by both glucose-1,6-bisphosphate and nucleotide-sugars. *FEBS Lett.* 581, 1035–1040.
- [25] Goobes, R., Kahana, N., Cohen, O. and Minsky, A. (2003) Metabolic buffering exerted by macromolecular crowding on DNA–DNA interactions: origin and physiological significance. *Biochemistry* 42, 2431–2440.
- [26] Munishkina, L.A., Cooper, E.M., Uversky, V.N. and Fink, A.L. (2004) The effect of macromolecular crowding on protein aggregation and amyloid fibril formation. *J. Mol. Recog.* 17, 456–464.
- [27] Candlish, J.K. and Tristram, G.R. (1963) The resistance to dispersion of collagen fibres formed in vitro in the presence of ascorbic acid. *Biochim. Biophys. Acta* 78, 289–294.
- [28] Laude, D., Odlum, K., Rudnicki, S. and Bachrach, N. (2000) A novel injectable collagen matrix: in vitro characterization and in vivo evaluation. *J. Biomech. Eng.* 122, 231–235.
- [29] Cavallaro, J.F., Kemp, P.D. and Kraus, K.H. (1994) Collagen fabrics as biomaterials. *Biotechnol. Bioeng.* 43, 781–791.
- [30] Minton, A.P. (2001) The influence of macromolecular crowding and macromolecular confinement on biochemical reactions in physiological media. *J. Biol. Chem.* 276, 10577–10580.

## Emulating a crowded intracellular environment *in vitro* dramatically improves RT-PCR performance

Ricky R. Lareu<sup>a,b</sup>, Karthik S. Harve<sup>a</sup>, Michael Raghunath<sup>a,c,\*</sup>

<sup>a</sup> Tissue Modulation Laboratory, Division of Bioengineering, Faculty of Engineering, National University of Singapore, Division Office Block E3A #04-15, 7 Engineering Drive 1, Singapore 117574, Singapore

<sup>b</sup> NUS Tissue Engineering Program and Department of Orthopedic Surgery, Yong Loo Lin School of Medicine, National University of Singapore, Singapore

<sup>c</sup> Department of Biochemistry, Yong Loo Lin School of Medicine, National University of Singapore, Singapore

Received 18 August 2007

Available online 5 September 2007

### Abstract

The polymerase chain reaction's (PCR) phenomenal success in advancing fields as diverse as Medicine, Agriculture, Conservation, or Paleontology is based on the ability of using isolated prokaryotic thermostable DNA polymerases *in vitro* to copy DNA irrespective of origin. This process occurs intracellularly and has evolved to function efficiently under crowded conditions, namely in an environment packed with macromolecules. However, current *in vitro* practice ignores this important biophysical parameter of life. In order to more closely emulate conditions of intracellular biochemistry *in vitro* we added inert macromolecules into reverse transcription (RT) and PCR. We show dramatic improvements in all parameters of RT-PCR including 8- to 10-fold greater sensitivity, enhanced polymerase processivity, higher specific amplicon yield, greater primer annealing and specificity, and enhanced DNA polymerase thermal stability. The faster and more efficient reaction kinetics was a consequence of the cumulative molecular and thermodynamic effects of the excluded volume effect created by macromolecular crowding.

© 2007 Elsevier Inc. All rights reserved.

**Keywords:** Macromolecular crowding; Excluded volume effect; Macromolecule; Polymerase chain reaction; DNA polymerase; Reverse transcriptase; Reverse transcription; Sensitivity

Biochemical reactions in cells function in a carefully controlled intracellular environment which biologists have, to a certain extent, reproduced *in vitro* by controlling factors such as pH, ionic strength, temperature, and supply of cofactors which constitute the buffer system. However, the biophysical effect of macromolecular crowding has not been transferred to the *in vitro* setting and has gone largely unnoticed and underappreciated [1]. In fact, all DNA modifying enzymes that are commonly used today (e.g. polymerases, nucleases, ligases) have evolved to function

efficiently within the crowded interior of cells. For example, the total concentration of protein and RNA inside bacteria (e.g. *Escherichia coli*) is in the range of 300–400 g/l [2] and this level of crowding is also present in eukaryotic cells [1]. Biological crowding occurs in the range of 5–40% w/v solute content [1,3,4] which translates to even higher excluded volume [5]. This high solute content, colloquially termed crowding, results from no single molecule species being present at a high concentration however, collectively, the consequence is expressed in the principle of the Excluded Volume Effect (EVE). It states that the volume of a solution that is excluded to a particular molecule in question is the result of the sum of non-specific steric hindrances (size and shape) and electrostatic repulsions (charge) of the other macromolecules [6]. This results in molecules constantly interacting non-specifically with an assortment of diverse macromolecular species which is responsible for a

\* Corresponding author. Address: Tissue Modulation Laboratory, Division of Bioengineering, Faculty of Engineering, National University of Singapore, Division Office Block E3A #04-15, 7 Engineering Drive 1, Singapore 117574, Singapore. Fax: +65 6872 3069.

E-mail address: [biern@nus.edu.sg](mailto:biern@nus.edu.sg) (M. Raghunath).

URL: <http://www.tissuemodulation.com> (M. Raghunath).



spectrum of molecular thermodynamic effects namely, reaction rate/kinetics [7], molecular assembly [8], and protein folding [9]. It has been postulated that macromolecular crowding is a key factor responsible for the phenomenally high rates of reactions and molecular interactions *in vivo* while seemingly relatively low amounts of reactants are present, at least when compared to their *in vitro* use [10,11].

Our aim was to more closely emulate the intracellular biophysical environment of the bacterium in the *in vitro* setting and thus enhance reverse transcription (RT) and polymerase chain reaction (PCR). Herein, for the first time with the addition of inert macromolecules we demonstrate significant improvements in all aspects of RT-PCR, including sensitivity, specificity, processivity, yield, and thermal stability of Taq DNA polymerase.

## Materials and methods

**General materials.** All reactions were performed on the real-time Mx3000P (Stratagene, CA, USA). Macromolecules: Ficoll™ (Fc) 70 kDa (Fc70) and Fc400 kDa (Fc400) (Amersham Pharmacia, Uppsala, Sweden); trehalose (Fluka–Sigma–Aldrich, Singapore); proline (Sigma–Aldrich); and polyethylene glycol (PEG) 4 kDa. Additives were dissolved in nuclease-free water as a concentrate and added freshly to the reaction buffers each time.

**RNA extraction.** RNA was extracted from human WI-38 fibroblasts (American Tissue Culture Collection, VA, USA) from which complementary DNA (cDNA) was prepared for all PCR assays except for aP2 (fatty acid binding protein 2) which used RNA from adipocytes differentiated from human mesenchymal stem cells. Extractions were performed with RNAqueous™ (Ambion Inc., TX, USA) according to the Manufacturer's protocol.

**Reverse transcriptase.** Complementary DNA synthesis was carried out according to the Manufacturer's protocol for SuperScript II reverse transcriptase with oligo(dT) primers with the following modifications when macromolecules were used. Fc70 (7.5 mg/ml) was added to the annealing buffer and mixture of Fc70/400 (7.5 and 2.5 mg/ml) was added to the polymerization step.

**Polymerase chain reaction.** Two microliters of cDNA was used as target for all PCRs in a final volume of 20  $\mu$ l and all samples were run in duplicates. Reactions as follows unless otherwise stated: 1 U Platinum Taq DNA polymerase in 1 $\times$  reaction buffer, 300 nM primers and 2.5 mM MgCl<sub>2</sub>. The thermal cycling program for all PCRs was the following, unless otherwise stated: 94 °C/5 min, 94 °C/30 s, 56 °C/30 s, 72 °C/30 s, for (collagen I set 1, 30; GAPDH, 35; aP2 and M13, 40; collagen I set 2, 42) cycles with a final dissociation step of 60–94 °C at 1.1 °C/s. The annealing temperature for collagen I set 1 and set 2 was 55 °C. Fluorescence was detected with SYBR Green I (Molecular Probes–Invitrogen). Primer sequences were: GAPDH, gtccactggcgtcttcacca, gtggcagtgatggcatggac; collagen I set 1, agccagcagatcgagaacat, tcttctcttgggggtcttg; aP2, tactggcagggaatttgac, gtggaagtgcagcaatttcat; M13, ttgcttcgggtctggttc, cacctcagagccaccac; collagen I set 2, gtgctaaaggtgccaatggt, ctctcgtcttctctct. Oligonucleotides poly-adenine (oligo(dA)<sub>20</sub>) and poly-thymine (oligo(dT)<sub>20</sub>) (both 20-mer) at 10  $\mu$ M were combined in the presence of reaction buffer, 2.5 mM MgCl<sub>2</sub> and SYBR Green 1 and thermal cycled through 94, 50, and 72 °C for 30 s each followed by a dissociation step 50–94 °C.

**Processivity experiments.** The single-stranded M13 (ssM13) processivity assay for Taq DNA polymerase was modified from Bambara et al. [12]. Briefly, 100 nM of primer (gtaaacgacggccagt) was added to 100 nM ssM13mp18 DNA (New England Biolabs Inc., MA, USA) in buffer with 1 U Taq DNA polymerase in the absence or presence of Fc400 (2.5 mg/ml). The samples were heated to 94 °C/5 min, cooled to 55 °C/1 min followed by 72 °C for 1 and 3 min, respectively. For the reverse transcriptase processivity assay, a standard RT was performed

without and with the macromolecules Fc70/Fc400 mixture, as above. Reaction products were separated on a denaturing 0.6% agarose gel.

**Agarose gel electrophoresis.** Reaction products were either resolved in 1XTAE agarose (Seakem, ME, USA) gels or in formamide-denaturing agarose gels [13] at the stipulated concentrations of 0.6% or 2.0%. The molecular weight markers were 1 kb (Promega Corporation, WI, USA), 50 and 100 bp (Invitrogen) DNA ladders. Post-staining was done with SYBR Gold (Molecular Probes–Invitrogen), images were captured with a Versadoc™ (Bio-Rad), and analysed using Quantity One v4.5.2 (Bio-Rad).

**Calculation of the area-under-the-curve and late phase PCR efficiency.** The method of Rasmussen et al. [14] which uses the NCSS™ software was used to calculate the area-under-the-curve from the PCR dissociation curves raw data values derived from the Stratgene software MxPro v3.20. The late-phase efficiency of PCR amplification was calculated according to the method of Liu and Saint [15].

## Results

### Sensitivity

Total RNA (1000 and 50 ng) was reverse transcribed in the presence and absence of a macromolecule mixture (Fc70 and Fc400) followed by amplification with collagen I PCR assay in the presence and absence of a single macromolecule (Fc400), respectively. Crowding resulted in a reduction of greater-than 3 Ct (threshold cycle) (green) compared to standard (i.e. non-crowded) RT-PCR samples (orange) (Fig. 1A; taken from the amplification plots Fig. 1B). This translates to enhanced sensitivity of >10-fold. The dissociation curves (Fig. 1C) in conjunction with the agarose gel electrophoresis (Fig. 1D) confirm amplification of the specific target. Complementary DNA was prepared from 500 ng of total RNA under standard condition (i.e. non-crowded) and subjected to amplification with GAPDH PCR in the absence or presence of macromolecule mixture Fc70/400 (7.5/2.5 mg/ml) or PEG 4 kDa at 2.5, 5 or 10 mg/ml concentrations. Unlike the macromolecules which enhanced an already optimized PCR by 2 Ct (i.e. 4-fold increase), PEG inhibited sensitivity by greater-than 4 Ct (i.e. 16-fold decrease) which was dose-dependent (Fig. 1E). In addition, the presence of PEG caused the amplification of a smaller, non-specific product, apparent by a shoulder on the left of the dissociation curves (Fig. 1F) and ~200 bp band on the agarose gel (Fig. 1G).

### Specificity

We were unable to amplify a particular collagen I template target region through standard RT-PCR due to its long distance from the oligo(dT) priming site (~4390 bp; NM\_000088). However, in the presence of a mixture of Fc70 and Fc400 the specific product was obtained with the lower range of primer concentrations (100–300 nM) (Fig. 2A). Although higher primer concentrations resulted in high background the specific product was still present and dominated the amplicons that were generated in the presence of macromolecules. In contrast, non-crowded reactions yielded only non-specific products. In fact, we

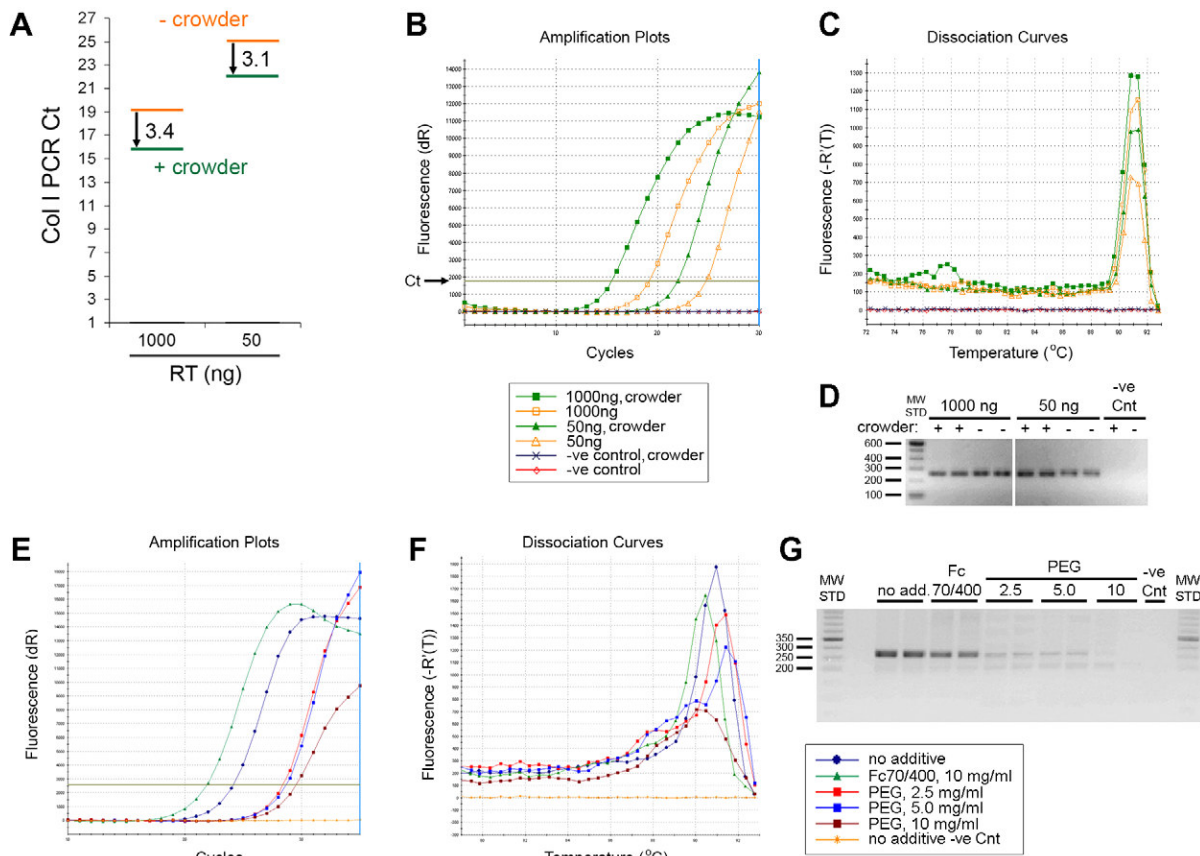


Fig. 1. Macromolecular crowding enhances the sensitivity of RT and PCR assays. (A) The average Ct (threshold cycle) values from samples amplified with the collagen I set 1 PCR in the presence (green) and absence (orange) of Fc400 from cDNA prepared in the presence and absence of mixed crowders (Fc70 7.5 and Fc400 2.5 mg/ml), respectively. The amount of total RNA used for the RT was 1000 and 50 ng. (B) Amplification plots and (C) dissociation curves of the PCR samples. (D) Composite of the same agarose gel (2%) demonstrating a specific 250 bp collagen I amplicon. (E) Amplification plots and (F) dissociation curves of the GAPDH PCR showing the relative performance of macromolecular mixture Fc70/Fc400 (7.5/2.5 mg/ml), PEG 4 kDa at either 2.5, 5 or 10 mg/ml, and standard conditions (without additives). (G) Agarose gel (2%) demonstrating a specific 261 bp GAPDH amplicon. All the graphs show one replicate per PCR sample for display clarity. –ve Cnt = PCR template-free control: no add = no additive. (For interpretation of the references to color in this figure legend, the reader is referred to the web version of this article.)

demonstrate that the presence of macromolecules directly enhances primer annealing. The total amount of duplex formation consisting of oligos of adenine and thymine was quantified with SYBR Green 1 dye. This primer configuration was chosen to avoid secondary structures and self-annealing. There was an average increase of 1.8-fold in specific duplex formation in the presence of macromolecules (Fig. 2B).

### Processivity

In order to assess the ability of macromolecules to enhance processivity of Taq DNA polymerase, we performed a classical ssM13 assay in the absence and presence of macromolecules. The presence of Fc400 resulted in an average increase in DNA product of 15% (Fig. 3A) and longer DNA fragment lengths after 1 and 3 min of extension time (Fig. 3B). Figs. 3A and B are based on the intensities and relative migration profiles of the bands from the denaturing agarose gel (Fig. 3C). The enhanced processivity induced by crowding was tested with a long PCR assay

with limited extension time of 40 s. The addition of macromolecule mixture Fc70/Fc400 enabled the amplification of the correct amplicon (1547 bp) under these limiting experimental conditions (Fig. 3D). In contrast, the reaction carried out in the absence of crowding did not amplify the correct and long amplicon. Total RNA was used to test the effect of crowders on the processivity of reverse transcriptase. We carried out cDNA synthesis in the absence and presence of crowding additives (Fc70/Fc400). Densitometric analysis of the denaturing agarose gel of reaction products (Fig. 3E) demonstrated an increase in total cDNA of 86% (Fig. 3F) and overall longer cDNA products under crowded condition (Fig. 3G).

### PCR product yield

Decreasing amounts of Taq DNA polymerase were used to amplify a specific aP2 product from cDNA in the absence and presence of Fc400. For all Taq DNA polymerase concentrations (units of activity (U)/reaction) the presence of a crowding agent resulted in > 2-fold yield of

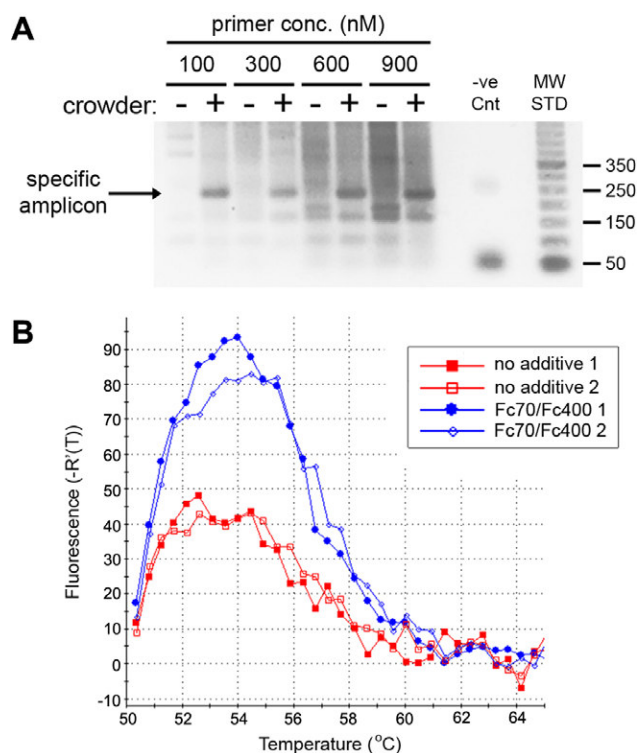


Fig. 2. Macromolecular crowding increased primer binding and specificity. Agarose gel of RT-PCR samples amplified with the collagen I set 2 PCR in the absence or presence of the macromolecule mixture Fc70/Fc400 (15/5 mg/ml) with increasing concentrations (conc.) of primers. The specific target is indicated at 228 bp. The cDNA was prepared from 250 ng total RNA. The -ve Cnt (control) was the PCR template-free control. (B) Dissociation curves of the hybridized oligonucleotide duplex between oligo(dA)<sub>20</sub> and oligo(dT)<sub>20</sub> in the absence (no additive) and presence of a mixture of macromolecules Fc70/Fc400 (15/5 mg/ml).

specific amplicon (Fig. 4A). These data were derived from integrating the area under the dissociation curves (Fig. 4C). In order to assess the relative reaction rates in the presence and absence of macromolecular crowders, we calculated the slopes of the amplification plots (Fig. 4D) at the late exponential phase for the above samples run with 1 U of enzyme (Fig. 4B). The presence of Fc400 resulted in a 2-fold greater value for the slope and an additional cycle in the exponential phase demonstrating faster reaction kinetics.

#### Thermal stability

We tested the thermal-protective property of macromolecules (i.e. Fc400) for Taq DNA polymerase against trehalose and proline, known, small molecules that have been shown to work as thermoprotectants. The enzyme was heat-stressed (95 °C for 45 min) in the absence and presence of the individual additives following which it was used to amplify a specific amplicon in the presence of the same additive. Only the presence of Fc400 and trehalose preserved the Taq DNA polymerase's enzymatic activity

(Fig. 4E). As expected, trehalose protected Taq while proline did not prevent the complete loss of activity.

#### Discussion

Macromolecular crowding has important thermodynamic consequences which influence reaction kinetics [2], however it has been neglected in biochemical and biological *in vitro* settings [1]. We have shown herein that reintroducing this parameter *in vitro* culminates in enhanced enzymatic properties expressed in dramatically more sensitive, specific and productive RT-PCR assays. Using molar concentration and hydrodynamic radii of the macromolecular additives, measured by Dynamic Light Scattering [16], all of which are hydrophilic, we have introduced fraction volume occupancies ranging from 5% to 15% based on steric repulsion, well within the accepted range of biological crowding [1]. However, the key to the success of crowding with macromolecules at relatively low concentrations is that the actual volume exclusion would be far greater as there is a non-linear relationship between macromolecular crowding concentration and excluded volume, which essentially has a magnifying effect due to steric exclusion of like-size molecules [5].

Although the addition of non-reacting molecules to improve RT and PCR is not new, the addition of inert “macromolecules” certainly is. Other studies have either been restricted to small molecules classified as compatible solutes or small molecular size polymers, such as PEG 4 kDa, with limited success. However, neither of which are classical macromolecules, defined by John R. Ellis [1]. In addition, PEG does not fit the description of EVE-causing models typically attributed to macromolecules because it displays hydrophobic interactions with proteins [1]. Their mode of action has been loosely referred to as molecular crowding but in actual fact their effects are due to improved hydration around substrate molecules. This is certainly true for trehalose [17], betaine and proline [18] which are classified as compatible solutes. They build water structures (kosmotropic effect) causing preferential hydration of other molecules like proteins [19]. They are able to stabilize the structures of protein/enzymes even at high temperatures [19,20]. We replicated this effect of trehalose and could show that the macromolecule Fc400 had the same protecting effect on Taq DNA polymerase.

Sensitivity and specificity are particularly crucial for diagnostic applications when the target is in low abundance (e.g. viral load in serum) or poor quality as found in archival sources. In using specific macromolecules as buffer additives we demonstrated dramatic increases in sensitivity up to 10-fold. Of note, the addition of PEG 4 kDa, in the same concentration range as macromolecules, to an optimized PCR assay was actually detrimental to the reaction with regards to sensitivity and yield, which was dose-dependent. Conversely, the addition of macromolecules still improved sensitivity of this assay. We were also able to specifically demonstrate enhanced primer specificity

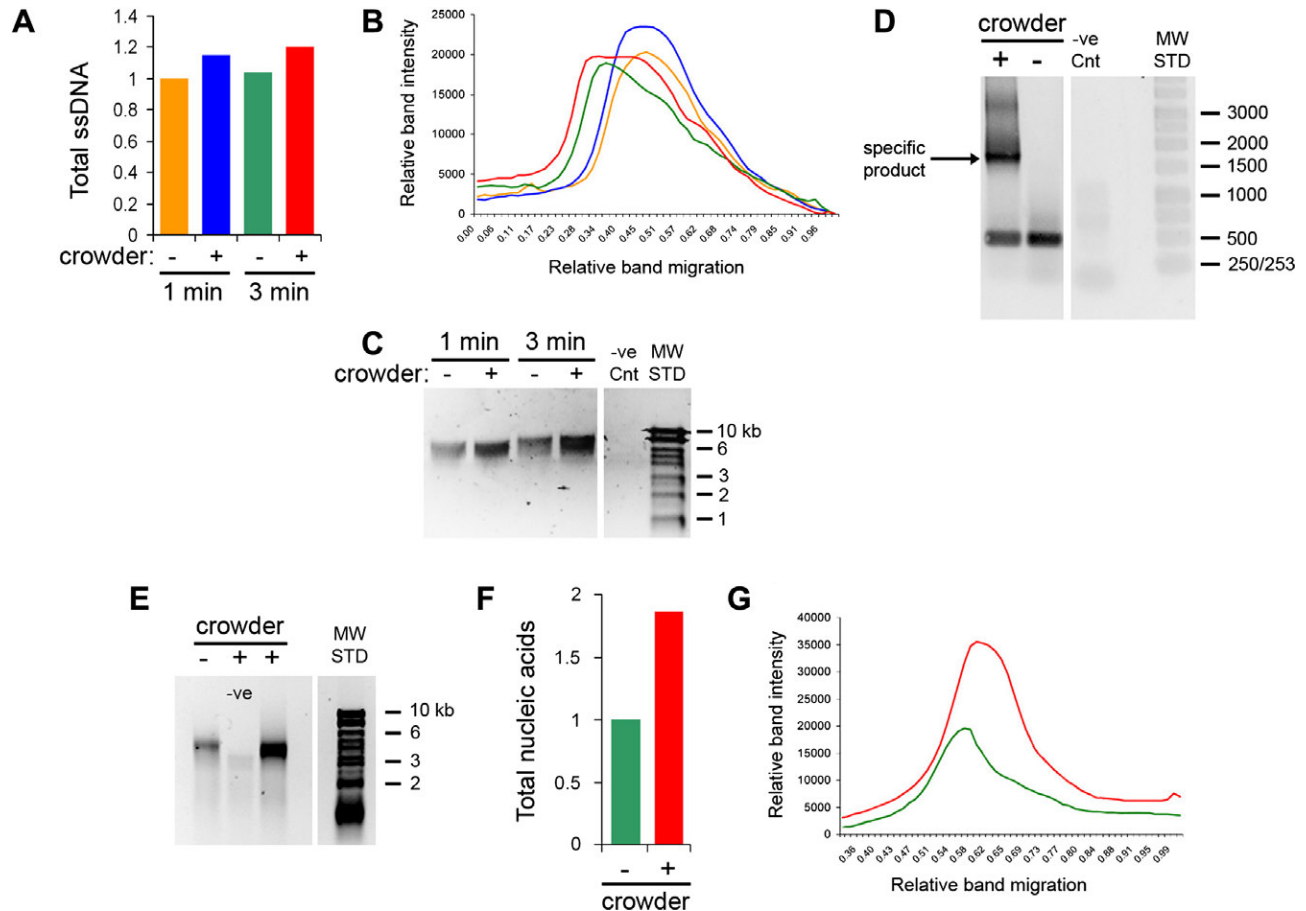


Fig. 3. Macromolecular crowding enhances enzyme processivity. The ssM13 processivity assay for Taq DNA polymerase was performed in the absence and presence of Fc400. (A) Densitometric analysis of the total amount of ssDNA products and (B) their relative migration through a (C) denaturing 0.6% agarose gel. The -ve Cnt was the enzyme-free negative control. (D) An agarose gel of the long M13 PCR products amplified in the absence and presence of macromolecule (mixture of Fc70 15 mg/ml and Fc400 5 mg/ml). One nanogram of ssM13 was used as target and the extension time was limited to 40 s. The -ve Cnt was without template. The arrow indicates the specific target which is 1547 bp. (E) A standard RT reaction was performed in the absence (green) and presence (red) of Fc70/Fc400 with 500 ng of total RNA and the subsequent reaction products were separated in a denaturing 0.6% agarose gels. (F) Densitometric analysis of total reaction products and (G) their relative migration through (E). “-ve” is the enzyme negative control. Gel images are composites of the respective gels omitting irrelevant sections. (For interpretation of the references to color in this figure legend, the reader is referred to the web version of this article.)

under crowded conditions, which in turn would result in increased sensitivity. Furthermore, we have shown that macromolecules cause a greater proportion of primer annealing. The usefulness of trehalose in improving sensitivity of PCR has been limited to the case of difficult cDNA templates with GC-rich regions [17]. Its effect is to reduce the melting temperature of these secondary structures. With regards to adding trehalose and betaine to RT reactions, an increase in the sensitivity was detected in the subsequent PCR but only when they were used at very high concentrations [21].

The increase in processivity, defined as greater product amount and length, which we attained with the addition of macromolecules would have been the direct consequence of both increased number of enzyme-nucleic acid initiation events and longer read-through of the enzymes, respectively. This is particularly significant for RT in faithfully generating enough copies of long cDNA molecules and for PCR in amplifying long amplicons. In fact, it has been

shown that a range of different molecular weight PEGs and dextrans were able to enhance the integrity and/or stability of the DNA-polymerase complex for *E. coli* T4 DNA polymerase [22,23]. However, they were not able to attain improved processivity. It has been reported that PEG destabilizes enzymes at high temperatures due to the inherent activity of its hydrophobic nature [24]. This may therefore hinder its application to PCR and the reason for the poor performance of PEG in our experiments and may have been responsible for the observed inability to improve processivity [22]. In comparison to an earlier study which used compatible solutes to enhance RT reactions [21], we employed high molecular weight macromolecules and attained an increase of both cDNA product and increased fragment length. However, in contrast to Spiess et al. [21] we achieved increased processivity at 50× lower additive concentrations. At these low mg concentrations viscosity was close to that of water (~1 centipoise) and therefore of no concern [16]. Conversely, the very high concentration

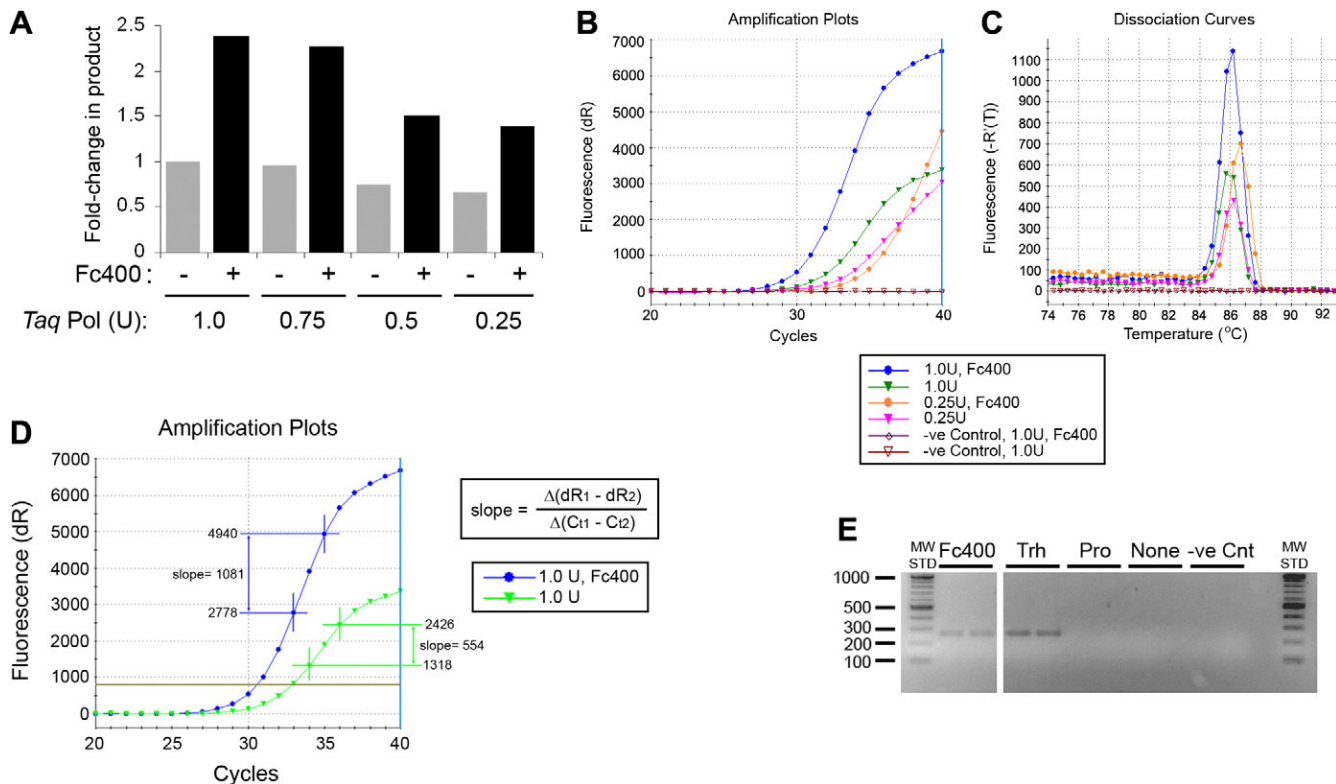


Fig. 4. Macromolecular crowding enhances activity of Taq DNA polymerase and protects it against thermal denaturation. (A) A range of Taq DNA polymerase concentrations (1–0.25 U/reaction) were used to amplify the aP2 product in the absence and presence of Fc400 (2.5 mg/ml). (B) Amplification plots and (C) dissociation curves for the PCR samples performed with 1 and 0.25 U of enzyme are only shown, for display clarity. (D) The slope of the late exponential phase was calculated for the samples amplified with 1 U of enzyme above. (E) Taq DNA polymerase was thermally stressed in the absence (None) and presence of 2.5 mg/ml Fc400, 100 mg/ml trehalose (Trh), or 113 mg/ml proline (Pro) and then the enzyme was used to amplify GAPDH PCR amplicons. Two replicates per treatment are shown on a 2% agarose gel demonstrating the presence of discrete bands of the correct size, 261 bp. The –ve Cnt (control) was without template.

required for compatible solutes to have an appreciable effect resulted in high viscosity to the point that it may have started acting like a “molecular brake” [21] and adversely affect other parameters of the reaction mixture and could possibly interfere with subsequent downstream processing of the products.

We attribute the success of the application of macromolecules to *in vitro* reactions in more closely emulating the intracellular environment of cells such as bacteria whence these enzymes were derived or naturally function in. This was clear from the overall better performance of the Taq DNA polymerase. Under these conditions we were able to reduce the amount of enzyme by 75% and still attained more reaction product due to faster reaction kinetics. We attribute these results to the cumulative molecular and thermodynamic effects of EVE created by macromolecular crowding, that is, lowering the entropy of the reaction and thus increasing the free energy of the reactants. We demonstrate that these gains were a consequence of or combination of enhanced enzyme thermal stability, more primer annealing to its target and greater specificity, and enhanced enzyme-nucleic acid complex formation and stability (i.e. processivity). This improvement did not necessitate the employment of a genetically upgraded DNA polymerase,

many of which are currently on the market, but by using low-cost additives. We believe this study comprehensively demonstrates the importance and potential that macromolecular crowding holds for *in vitro* enzymatic settings with far-reaching consequences to the fields of Biochemistry, Molecular Biology and Biotechnology in general.

## Acknowledgments

MR acknowledge funding by a start-up grant from Provost and the Office of Life Sciences of NUS (R-397-000-604-101; R-397-000-604-712, the Faculty of Engineering (FRC) (R-397-000-017-112) and the National Medical Research Council (R397-000-018-213).

## References

- [1] R.J. Ellis, Macromolecular crowding: obvious but underappreciated, *Trends Biochem. Sci.* 26 (2001) 597–604.
- [2] S.B. Zimmerman, A.P. Minton, Macromolecular crowding: biochemical, biophysical, and physiological consequences, *Annu. Rev. Biophys. Biomol. Struct.* 22 (1993) 27–65.
- [3] A. Partikian, B. Ölveczky, R. Swaminathan, Y. Li, A.S. Verkman, Rapid diffusion of green fluorescent protein in the mitochondrial matrix, *J. Cell Biol.* 140 (1998) 821–829.

- [4] R. Hancock, Internal organisation of the nucleus: assembly of compartments by macromolecular crowding and the nuclear matrix model, *Biol. Cell* 96 (2004) 595–601.
- [5] P.D. Ross, A.P. Minton, Analysis of nonideal behaviour in concentrated haemoglobin solutions, *J. Mol. Biol.* 112 (1977) 437–452.
- [6] C.C. Gyenge, O. Tenstad, H. Wiig, In vivo determination of steric and electrostatic exclusion of albumin in rat skin and skeletal muscle, *J. Physiol.* 552 (2003) 907–916.
- [7] S. Schnell, T.E. Turner, Reaction kinetics in intracellular environments with macromolecular crowding: simulations and rate laws, *Prog. Biophys. Mol. Biol.* 85 (2004) 235–260.
- [8] D. Hall, A.P. Minton, Macromolecular crowding: qualitative and semi-quantitative successes, quantitative challenges, *Biochim. Biophys. Acta* 1649 (2003) 127–139.
- [9] M.S. Cheung, D. Klimov, D. Thirumalai, Molecular crowding enhances native state stability and refolding rates of globular proteins, *Proc. Natl. Acad. Sci. USA* 102 (2005) 4753–4758.
- [10] L. Acerenza, M. Grana, On the origins of a crowded cytoplasm, *J. Mol. Evol.* 63 (2006) 583–590.
- [11] J.M. Rohwer, P.W. Postma, B.N. Kholodenko, H.V. Westerhoff, Implications of macromolecular crowding for signal transduction and metabolite channeling, *Proc. Natl. Acad. Sci. USA* 95 (1998) 10547–10552.
- [12] R.A. Bambara, D. Uyemura, T. Choi, On the processive mechanism of *Escherichia coli* DNA polymerase I, *J. Biol. Chem.* 253 (1978) 413–423.
- [13] S. Bryant, D.L. Manning, Formaldehyde gel electrophoresis of total RNA, *Meth. Mol. Biol.* 86 (1998) 69–72.
- [14] R. Rasmussen, T. Morrison, M. Hermann, C. Wittwer, Quantitative PCR by continuous fluorescence monitoring of a double strand DNA specific binding dye, *Biochimica* 2 (1998) 8–11.
- [15] W. Liu, D.A. Saint, A new quantitative method of real time reverse transcription polymerase chain reaction assay based on simulation of polymerase chain reaction kinetics, *Anal. Biochem.* 302 (2002) 52–59.
- [16] K.S. Harve, R.R. Lareu, R. Rajagopalan, M. Raghunath, Macromolecular crowding in biological systems: dynamic light scattering (DLS) to quantify the excluded volume effect (EVE), *Biophys. Rev. Lett.* 1 (2006) 317–325.
- [17] A.N. Spiess, N. Mueller, R. Ivell, Trehalose is a potent PCR enhancer: lowering of DNA melting temperature and thermal stabilization of Taq polymerase by the disaccharide trehalose, *Clin. Chem.* 50 (2004) 1256–1259.
- [18] C.S. Rajendrakumar, T. Suryanarayana, A.R. Reddy, DNA helix destabilization by proline and betaine: possible role in the salinity tolerance process, *FEBS Lett.* 410 (1997) 201–205.
- [19] E.A. Galinski, M. Stein, B. Amendt, M. Kinder, The kosmotropic (structure-forming) effect of compensatory solutes—evolution of osmolyte systems, *Comp. Biochem. Physiol. (A Comp. Physiol.)* 117 (1997) 357–365.
- [20] N.A. Chebotareva, B.I. Kurganov, N.B. Livanova, Biochemical effects of molecular crowding, *Biochemistry (Mosc)* 69 (2004) 1239–1251.
- [21] A.N. Spiess, R.A. Ivell, Highly efficient method for long-chain cDNA synthesis using trehalose and betaine, *Anal. Biochem.* 301 (2002) 168–174.
- [22] S.B. Zimmerman, B. Harrison, Macromolecular crowding increases binding of DNA polymerase to DNA: an adaptive effect, *Proc. Natl. Acad. Sci. USA* 84 (1987) 1871–1875.
- [23] T.C. Jarvis, D.M. Ring, S.S. Daube, P.H. von Hippel, “Macromolecular crowding”: thermodynamic consequences for protein–protein interactions within the T4 DNA replication complex, *J. Biol. Chem.* 265 (1990) 15160–15167.
- [24] L.L. Lee, J.C. Lee, Thermal stability of proteins in the presence of poly(ethylene glycols), *Biochemistry* 26 (1987) 7813–7819.

**(WO/2008/018839) METHOD FOR MOLECULAR BIOLOGY APPLICATIONS**

Biblio. Data

Description

Claims

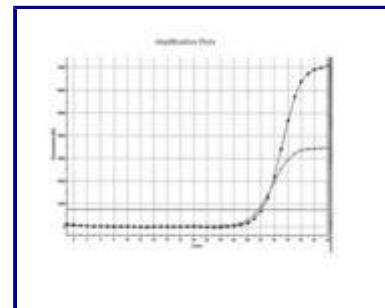
National Phase

Notices

Documents

**Latest bibliographic data on file with the International Bureau****Pub. No.:** WO/2008/018839 **International Application No.:** PCT/SG2007/000248**Publication Date:** 14.02.2008**International Filing Date:** 10.08.2007**Chapter 2 Demand Filed:** 06.06.2008**IPC:** **C12Q 1/68** (2006.01)**Applicants:** **NATIONAL UNIVERSITY OF SINGAPORE** [SG/SG]; 21 Lower Kent Ridge Road, Singapore 119077 (SG) (*All Except US*).**RAGHUNATH, Michael** [DE/SG]; (SG) (*US Only*).**LAREU, Ricardo, Rodolfo** [AU/SG]; (SG) (*US Only*).**HARVE, Subramhanya, Karthik** [IN/SG]; (SG) (*US Only*).**Inventors:** **RAGHUNATH, Michael**; (SG).**LAREU, Ricardo, Rodolfo**; (SG).**HARVE, Subramhanya, Karthik**; (SG).**Agent:** **MATTEUCCI, Gianfranco**; Lloyd Wise, Tanjong Pagar, P.O. Box 636, Singapore 910816 (SG).**Priority Data:** 60/836,374 09.08.2006 US**Title:** METHOD FOR MOLECULAR BIOLOGY APPLICATIONS

**Abstract:** The invention provides a method of nucleic acid synthesis and/or amplification, and/or of improving the efficiency, activity and/or stability of at least one nucleic acid-modifying enzyme, comprising carrying out the method in the presence of (a) at least one organic-based macromolecule having a molecular weight of 50kDa to 500kDa and neutral surface charge; or (b) at least one organic-based macromolecule of radius 2 to 50nm and neutral surface charge. There is also provided a method of determining the optimum crowding conditions of macromolecule(s) in solution.



**Designated States:** AE, AG, AL, AM, AT, AU, AZ, BA, BB, BG, BH, BR, BW, BY, BZ, CA, CH, CN, CO, CR, CU, CZ, DE, DK, DM, DO, DZ, EC, EE, EG, ES, FI, GB, GD, GE, GH, GM, GT, HN, HR, HU, ID, IL, IN, IS, JP, KE, KG, KM, KN, KP, KR, KZ, LA, LC, LK, LR, LS, LT, LU, LY, MA, MD, ME, MG, MK, MN, MW, MX, MY, MZ, NA, NG, NI, NO, NZ, OM, PG, PH, PL, PT, RO, RS, RU, SC, SD, SE, SG, SK, SL, SM, SV, SY, TJ, TM, TN, TR, TT, TZ, UA, UG, US, UZ, VC, VN, ZA, ZM, ZW.

African Regional Intellectual Property Org. (ARIPO) (BW, GH, GM, KE, LS, MW, MZ, NA, SD, SL, SZ, TZ, UG, ZM, ZW)

Eurasian Patent Organization (EAPO) (AM, AZ, BY, KG, KZ, MD, RU, TJ, TM)

European Patent Office (EPO) (AT, BE, BG, CH, CY, CZ, DE, DK, EE, ES, FI, FR, GB, GR, HU, IE, IS, IT, LT, LU, LV, MC, MT, NL, PL, PT, RO, SE, SI, SK, TR)

African Intellectual Property Organization (OAPI) (BF, BJ, CF, CG, CI, CM, GA, GN, GQ, GW, ML, MR, NE, SN, TD, TG).

**Publication Language:** English (EN)**Filing Language:** English (EN)